

## PHYS 6751 Laboratory: $^{197}\text{Au}(n,\gamma)$ Cross Section Measurement via $\gamma$ -Spectroscopy

### Lab overview:

- *Objective:* Measure the radiative neutron-capture cross section of  $^{197}\text{Au}$  by irradiating gold powder with a neutron howitzer and counting radioactive decays from  $^{198}\text{Au}$  using a sodium-iodide  $\gamma$ -detection set-up, comparing the result to calculations performed with the software TALYS and previously published data
- *Gain familiarity with:* neutron activation,  $\gamma$  calibration sources,  $\gamma$ -spectroscopy, Hauser-Feshbach cross section calculations, the EXFOR database from the National Nuclear Data Center
- *Report style:* Physical Review Letters (PRL)

### Brief description:

Radiative neutron-capture reactions play a key role in low-energy nuclear physics. These reactions have been employed for nuclear mass measurements and nuclear structure studies, and are the primary means by which nearly half of the elements in the universe were made. Activation measurements, where radioactive decay from target material is monitored after a period of target irradiation, are often the go-to technique for measuring  $(n,\gamma)$  reaction cross sections, so that sensitive  $\gamma$ -detectors can safely be used far from the damagingly high neutron flux.

In this experiment, we will use a strong neutron source to irradiate a sample of  $^{197}\text{Au}$  over a period of days to generate a significant amount of  $^{198}\text{Au}$ . Following irradiation, a sodium-iodide (NaI) counting set-up, which must be calibrated with  $\gamma$ -sources, will be used to detect  $\gamma$ -decays from the gold sample in order to determine the amount of  $^{198}\text{Au}$  which was made. Using an estimate for the incident neutron flux, the  $^{197}\text{Au}(n,\gamma)$  cross section will be determined. This cross section will be compared to calculations performed with the Hauser Feshbach code Talys, as well as previous measurement data. Additional tasks include determining the contamination of the  $^{197}\text{Au}$  sample using a germanium detection set-up.

### Expectations for Run-plan:

The run-plan should consist of time-saving calculations and an order of operations. For instance,

- What is the expected decay energy for  $^{198}\text{Au}$  and what background lines are nearby?
- How will the data analysis be performed? (e.g. peak-fitting, background subtraction)
- How will the cross-section calculation be performed?
- How will the efficiency and energy-calibration of the  $\gamma$ -detection set-up be determined?
- What is the experiment order-of-operations? (e.g. What measurements do we need to take? What is the bias voltage for our detectors?)

- What is the expected cross section for thermal neutrons? (Data or calculation results)
- Given a nominal mass of gold (e.g. 1 gram) in a powder and a nominal flux of thermal neutrons (e.g.  $10^7$  per  $\text{cm}^2$  per second), how many reactions do we expect to occur?
- How long do we need to perform the irradiation?
- ...of course, other preparatory notes are welcome, so long as they're useful!

**NOTE:** The above examples are suggestions. Please do not feel obligated to have all of them done prior to the lab start. You will be working in a group, so with any luck your partners will have prepared for some different portions of the lab.

### Expectations for Lab Report:

The lab report should be a publication-quality paper typeset in the style of Physical Review Letters. As such, it should include an exciting motivation for the measurement, emphasizing the scientific advance this measurement represents. This should be followed by a concise but comprehensive description of the experimental and analysis technique, followed by a comparison to prior data and/or calculations. Finally, the impact of the measurement should be discussed; generally this describes what problem has been solved or what the future applications will be.

The reports will be written individually, but your group members should appear as co-authors on the paper. As such, you are free to share calculations and plots. In fact, sharing in this sense is expected, as this is how real experiments work. However, all writing must be your own.

**NOTE:** It is quite possible that the lab contains more work than you could possibly get done during the experiment time allotted. This is OK, as I don't expect you to necessarily complete every single task. However, a reasonable amount of work must be completed and that work must be thoroughly described in an articulate way.

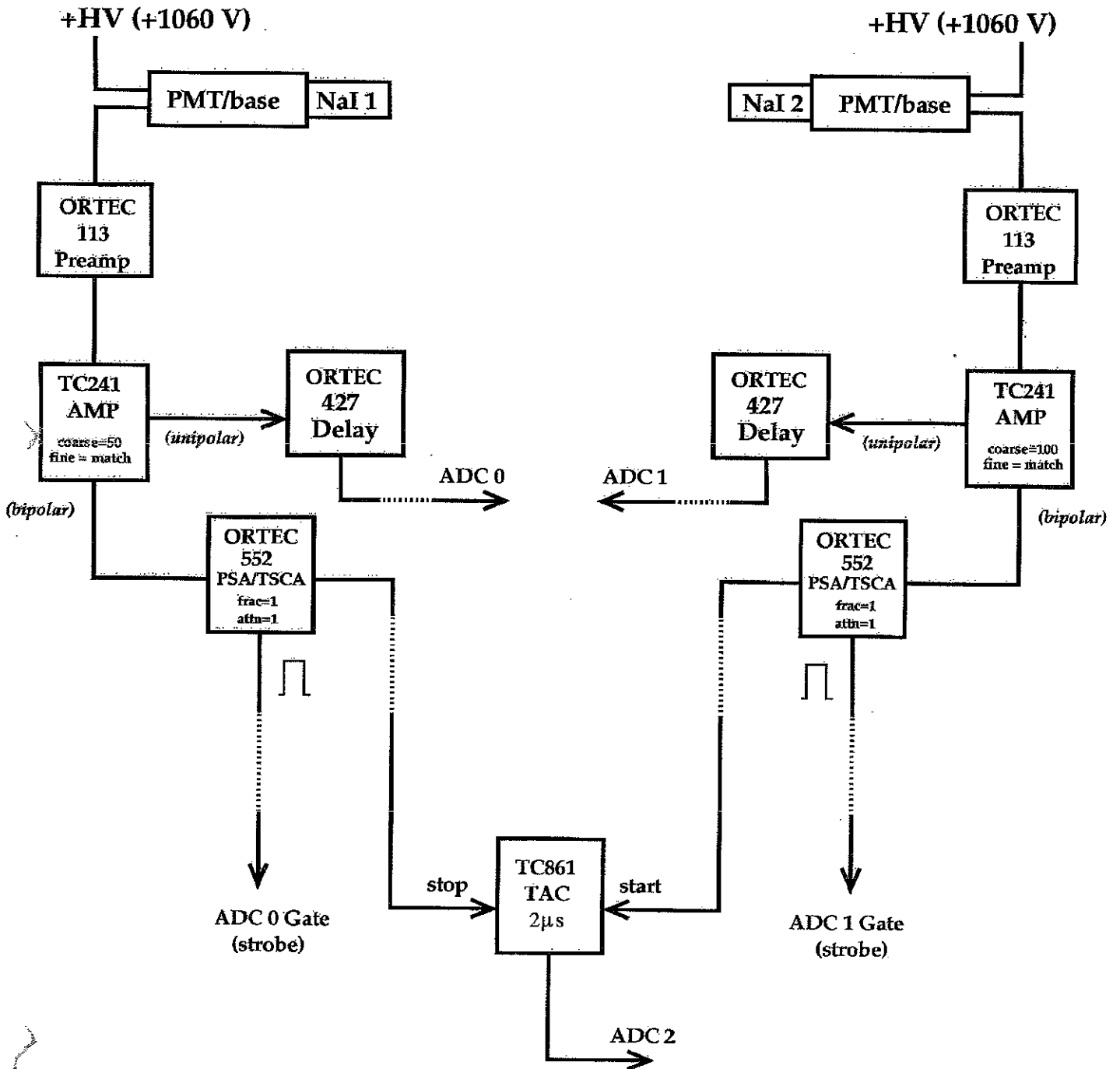
### WARNINGS:

- Be careful with the bias voltage
  - Don't electrocute yourself
  - Don't exceed the maximum bias voltage for the detector
  - Don't touch the high-voltage supply cables or the detector when the bias voltage is on
- Be careful with the  $\gamma$ -sources and the activated gold sample
  - Only handle with gloves
  - Never touch the surface of the  $\gamma$ -source to any other surface
  - Report any incidents (e.g. dropped the source) immediately to Zach Meisel or Tom Massey or Carl Brune
- If you aren't sure, ask!

# Appendices

1. Electronics set-up for NaI
2. NaI data acquisition instructions
3.  $^{198}\text{Au}$   $\gamma$ -decay spectrum
4.  $^{197}\text{Au}(n,\gamma)$  cross-section measurement paper
5. How to find a cross section on EXFOR
6. Talys information
7. Edwards Lab radioactive source list
8.  $\gamma$ -ray energy and intensity standards
9. Comments on reaction network equilibria
10. Ortec NaI  $\gamma$ -spectroscopy information
11. Electronics set-up for HpGe
12. ~~HpGe and NIST source specifications~~
13. Information on typical gold impurities
14. Ortec HpGe  $\gamma$ -spectroscopy information
15. Comments on  $\gamma$  interactions in matter

# Electronics Set-up



## Pre-Defined Histograms

vector	histogram name	type	comment
0	gam1	1D	energy of NaI 1
1	gam2	1D	energy of NaI 2
2	gtac	1D	time between NaI 1 and NaI 2
3	g1_t	2D	time vs. gam1
4	g2_t	2D	time vs. gam2
5	g1_g2	2D	gam2 vs. gam1
10	g11 <small>475-625</small>	1D	gam1 cond. $\equiv$ gate 0 $\cdot$ gate 1
11	g21 <small>61-100</small>	1D	gam2 cond. $\equiv$ gate 0 $\cdot$ gate 1
12	g12 <small>242-300</small>	1D	gam1 cond. $\equiv$ gate 0 $\cdot$ gate 2
13	g22	1D	gam2 cond. $\equiv$ gate 0 $\cdot$ gate 2
14	g13	1D	gam1 cond. $\equiv$ gate 0 $\cdot$ gate 3
15	g23	1D	gam2 cond. $\equiv$ gate 0 $\cdot$ gate 3

### TO SET GATES:

475-625

*sysk list to see*

Use the command "*gate i limlo limhi*"

Here *i* is the gate number (0,1,2) and the lower and upper limits are given by *limlo* and *limhi*, respectively.

### TO RUN FOR A FIXED TIME DURATION

Use the command "*time*" to set the time duration in seconds.

Use the command "*run*" to run the DAQ system for this duration.

## Four-Input Multi-Channel Analyzer

The "home-made" multi-channel analyzer consists of 4 "sample-and-hold" units that can measure the amplitude of an input signal and hold this amplitude (0 to 10 volts) until it is digitized by a single fast-successive approximation analog-to-digital converter (ADC). The digitized data are stored in a first-in-first-out (FIFO) buffer after averaging out the differential non-linearity of the ADC's, providing a very linear response (this is referred to as channel width averaging). The unique feature of the buffered data is its sequenced storage as input 0 to input 3, which allows the four input channels to be analyzed separately within the time resolution of the analyzer. The data can then be saved for later analysis or plotted for on-line observation.

The computer interrupt routine (the controlling program of the Data Acquisition system, or DAQ) also allows the user to set gates. In the  $\gamma - \gamma$  coincidence interrupt, the gates sort the data on-line, i.e. as it is being acquired. The gates are pre-defined (in the `ugl1` interrupt) as follows:

Gate 0 : The coincidence time overlap of the two NaI signals from the output of the time-to-amplitude converter (TAC). This spectrum is called `gtac`.

Gate 1: Set on the `gam2` spectrum to identify the 0.511 MeV gamma ray peak of  $^{22}\text{Na}$ .

Gate 2: Set on the `gam2` spectrum to identify the 1.275 MeV gamma ray peak of  $^{22}\text{Na}$ .

**Differential non-linearity:** Ideally any two adjacent digital codes correspond to output analog voltages that are exactly one LSB apart. Differential non-linearity is a measure of the worst case deviation from the ideal 1 LSB step. Ideally one should expect that if the detector is irradiated by a sufficiently homogeneous source, then the number of counts in each ADC pixel is linearly proportional to the size of the pixel. To put it differently, the relative deviation from the average size of the pixels is a measure for the differential non-linearity.

## TO SAVE DATA

- 1). At the *DAQ* prompt enter the subdirectory where you want the data to be stored. The subdirectories are created on */home/ugl1/data*. You carry out this process by defining a "disk number" via the command: *disk #*. This will create the subdirectory */home/ugl1/data/disk#* where all of the histograms will be saved. You should choose a number that does not yet exist.
- 2). At the *DAQ* prompt enter the starting label (called a "tag") for the histogram set. Use the command: *tag #*.
- 3). At the *DAQ* prompt type *sav* to save all histograms.

## TO RECOVER THE DATA FOR PLOTTING

- 1). Clear out all histograms already in memory with the command: *clear \**.
- 2). At the *DAQ* prompt use the script command *review*. This will load all histograms in the defined *disk* area starting with the defined *tag* number.
- 3). Note that individual histograms can be printed using the on-screen "print" button.

File: IPL.daq (also called setup.daq)

```
define gam1 1024
define gam2 1024
define gtac 1024
define g1_t 4096 type 1
define g2_t 4096 type 1
define g1_g2 4096 type 1
define g11 1024
define g21 1024
define g12 1024
define g22 1024
define g13 1024
define g23 1024
vector 0 gam1 1024
vector 1 gam2 1024
vector 2 gtac 1024
vector 3 g1_t 4096
vector 4 g2_t 4096
vector 5 g1_g2 4096
vector 10 g11 1024
vector 11 g21 1024
vector 12 g12 1024
vector 13 g22 1024
vector 14 g13 1024
vector 15 g23 1024
loadint ugl1
t0 10
gate 0 280 330
gate 1 145 180
gate 2 285 335
gate 3 380 455
```

Note: ugl1 is one of the many interrupt routines in int8.c (so it acts like a subroutine).



## Interrupt Routine: ugl1

```
#include <dos.h>
#include <bios.h>
#include <stdio.h>
#include <oual.h>
#include <signal.h>
#include <conio.h>
#include <stdlib.h>
#include <time.h>
#include <string.h>

char oual_system_name[] = "UGL Gamma-Gamma_Coinc 27 March 1996\n"; /*
/* gamma1 energy signal applied to adc0
 * gamma2 energy signal applied to adc1
 * coincidence tac signal applied to adc2
 * vector 0 = gam1
 * vector 1 = gam2
 * vector 2 = g1-g2 tac
 * vector 3 = gam1_coinc 2d
 * vector 4 = gam2_coinc 2d
 * vector 5 = gam1_gam2 2d
 * vector 10 = gam1 gated
 * vector 11 = gam2 gated/

extern int oual_event_flag;
void ugl_int(void)

{
unsigned g1,g2,g12t,flag;
unsigned g1_g2,g1_t,g2_t;

databufferptr = (struct databuffer *) shmptr;
databufferptr->dav = 1;
if(databufferptr->nevents <= 0) goto ret; //return;

if(oual_anal == 0) goto ret;

oual_lastadc=-1;
ouindex=0;

while(databufferptr->nevents-- > 0)
  {if(((oual_rawdata=databufferptr->data[ouindex++]) & 0x3000) == 0) /* is data present */
    {if (oual_anal == 0) goto ret;
      oual_adcdata=oual_rawdata & 0xff;
      oual_adcnumber=(oual_rawdata & 0x3000) >> 12;
      if (oual_adcnumber == 0)
        {g1 = oual_adcdata;
          oual_lastadc = 0;
          histogram(0,g1);}
      if ((oual_adcnumber == 1) && (oual_lastadc == 0))
        {g2 = oual_adcdata;
          oual_lastadc = 1;
          histogram(1,g2);
          g1_g2=(((g2 & 0xfc0) << 6) | g1) >> 6);
```

```

        histogram(5, g1_g2);}
else if (oual_adcnumber == 1)
    {histogram(1,oual_adcdata);
    oual_lastadc = -1;}
if ((oual_adcnumber == 2) && (oual_lastadc == 1))
    {g12t = oual_adcdata;
    histogram(2,g12t);
    g1_t=(((g12t & 0xfc0) << 6) | g1) >> 6);
    histogram(3, g1_t);
    g2_t=(((g12t & 0xfc0) << 6) | g2) >> 6);
    histogram(4, g2_t);
    if((checkgate(1,1,g2) == 1) && (checkgate(0,2,g12t) == 1))
        {histogram(10,g1);
        histogram(11,g2);}
    if((checkgate(2,1,g2) == 1) && (checkgate(0,2,g12t) == 1))
        {histogram(12,g1);
        histogram(13,g2);}
    if((checkgate(3,1,g2) == 1) && (checkgate(0,2,g12t) == 1))
        {histogram(14,g1);
        histogram(15,g2);}
    oual_lastadc = -1;}
else if (oual_adcnumber == 2)
    {histogram(2,oual_adcdata);
    oual_lastadc = -1;}
}
}

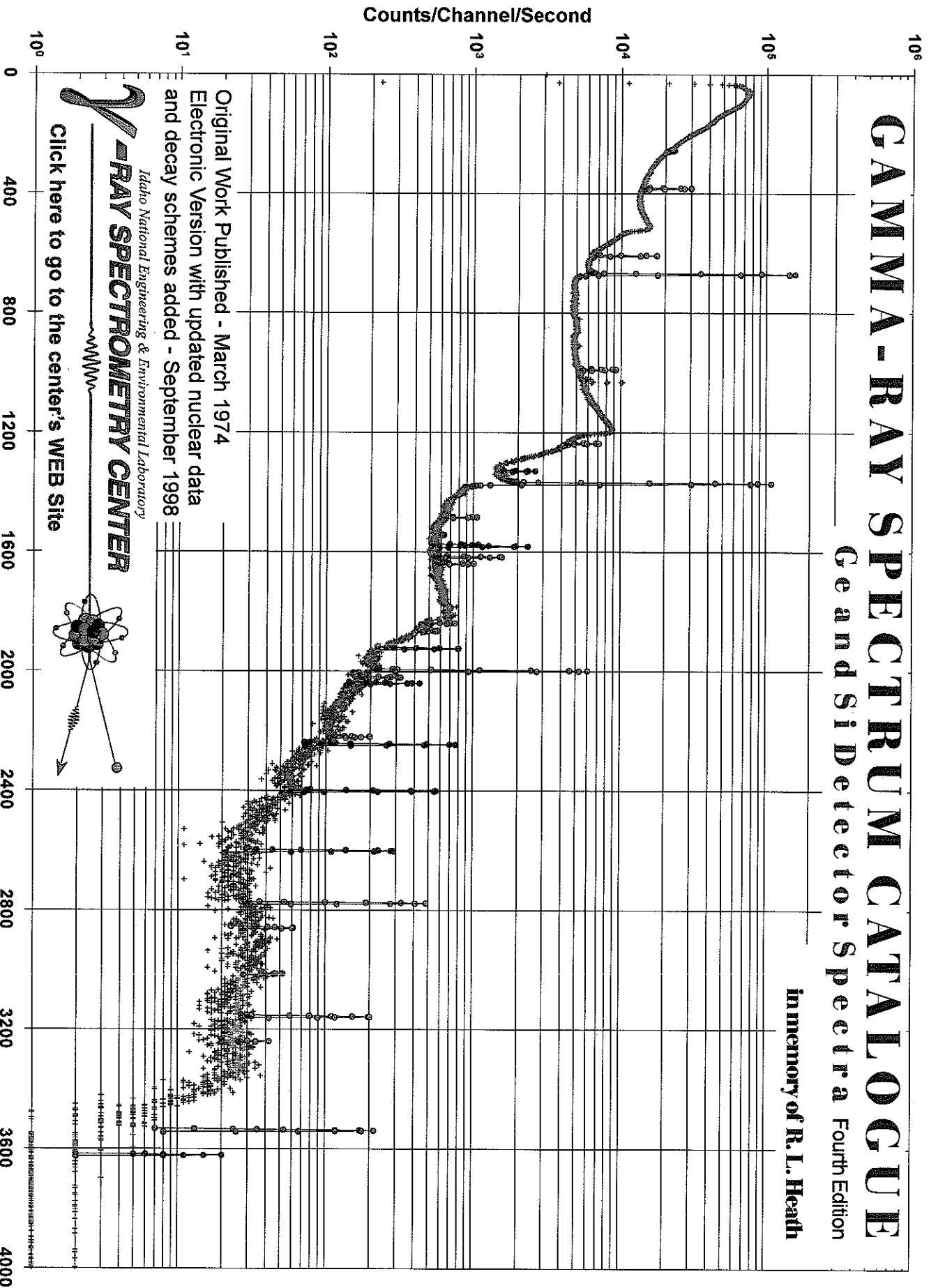
ret:
databufferptr->nevents = 0;
databufferptr->dav = 0; /* set no data available */
return;}

```


# GAMMA-RAY SPECTRUM CATALOGUE

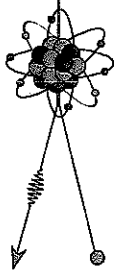
GeantSi Detector Spectra Fourth Edition

In memory of R.L. Heath



Original Work Published - March 1974  
Electronic Version with updated nuclear data  
and decay schemes added - September 1998

  
Idaho National Engineering & Environmental Laboratory  
**RAY SPECTROMETRY CENTER**



[Click here to go to the center's WEB Site](#)

Table of Contents



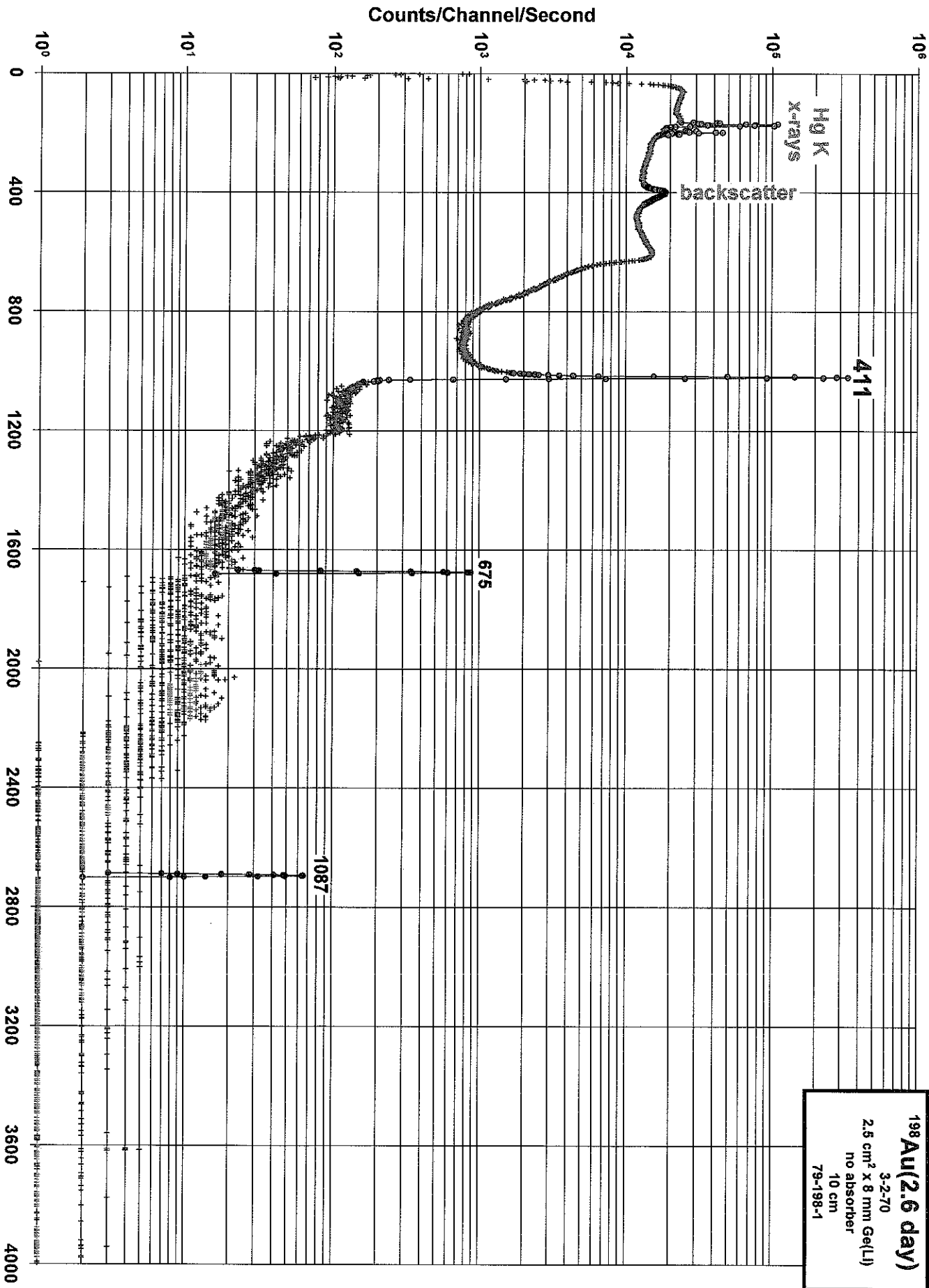
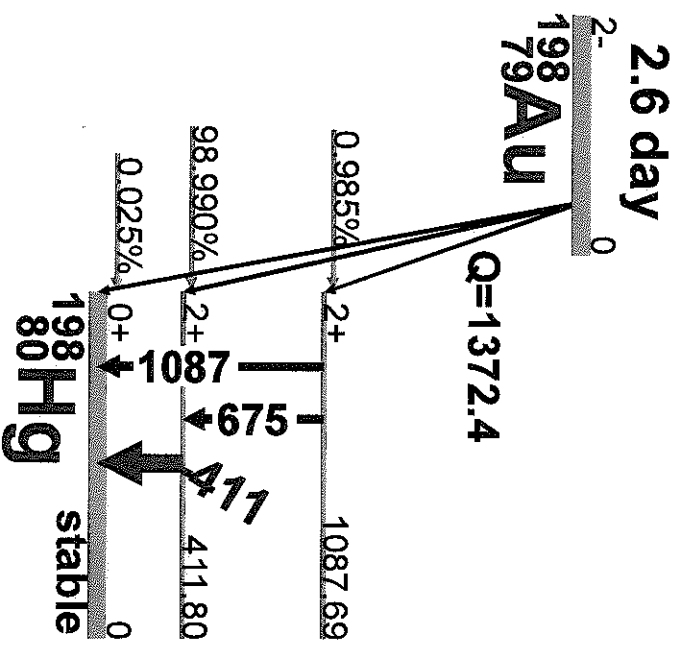


Table of Contents



**<sup>198</sup>Au(2.6 day) Decay Scheme**



**GAMMA-RAY ENERGIES AND INTENSITIES**

Nuclide: <sup>198</sup>Au

Half Life: 2.69517(2) day

Detector: 2.5 cm<sup>2</sup> x 8 mm Ge (Li)

Method of Production: <sup>197</sup>Au(n,γ)

E <sub>γ</sub> (keV)	σ E <sub>γ</sub>	I <sub>γ</sub> (rel)	I <sub>γ</sub> (%)	σ I <sub>γ</sub>	S
411.802			95.58	0.12	1
675.884	0.001		0.804	0.003	2
1087.684	0.003		0.1590	0.0020	2

E<sub>γ</sub>, σE<sub>γ</sub>, I<sub>γ</sub>, σI<sub>γ</sub> - 1998 ENSDF Data



$Y_B(E)$  is unity as mentioned above. In the case of Sb, since it also has a large capture width at 6.3 eV resonance and the ratio of capture-to-neutron width is sufficiently large, the saturated yield method can be applicable. Then, the detection efficiency  $\epsilon_{Sb}$  and the capture yield  $Y_{Sb}(E)$  for Sb could be derived through Eqs.(6) to (9) as same as Au sample. In this measurement, the detection efficiency  $\epsilon_{Sb}$  was determined to be 0.91.

#### 4. Correction for Capture Yield

For the capture cross section measurement, capture yield is the primary quantity to be determined from the number of capture events occurring in the sample. The neutron capture yield is given as

$$Y_c(E) = (1 - e^{-N\sigma_t(E)t}) \frac{\sigma_c(E)}{\sigma_t(E)} f_c, \quad (10)$$

where  $N$  is the atomic density of sample material,  $\sigma_t$  the neutron total cross section,  $t$  the sample thickness,  $\sigma_c$  the neutron capture cross section, and  $f_c$  the correction factor for neutron scattering in the sample. When  $t$  is thin enough, Eq.(10) can be written as

$$Y_c(E) = N\sigma_c(E)t. \quad (11)$$

In the neutron capture cross section measurement, the effect of single and multiple neutron scattering in the sample is quite important in determining a capture cross section. This effect, which increases the effective thickness of the sample relative to geometrical thickness in the direction of the incident neutrons, must be considered in a capture cross section measurement in which the total number of capture events in a sample is measured. In the present work, we have made a Monte Carlo code to simulate the neutron capture and multiple scattering events in the sample and to carry out the corrections. The correction factor  $f_c$  was 0.975 to 0.985 for Au, and 0.965 to 0.971 for Sb. Then, the cross sections for the  $^{197}\text{Au}(n, \gamma)$  and  $\text{Sb}(n, \gamma)$  reactions were derived from the corrected yield data for the present measurements.

### IV. RESULTS OF CAPTURE CROSS SECTIONS

The results of Au are given in Fig. 4. Table 1 also shows the comparison of mean cross sections in the present work with those in ENDF/B-VI and JENDL Dosimetry File. The statistical uncertainties are about 0.3% to 1.5%. Other uncertainties are due to detection efficiency of about 1.5% for the  $^{10}\text{B}$  sample measurement and 1.8% for the Au sample measurement, sample thickness of about 0.5% and correction for capture yield of about 0.3%. The present result is in good agreement with the evaluated data in JENDL Dosimetry File and ENDF/B-VI. It could be considered that in the energy range below 10 eV the BGO detection system can be verified to be applicable to the absolute measurement of capture cross sections by detecting prompt capture

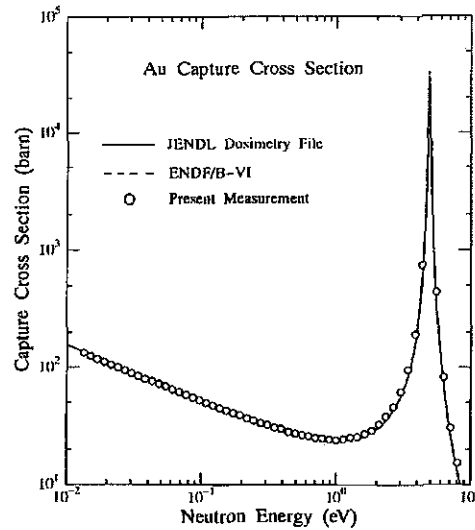


Fig. 4 Capture cross section for the  $^{197}\text{Au}(n, \gamma)$  reaction.

Table 1 Comparison of mean values of the  $^{197}\text{Au}(n, \gamma)$  cross section from the present work with those from ENDF/B-VI and JENDL Dosimetry File

Energy range (eV)	ENDF/B-VI (barn)	JENDL-DF (barn)	Present (barn)
0.0134 - 0.0213	119.7	117.7	117.7±2.9
0.0213 - 0.0338	95.4	95.8	94.1±2.3
0.0338 - 0.0538	76.1	76.2	75.7±1.8
0.0538 - 0.0855	60.9	61.0	61.2±1.5
0.0855 - 0.136	49.1	49.2	49.4±1.2
0.136 - 0.217	39.9	39.9	40.3±1.0
0.217 - 0.347	32.9	32.8	33.4±0.8
0.347 - 0.554	27.9	27.7	28.3±0.7
0.554 - 0.886	24.8	24.5	25.3±0.7
0.886 - 1.438	24.1	23.6	24.7±0.6

$\gamma$ -rays using the linac TOF method.

For the Sb measurement, statistical errors are about 1.0% to 4.5%, and the total uncertainties are from 2.6 to 5.1%, including the error of detection efficiencies, sample thickness and correction of capture yield. The measured result is shown in Fig. 5 and Table 2, and compared with the evaluated data in JENDL-3.2 and ENDF/B-VI. The present result shows good agreement with the data in JENDL-3.2 and ENDF/B-VI.

Since the resonance parameters have not been obtained in the present measurement, the capture cross sections in the resonance region are not compared in Tables 1 and 2.

### V. CONCLUSION

The present study can be concluded as follows:

- (1) Making use of BGO scintillators, a total energy absorption  $\gamma$ -ray detection system was prepared for the absolute measurement of capture cross sections

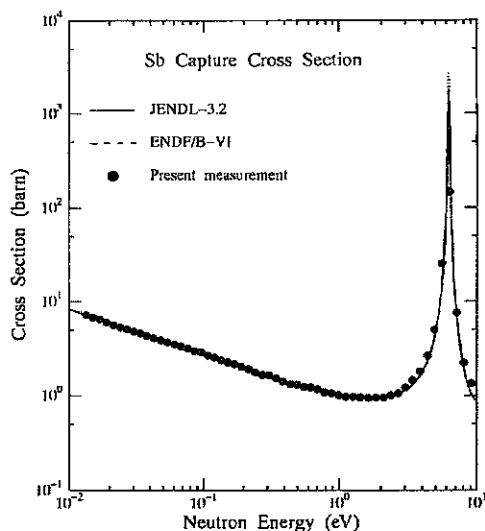


Fig. 5 Capture cross section for the  $\text{Sb}(n, \gamma)$  reaction.

Table 2 Comparison of mean values of the  $\text{Sb}(n, \gamma)$  cross section from the present work with those from ENDF/B-VI and JENDL-3.2

Energy range (eV)	ENDF/B-VI (barn)	JENDL-3.2 (barn)	Present (barn)
0.0134-0.0213	6.62	6.35	$6.31 \pm 0.18$
0.0213-0.0338	5.26	5.05	$5.00 \pm 0.13$
0.0338-0.0538	4.18	4.01	$4.05 \pm 0.10$
0.0538-0.0855	3.33	3.20	$3.30 \pm 0.08$
0.0855-0.136	2.66	2.55	$2.64 \pm 0.07$
0.136-0.217	2.13	2.04	$2.10 \pm 0.06$
0.217-0.347	1.71	1.65	$1.67 \pm 0.05$
0.347-0.554	1.40	1.35	$1.34 \pm 0.05$
0.554-0.886	1.17	1.13	$1.14 \pm 0.04$
0.886-1.438	1.01	0.98	$0.98 \pm 0.03$
1.438-2.344	0.96	0.94	$0.95 \pm 0.03$

below 10 eV using the linac TOF method. It is necessary for this absolute measurement that samples have an appropriate resonance for the saturated yield method.

- (2) This detection system was firstly calibrated with a Sm sample for thermal neutrons. After that, the  $^{10}\text{B}$  sample was employed to determine the absolute neutron flux from thermal to higher neutron energies by the  $^{10}\text{B}(n, \alpha\gamma)$  reaction.
- (3) The detection system was applied to the absolute measurement of the  $^{197}\text{Au}(n, \gamma)$  reaction cross section which was one of the well known cross sections as a standard. The measured result showed satisfactory agreement with the evaluated data in JENDL Dosimetry File and ENDF/B-VI.
- (4) To extend the application of the BGO detection system, Sb was selected as a sample, which has a

large scattering-to-capture cross section ratio. The measured result showed good agreement with the evaluated data in JENDL-3.2 and ENDF/B-VI.

- (5) From above results, it could be verified that the BGO detection system is applicable to the absolute measurement of capture cross sections below 10 eV except resonance energy region.

It can be expected in future that the BGO detection system is applicable to the absolute measurement of some other capture cross sections as a total energy absorption detector.

#### ACKNOWLEDGMENTS

The authors would like to express their sincere thanks to Prof. I. Kimura of Kyoto University for his continuous encouragement and invaluable suggestions throughout this study. The cooperation of Mr S. Kanazawa of Kyoto University is deeply appreciated throughout this work. This study was partially supported by the Special Project Research on Energy under a Grant in Aid for Scientific Research of the Ministry of Education, Science, Sports and Culture of Japan.

#### REFERENCES

- (1) Chrien, R.E. (Ed.): "Neutron Physics and Nuclear Data in Science and Technology", Neutron Radiative Capture, OECD/NEA, Pergamon Press, Vol.3, (1984).
- (2) Yamamoto, S., Fujita, Y., Shibata, T., Selvi, S.: *Nucl. Instrum. Methods.*, **A249**, 484 (1986).
- (3) Wisshak, K., Guber, K., Käppeler, F., Krisch, J., Müller, H., Rupp, G., Voss, F.: *Proc. Int. Conf. on Nucl. Data for Sci. and Technol., at Mito*, p.387 (1988).
- (4) Block, R.C., Marano, P.J., Drindak, N.J., Feiner, F., Seeman, K.W., Slovacek, R.E.: *ibid.*, p.383 (1988).
- (5) Muradyan, G.V., Shchepkin, Yu.G., Adamchuk, Yu.V., Ustrov, G.I.: *Preprint IAEA-2634*, (1976).
- (6) Knoll, G.F.: "Radiation Detection and Measurement", John Wiley & Sons, p.257 (1979).
- (7) Kobayashi, T., Kanda, K.: *KURRI-TR-198*, (1980).
- (8) Mughabghab, S.F., Divadeenam, M., Holden, N.E.: "Neutron Cross Sections", Academic Press, Vol.1, (1981).
- (9) Nakagawa, T., Shibata, K., Chiba, S., Fukahori, T., Nakajima, Y., Kikuchi, Y., Kawano, T., Kanda, Y., Ohsawa, T., Matsumobu, H., Kawai, M., Zukeran, A., Watanabe, T., Igarasi, S., Kosako, K., Asami, T.: *J. Nucl. Sci. Technol.*, **32**[12], 1259 (1995).
- (10) Nakazawa, M., Kobayashi, K., Iwasaki, S., Iguchi, T., Sakurai, K., Ikeda, Y., Nakagawa, T.: JENDL Dosimetry File, *JAERI 1325*, (1992).
- (11) Rose, R.F. (Compiled and Edited): *BNL-NCS-17541*, (4th ed.) (ENDF/B-VI), (1991).
- (12) Kobayashi, K., Jin, G., Yamamoto, S., Takami, K., Kimura, Y., Kozuka, T., Fujita, Y.: *Annu. Rep. Res. Reactor Inst., Kyoto Univ.*, **22**, 142 (1987).
- (13) Reactor Physics Constants, *ANL-5800*, (2nd ed.), USAEC, p.631 (1963).
- (14) IAEA Technical Series No.227, "Nuclear Data Standards for Nuclear Measurements", IAEA, Vienna, (1983).
- (15) Schmitt, H.W.: *ORNL-2883*, 1-28-60, (1960).

# National Nuclear Data Center



Site Index -

Go

NSR XUNDL ENSDF  
 NUDat Databases MIRD  
 SUMMA ENDS  
 Chart of Nuclides  
 Networks CSEWG USNDP  
 Nuclear reaction experimental data  
 Empire Resonances  
 Nuclear Walllet  
 Cards Nuclear Publications  
 Nuclear Data Sheets

Nuclear Data Survey

Please take a moment to fill out the nuclear data survey!

USNDP Workshop  
 Nuclear Data Week 2016  
 MINHSEWG

- Main
- Structure & Decay
- Reactions
- Bibliography
- Networks & Links
- Publications
- Meetings

- AMDC Atomic Mass Data Center, *Q-value Calculator*
- Coveriances of Neutron Reactions
- ENDF Evaluated Nuclear (reaction) Data File, *Sigma*
- MMSS & DOE NMIRD  
Safeguards & inventory decay data standards
- NuCRates MACS & Astro-physical reaction rates
- XUNDL Experimental Un-
- Atlas of Neutron Resonances Parameters & thermal values
- CSEWG Cross Section Evaluation Working Group
- ENSDF Evaluated Nuclear Structure Data File
- NSR Nuclear Science References
- NUDat Nuclear structure & decay Data
- CapGam Thermal Neutron Capture  $\gamma$ -rays
- CSRSRS alias EXFOR Nuclear reaction experimental data
- IRDF International Reactor Dosimetry File
- Nuclear Data Sheets Nuclear structure & decay data journal, *Special Issues on reactor data*
- USNDP U.S. Nuclear Data Program
- Chart of Nuclides Basic properties of atomic nuclei
- Empire Nuclear reaction model code system, *Reference paper*
- MIRD Medical Internal Radiation Dose
- Nuclear Walllet Cards Ground & isomeric states properties, *Homeland Security version*
- USNDP/CSEWG G-Forge Collaboration Server





A : Automatic data re-normalized  Tabulated data...

[Info] : Show Summary (with code explanation, links to dependent data, etc.)

[X4+] : Extended EXFOR (original file with code explanation, links to Web-Journals)

[T4] : Tabulated Data

...leads to:

```

#SUBENT          V1002484
#AUTHORS        S.F.Mughabghab
#REFERENCE       Atlas of Neutron Resonances, S.F.Mughabghab, 2006
#TITLE          Atlas of neutron resonances resonance parameters and
#+             thermal cross sections Z=1-100
#REACTION        79-AU-197(N,G) 79-AU-198-M, SIG,,, RECOM
#QUANTITY        Cross section
#SUBR           V1002484?
#Ene, eV         8          Sig, mb          dSig, mb
0.0253          8          2
#END
  
```



# TALYS

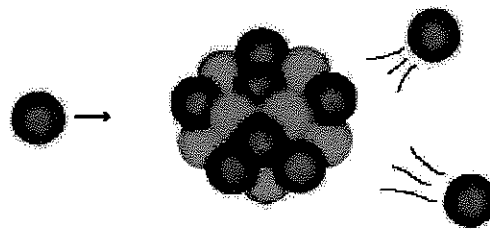
- Home
- More about TALYS
- Download TALYS
- Documentation**
- Links
- Random nuclear data files
- TENDL-2008
- TENDL-2009
- TENDL-2010
- TENDL-2011
- TENDL-2012
- TENDL-2013
- TENDL-2014
- TENDL-2015
- Contact

## What is TALYS?

**TALYS** is software for the simulation of nuclear reactions. Many state-of-the-art nuclear models are included to cover all main reaction mechanisms encountered in light particle-induced nuclear reactions. **TALYS** provides a complete description of all reaction channels and observables, and is user-friendly.

**TALYS** is a versatile tool to analyse basic microscopic experiments and to generate nuclear data for applications.

**TALYS** is created at [NRG in Petten](#), the Netherlands, and [CEA in Bruyères-le-Châtel](#), France, and is available free of charge.



Schematic illustration of an (n,2n) reaction on a nucleus

## News

### **Download TALYS-1.8!**

The official TALYS-1.8 is now available. Go to the TALYS download page. [\[more\]](#)

[\[more\]](#)

# Chapter 6

## Input description

For the communication between TALYS and its users, we have constructed an input/output method which shields beginners from all the possible options for nuclear model parameters that can be specified in TALYS, while enabling at the same time maximal flexibility for experienced users.

An input file of TALYS consists of keywords and their associated values. Before we list all the input possibilities, let us illustrate the use of the input by the following example. It represents a minimum input file for TALYS:

Run in terminal:

```
projectile n
element    al
mass      27
energy    14.
```

`talys <InputFileName> OutputFileName`  
↑  
you specify these

This input file represents the simplest question that can be asked to TALYS: if a  $^{27}\text{Al}$  nucleus is hit by 14 MeV neutrons, what happens? Behind this simple input file, however, there are more than a few hundred default values for the various nuclear models, parameters, output flags, etc., that you may or may not be interested in. When you use a minimal input file like the one above, you leave it to the authors of TALYS to choose all the parameters and models for you, as well as the level of detail of the output file. If you want to use specific nuclear models other than the default, adjust parameters or want to have more specific information in the output file(s), more keywords are required. Obviously, more keywords means more flexibility and, in the case of adequate use, better results, though often at the expense of increasing the level of phenomenology. In this Chapter, we will first give the basic rules that must be obeyed when constructing an input file for TALYS. Next, we give an outline of all the keywords, which have been categorised in several groups. Finally, we summarize all keywords in one table.

## 6.1 Basic input rules

Theoretically, it would be possible to make the use of TALYS completely idiot-proof, i.e. to prevent the user from any input mistakes that possibly can be made and to continue a calculation with “assumed” values. Although we have invested a relatively large effort in the user-friendliness of TALYS, we have not taken such safety measures to the extreme limit and ask at least some minimal responsibility from the user. Once you have accepted that, only very little effort is required to work with the code. Successful execution of TALYS can be expected if you remember the following simple rules and possibilities of the input file:

1. One input line contains one keyword. Usually it is accompanied by only one value, as in the simple example given above, but some keywords for model parameters need to be accompanied by indices (usually  $Z$  and  $A$ ) on the same line.
2. A keyword and its value(s) *must* be separated by at least 1 blank character.
3. The keywords can be given in arbitrary order. If, by mistake, you use the same keyword more than once, the value of the last one will be adopted. This does not hold for keywords which are labeled with different  $Z$  and  $A$  indices, see the beginning of Section 6.2.
4. All characters can be given in either lowercase or uppercase.
5. A keyword *must* be accompanied by a value. (There is one exception, the **rotational** keyword). To use default values, the keywords should simply be left out of the input file.
6. An input line starting with a  $\#$  in column 1 is neglected. This is helpful for including comments in the input file or to temporarily deactivate keywords.
7. A minimal input file always consists of 4 lines and contains the keywords **projectile**, **element**, **mass** and **energy**. These 4 keywords *must* be given in any input file.
8. An input line may not exceed 80 characters.

As an example of rules 2, 3, 4 and 6, it can be seen that the following input file is completely equivalent to the one given in the beginning of this Chapter:

```
# Equivalent input file
energy          14.
projectile n
mass 27
Element AL
#outbasic y
```

In the following erroneous input file, only the first 2 lines are correct, while rules 2 and 5 are violated in the other lines.

```

projectile n
element al
mass27
energy

```

In cases like this, the execution will be stopped and TALYS will give an appropriate error message for the first encountered problem. We like to believe that we have covered all such cases and that it is impossible to let TALYS crash (at least with our compilers, see also Chapter 7), but you are of course invited to prove and let us know about the contrary (Sorry, no cash rewards). Typing errors in the input file will be spotted by TALYS, e.g. if you write **projjectile n**, it will tell you the keyword is not in our list.

## 6.2 Keywords

The four-line input file given above was an example of a minimum input file for TALYS. In general, you probably want to be more specific, as in the following example:

```

projectile  n
element     nb
mass       93
energy     1.
ltarget    1
relativistic n
widthmode  2
outinverse y
a 41 93 13.115
a 41 94 13.421

```

which will simulate the reaction of a 1 MeV neutron incident on  $^{93}\text{Nb}$ , with the target in its first excited state (**Ltarget 1**, a 16-year isomer), using non-relativistic kinematics, the HRTW-model for width fluctuation corrections (**widthmode 2**) in the compound nucleus calculation, with the particle transmission coefficients and inverse reaction cross sections written on the output file (**outinverse y**) and with user-defined level density parameters **a** for  $^{93}\text{Nb}$  and  $^{94}\text{Nb}$ .

In this Section, we will explain all the possible keywords. We have classified them according to their meaning and importance. For each keyword, we give an explanation, a few examples, the default value, and the theoretically allowed numerical range. As the input file above shows, there is usually one value per keyword. Often, however, in cases where several residual nuclides are involved, nuclear model parameters differ from nuclide to nuclide. Then, the particular nuclide under consideration must also be given in the input line. In general, for these model parameters, we read keyword,  $Z$ ,  $A$ , a physical value and sometimes a possible further index (e.g. the fission barrier, index for the giant resonance, etc.), all separated by blanks. As the example above shows for the level density parameter  $a$ , the same keyword can appear more than once in an input file, to cover several different nuclides. Again, remember that all such keywords, if you don't specify them, have a default value from either the nuclear structure and model parameter database or from systematics. The usual reason to change them is to fit experimental

data, to use new information that is not yet in the TALYS database, or simply because the user may not agree with our default values. A final important point to note is that some keywords induce defaults for other keywords. This may seem confusing, but in practice this is not so. As an example, for a  $^{56}\text{Fe}$  target the **fission** keyword is automatically disabled whereas for  $^{232}\text{Th}$  it is by default enabled. Hence, the default value of the **fission** keyword is mass dependent. In the input description that follows, you will find a few similar cases. Anyway, you can always find all adopted default values for all parameters at the top of the *output* file, see which values have been set by the user or by default, and overrule them in a new input file.

### 6.2.1 Four main keywords

As explained above there are 4 basic keywords that form the highest level of input. They determine the fundamental parameters for any nuclear reaction induced by a light particle.

#### projectile

Eight different symbols can be given as **projectile**, namely **n**, **p**, **d**, **t**, **h**, **a**, **g** representing neutron, proton, deuteron, triton,  $^3\text{He}$ , alpha and gamma, respectively, and **0**, which is used if instead of a nuclear reaction (projectile + target) we start with an initial population of an excited nucleus.

*Examples:*

**projectile n**

**projectile d**

*Range:* **projectile** must be equal to **n**, **p**, **d**, **t**, **h**, **a**, **g** or **0**.

*Default:* None.

#### element

Either the nuclear symbol or the charge number  $Z$  of the target nucleus can be given. Possible values for **element** range from Li (3) to C4 (124). To accommodate target nuclides with  $Z > 110$  the element names are defined as follows: Rg(111), Cn(112), Fl(114) and Lv(116), B3(113), B5(115), B7-9(117-119), C0-4(120-124). Obviously the symbols, for  $Z=113,115$  and above 116 will be changed when official names are assigned to them.

*Examples:*

**element pu**

**element 41**

**element V**

**element B3**

*Range:*  $3 \leq \text{element} \leq 124$  or  $\text{Li} \leq \text{element} \leq \text{C4}$ .

*Default:* None.

### mass

The target mass number  $A$ . The case of a natural element can be specified by **mass 0**. Then, a TALYS calculation for each naturally occurring isotope will be performed (see also the **abundance** keyword, p. 173), after which the results will be properly weighted and summed.

*Examples:*

**mass 239**

**mass 0**

*Range:* **mass 0** or  $5 < \text{mass} \leq 339$ . The extra condition is that the target nucleus, i.e. the combination of **mass** and **element** must be present in the mass database, which corresponds to all nuclei between the proton and neutron drip lines.

*Default:* None.

### energy

The incident energy in MeV. The user has four possibilities: (1) A single incident energy is specified in the input as a real number, (2) A filename is specified, where the corresponding file contains a series of incident energies, with one incident energy per line. Any name can be given to this file, provided it starts with a character, and it is present in your working directory. Option (2) is helpful for the calculation of excitation functions or for the creation of nuclear data libraries. Option (2) is mandatory if **projectile 0**, i.e., if instead of a nuclear reaction we start with a population of an excited nucleus (see the **Special cases** below). Since TALYS-1.6, there are an additional 2 options which allows to use a whole range of incident energies without having to make a file for this: (3) A filename that is predefined by TALYS. This contains a hardwired energy grids with for example for neutrons a finer energy grid at low energies and a progressively wider grid at high energies. These have the form  $pE-E.grid$  where  $p$  is the name of the projectile, and the two  $E$ 's are the start and end energy in integer form respectively. The *.grid* specifies that this concerns a predefined energy grid. An often used example is *n0-200.grid* which is the neutron energy grid of the TENDL library. More energies are used in the eV and keV range while at high energies automatically a course grid is used. With the file *n0-20.grid* exactly the same incident energy grid is used, but only up to the final energy of 20 MeV. Finally, option (4) is to give after the *energy* keyword 3 numbers: the starting energy, the end energy and the energy step. Next, an equidistant grid is made based on these 3 numbers.

*Examples:*

**energy 140.**

**energy 0.002**



**energy range**

**energy n0-30.grid**

**energy p10-100.grid**

**energy 0.5 20. 0.5** (Incident energies: 0.5, 1, 1.5, ...20 MeV)

*Range:*  $10^{-11}$  MeV  $\leq$  **energy** < 1000 MeV or a *filename*, whereby the corresponding file contains at least 1 and a maximum of **numenin** incident energies, where **numenin** is an array dimension specified in *talys.cmb*. Currently **numenin=500**.

*Default:* None.

### Using the four main keywords

To summarize the use of the four basic keywords, consider the following input file

```
projectile n
element   pd
mass      110
energy range
```

The file *range* looks e.g. as follows

```
0.1
0.2
0.5
1.
1.5
2.
5.
8.
10.
15.
20.
```

In the source code, the number of incident energies, here 11, is known as **numinc**. For the four-line input given above, TALYS will simulate all open reaction channels for  $n + {}^{110}\text{Pd}$  for all incident energies given in the file *range*, using defaults for all models and parameters. The most important cross sections will automatically be written to the output file, see Chapter 7.

### Special cases

There are two examples for which the **energy** keyword does not represent the incident energy of the projectile.

Edwards Lab Source List as of Aug. 2016, T. Massey

All\_Sources

Gamma  
Alpha  
Electron (beta)  
Neutron  
Fission Foils

Source #	Isotope	Half-life	Date Purchased	Half Life	Int. Act. $\mu$ Ci	Comments
0	Co-57	271.8 d	3/31/1984	271.8 d	8,000	On loan from Ranger Scientific. Lead cylinder w/3 screws on bottom plate 2 1/4" diam., 2 1/4" ht.
1	Ra-226	1,622 y		1,622 y	10	1/2" thick, 2" diam. disk. Ra-A Plastic disc with metal rim.
2	Ra-226	1,622 y		1,622 y	5	Plastic disc with metal rim. Ra-B
3	Ra-226	1,622 y		1,622 y	120	Glass jar with black lid. 1/2" silvery cylinder mylar on source is cracked. Ra-C
4	Ra-226	1,622 y		1,622 y	5	Plastic. 1 1/2" disk wrapped in scotch tape. Ra-D
10	Cs-137	30.17 y	6/9/1958	30.17 y	60	In lead pig 2" x 2". F
18	Cs-137	30.17 y	6/8/1971	30.17 y	23,100	1/4" x 1/2" cylinder with big tag in 3" x 3" lead pig with leather handle.
24	Co-60	5.27 y	6/8/1955	5.27 y	1,200	Lead shield source in shield (rod) - pull out #312 Serial #Tracer Lab. Inc. B-312
26	Co-60	5.27 y	6/8/1965	5.27 y	1,250	W/O Rad tape. In 4" high cylindrical Pb pig.
27	Co-60	5.27 y	6/8/1964	5.27 y	320	W/Rad tape. In 4" high cylindrical Pb pig.
30	Na-22	2.605 y	6/8/1960	2.605 y	10	Looks like a radiation token. Small, flat paper like. Past 10 half-lives (dead)
33	Eu-154	8.59 y		8.59 y	4	2" x 2" lead cylinder with radiation tape. (7.8 y) B
43	Bi-207	32.2 y	6/8/1959	32.2 y	5	Brass metal cylinder 1" x 1", hole through middle. Label says Bi-209T.
44	Am-241	458 y	6/8/1964	458 y	0.083234	1/2" x 1/4" disc blue yellow plastic container. On back M1076 + .030 silver disc attached to small metal plate with screw.
52	PuBe	2.41E4 y	6/9/1964	2.41E4 y	1000000	(M712) Solid metal peg - 1" x 2".
53	PuBe	2.41E4 y	6/9/1964	2.41E4 y	1000000	# at bottom (M713) Short cylinder - 1" x 2".
54	PuBe	2.41E4 y	6/9/1964	2.41E4 y	1000000	Solid metal peg - 1" x 2". (M714)
55	PuBe	2.41E4 y	6/9/1964	2.41E4 y	1000000	Solid metal peg - 1" x 2". (M715)
56	PuBe	2.41E4 y	6/9/1964	2.41E4 y	1000000	Solid metal peg - 1" x 2". (M716)
57	PuBe	2.41E4 y	6/9/1964	2.41E4 y	5000000	Short cylinder. (M168)
58	U-235	7.04E8 y	6/9/1964	7.04E8 y	5	Silvery cylinder - 1 ft. long. ~ 2" diam.
60	Fe-55	2.73 y	6/9/1966	2.73 y	100	In plastic box. Serial #215794. Red disk silvery center 3/4" diam. 1/10" ht.
69	Am-241	458 y	6/9/1968	458 y	1.21	Isotope Products Lab. in plastic disc holder 1/2" x 1/4" - has #69 on top of container B on back.
70	Am-241 (#1085-1)	458 y	6/9/1968	458 y	9.85	Isotope Prod. Lab. plastic rod 5" long x 5/8" wide. Tip separated but still enclosed in plexiglass.
81.1	Cd-109	462 d	6/9/1970	30.17 y	4,500	Flat wooden box with 7 plastic rod/sources - 5" long. Orange top.
81.2	Ba-133	10.5 y	6/9/1972	462 d	57	Flat wooden box with 7 plastic rod/sources - 5" long. Black top.
81.3	Co-57	271.8 d	6/15/1972	10.5 y	57	Flat wooden box with 7 plastic rod/sources - 5" long. Red top.
81.4	Co-60	5.27 y	6/15/1972	271.8 d	57	Flat wooden box with 7 plastic rod/sources - 5" long. Blue top.
81.5	Mn-54	312.2 d	6/15/1972	5.27 y	57	Flat wooden box with 7 plastic rod/sources - 5" long. Brown top.
81.6	Na-22	2.605 y	6/15/1972	312.2 d	57	Flat wooden box with 7 plastic rod/sources - 5" long. Yellow
84	Th-228	1.913 y	6/15/1972	2.605 y	57	5" x 1/2" plastic rod. Ask Finlay and Rapaport about disposal. Am. Nucl. Products Springfield, MO Lot #867
89	Cm-244	18.11 y	10/14/1972	1.913 y	10	1" disc flat disc - Isotope Prod. Lab #37040 - blue rim. 9/1/78?
96	Th-228	1.913 y	6/9/1974	18.11 y	67	Doubly contained in plastic boxes. DIOS IPL - No Card
97	Cm-244	18.11 y	6/9/1975	1.913 y	0.1	#37055 Flat silvery disk with gold center. ~ 2" diam. July 8, 1980
101	Sr-90	29.1 y	6/9/1980	29.1 y	10,000	In plastic housing on side IPL; Sr-90 1/4" x 1/3" disc, 10 mCi - silver metallic disc. IPL F741
102	Eu-154 Eu-155	8.59 y 4.73 y	6/9/1981	8.59 y 4.73 y	5	Metal ring with brown spot in middle in plastic covering SRM 4275B 1 1/2" disc. All inside 3/4" diam. round case.
103	Co-57	271.8 d	6/9/1980	271.8 d	10,800	1/2" Thin foil in small plastic. S.N. 103-1439 - Lead container = 3" dia.
105	Pm-145	17.7 y	5/31/1966	17.7 y	1	Orange ring w/silvery center 3/4" in diam. NEN. Electron Capture.
106	Pb-210	22.3 y		22.3 y	<1	1.5" plastic ring 1" silvery ring, brown center. 202 scratched on back.
109	Co-60	5.27 y		5.27 y	>100	Clear plastic rod w/black end. Green dymo tape w/Co-60. 5" long.
110	Cs-137	30.17 y		30.17 y	>100	Silvery disk. 1/2" thick, 1" diam. blue & silver label. Nucleonic Corp. of Am.
111	Ra-226	1,622 y	2/16/1985	1,622 y	0.1366	1/2" diam. 1/4" in ht. Isotope Products Lab. K-903 0.1 $\mu$ Ci

Traceable to NIST standard

Handwritten checkmarks and symbols on the right margin of the table.

All\_Sources

112	Ra-226	1,622 y	2/16/1985	1,622 y	0.977	1/2" diam. 1/4" in ht. Isotope Products Lab. K-904 1.0 uCi
113	Co-60	5.27 y		5.27 y	100	On a long rod. The end is broken off.
119	Sr-90	29.1 y	3/13/1973	29.1 y	25	Serial No. 29780. Source at the end of a pencil-like config. w/ a wire attached.
120	Sr-90	29.1 y		29.1 y	10	Serial No. 19763. Source at the end of a pencil-like config. w/ a wire attached.
121	Sr-90	29.1 y		29.1 y	25	Serial No. 19832.
122	Sr-90	29.1 y		29.1 y	25	Serial No. 19830.
123	Cs-137	30.17 y		30.17 y	10	Disk shaped source.
127	Cm-244	18.11 y		18.11 y	1	Tissue Eq. for West Tech. Ionization Chamber - Model 1/2" - LET Counter S. N. 1001. Purchased 20 yr. Ago.
128	Na-22	2.605 y	2/27/1991	2.605 y	8.77	IPL Ref. Date 3/1/95, Ser. #472-106-1. Clear with black tip - 5" long and width 9/8"
129	Pu-239	2.41E4 y	1/31/1991	2.41E4 y	1.83 µg nCi	114 On loan from NIST49K-001-4 [FFTF] Plastic cap stainless steel backing.
131	U-235	7.04E8 y	8/17/1991	7.04E8 y	10.4 mg nCi	22.5 On loan U-235 Fission chambers. Foils contained in "coffee cans." Foils in plexiglass cases with screws. J
132	U-235	7.04E8 y	8/17/1991	7.04E8 y	9.7 mg nCi	20.9 On loan U-235 Fission chambers P enrichment for foils J, P, S and T (U-235) is 93.0%
133	U-235	7.04E8 y	8/17/1991	7.04E8 y	10.2 mg nCi	22.3 On loan U-235 Fission chambers S
134	U-235	7.04E8 y	8/17/1991	7.04E8 y	11.7 mg nCi	25.3 On loan U-235 Fission chambers T
135	U-238	4.47E9 y	8/17/1991	4.47E9 y	12.0 mg nCi	4.32 On loan U-238 Fission chambers K natural uranium
136	U-238	4.47E9 y	8/17/1991	4.47E9 y	11.1 mg nCi	3.73 On loan U-238 Fission chambers L natural uranium
137	U-238	4.47E9 y	8/17/1991	4.47E9 y	7.4 mg nCi	2.49 On loan U-238 Fission chambers M natural uranium
138	U-238	4.47E9 y	8/17/1991	4.47E9 y	13.0 mg nCi	4.37 On loan U-238 Fission chambers O natural uranium
139	U-238	4.47E9 y	12/20/1991	4.47E9 y	1.18 mg 0.39 nCi	On loan U-238 Fission chambers -210 enrichment is slightly above natural uranium (U-238) at 2.34 %
140	U-235	7.04E8 y	12/20/1991	7.04E8 y	364 µg 0.78 nCi	On loan U-235 Fission chambers -5-4 enrichment is 98.49%
141	Be-10	1.6E6 y	9/8/1992	1.6E6 y	0.5	
148	Np-237	2.14E6 a	9/13/1996	2.14E6 a	0.358mg 264 nCi	ID #77; Fission Foils
149	Np-237	2.14E6 a	9/13/1996	2.14E6 a	0.262 mg 193 nCi	ID #78; Fission Foils
150	Np-237	2.14E6 a	9/13/1996	2.14E6 a	0.633 mg 466 nCi	ID #80; Fission Foils
151	U-238/U-235	4.47E9 a	9/12/1996	4.47E9 a	0.005 mg 1.7 pCi	ID #5; U-235 fissile excepted 3.54 E -4 uCi; 0.161 mg; Fission Foils
152	U-236/U-235	2.342E7 a	9/12/1996	2.342E7 a	0.384 mg 0.025	ID #34; U-235 fissile excepted 3.54 E -4 uCi; 0.161 mg; Fission Foils
153	U-233	1.592E5 a	9/18/1996	1.592E5 a	0.189 mg 1.81	ID #10; Fission Foils
154	U-233	1.592E5 a	9/18/1996	1.592E5 a	0.259 mg 2.53	ID #11; Fission Foils
155	U-233	1.592E5 a	9/18/1996	1.592E5 a	0.299 mg 2.89	ID #12; Fission Foils
156	Ra-226	1,622 y	10/25/1996	1,622 y	1.205	AF-226 type A-1 plated disc
	Pu-239	2.41E4y		2.41E4y		
	Am-241	458y		458y		
161	Cm-244	18.1y	Spring 03	18.1y	0.01	Trinucleide 3/4" square plastic box
162	Co-60	5.271 y	Spring 03	5.271 y	0.1	3/4" square plastic box
163	Cs-137	30.07 y	Spring 03	30.07 y	0.1	3/4" square plastic box
164	Eu-152	13.54 y	Spring 03	13.54 y	0.1	3/4" square plastic box
165	Ba-133	10.5 y	4/30/1999	10.5 y	0.1	3/4" square plastic box
168	Ra-226	1,622 y	8/31/2002	1,622 y	0.08827	Electroplated, 5 mm disk, IPL Ref. Date 9/1/96; source no. 1198-84
169	U-235	7.04E8 y	2/12/2004	7.04E8 y	170.9 mg 0.376	NIST U-235 Fission foils
172	Cf-252	2.64 y	1/10/2006	2.64 y	49.9µCi	
173	U-235/U-238	4.47E9 y		4.47E9 y		LANL fission chamber

of 10  
 2003  
 2004  
 2005  
 2006  
 2007  
 2008  
 2009  
 2010  
 2011  
 2012  
 2013  
 2014  
 2015  
 2016  
 2017  
 2018  
 2019  
 2020  
 2021  
 2022  
 2023  
 2024  
 2025  
 2026  
 2027  
 2028  
 2029  
 2030  
 2031  
 2032  
 2033  
 2034  
 2035  
 2036  
 2037  
 2038  
 2039  
 2040  
 2041  
 2042  
 2043  
 2044  
 2045  
 2046  
 2047  
 2048  
 2049  
 2050  
 2051  
 2052  
 2053  
 2054  
 2055  
 2056  
 2057  
 2058  
 2059  
 2060  
 2061  
 2062  
 2063  
 2064  
 2065  
 2066  
 2067  
 2068  
 2069  
 2070  
 2071  
 2072  
 2073  
 2074  
 2075  
 2076  
 2077  
 2078  
 2079  
 2080  
 2081  
 2082  
 2083  
 2084  
 2085  
 2086  
 2087  
 2088  
 2089  
 2090  
 2091  
 2092  
 2093  
 2094  
 2095  
 2096  
 2097  
 2098  
 2099  
 2100  
 2101  
 2102  
 2103  
 2104  
 2105  
 2106  
 2107  
 2108  
 2109  
 2110  
 2111  
 2112  
 2113  
 2114  
 2115  
 2116  
 2117  
 2118  
 2119  
 2120  
 2121  
 2122  
 2123  
 2124  
 2125  
 2126  
 2127  
 2128  
 2129  
 2130  
 2131  
 2132  
 2133  
 2134  
 2135  
 2136  
 2137  
 2138  
 2139  
 2140  
 2141  
 2142  
 2143  
 2144  
 2145  
 2146  
 2147  
 2148  
 2149  
 2150  
 2151  
 2152  
 2153  
 2154  
 2155  
 2156  
 2157  
 2158  
 2159  
 2160  
 2161  
 2162  
 2163  
 2164  
 2165  
 2166  
 2167  
 2168  
 2169  
 2170  
 2171  
 2172  
 2173  
 2174  
 2175  
 2176  
 2177  
 2178  
 2179  
 2180  
 2181  
 2182  
 2183  
 2184  
 2185  
 2186  
 2187  
 2188  
 2189  
 2190  
 2191  
 2192  
 2193  
 2194  
 2195  
 2196  
 2197  
 2198  
 2199  
 2200  
 2201  
 2202  
 2203  
 2204  
 2205  
 2206  
 2207  
 2208  
 2209  
 2210  
 2211  
 2212  
 2213  
 2214  
 2215  
 2216  
 2217  
 2218  
 2219  
 2220  
 2221  
 2222  
 2223  
 2224  
 2225  
 2226  
 2227  
 2228  
 2229  
 2230  
 2231  
 2232  
 2233  
 2234  
 2235  
 2236  
 2237  
 2238  
 2239  
 2240  
 2241  
 2242  
 2243  
 2244  
 2245  
 2246  
 2247  
 2248  
 2249  
 2250  
 2251  
 2252  
 2253  
 2254  
 2255  
 2256  
 2257  
 2258  
 2259  
 2260  
 2261  
 2262  
 2263  
 2264  
 2265  
 2266  
 2267  
 2268  
 2269  
 2270  
 2271  
 2272  
 2273  
 2274  
 2275  
 2276  
 2277  
 2278  
 2279  
 2280  
 2281  
 2282  
 2283  
 2284  
 2285  
 2286  
 2287  
 2288  
 2289  
 2290  
 2291  
 2292  
 2293  
 2294  
 2295  
 2296  
 2297  
 2298  
 2299  
 2300  
 2301  
 2302  
 2303  
 2304  
 2305  
 2306  
 2307  
 2308  
 2309  
 2310  
 2311  
 2312  
 2313  
 2314  
 2315  
 2316  
 2317  
 2318  
 2319  
 2320  
 2321  
 2322  
 2323  
 2324  
 2325  
 2326  
 2327  
 2328  
 2329  
 2330  
 2331  
 2332  
 2333  
 2334  
 2335  
 2336  
 2337  
 2338  
 2339  
 2340  
 2341  
 2342  
 2343  
 2344  
 2345  
 2346  
 2347  
 2348  
 2349  
 2350  
 2351  
 2352  
 2353  
 2354  
 2355  
 2356  
 2357  
 2358  
 2359  
 2360  
 2361  
 2362  
 2363  
 2364  
 2365  
 2366  
 2367  
 2368  
 2369  
 2370  
 2371  
 2372  
 2373  
 2374  
 2375  
 2376  
 2377  
 2378  
 2379  
 2380  
 2381  
 2382  
 2383  
 2384  
 2385  
 2386  
 2387  
 2388  
 2389  
 2390  
 2391  
 2392  
 2393  
 2394  
 2395  
 2396  
 2397  
 2398  
 2399  
 2400  
 2401  
 2402  
 2403  
 2404  
 2405  
 2406  
 2407  
 2408  
 2409  
 2410  
 2411  
 2412  
 2413  
 2414  
 2415  
 2416  
 2417  
 2418  
 2419  
 2420  
 2421  
 2422  
 2423  
 2424  
 2425  
 2426  
 2427  
 2428  
 2429  
 2430  
 2431  
 2432  
 2433  
 2434  
 2435  
 2436  
 2437  
 2438  
 2439  
 2440  
 2441  
 2442  
 2443  
 2444  
 2445  
 2446  
 2447  
 2448  
 2449  
 2450  
 2451  
 2452  
 2453  
 2454  
 2455  
 2456  
 2457  
 2458  
 2459  
 2460  
 2461  
 2462  
 2463  
 2464  
 2465  
 2466  
 2467  
 2468  
 2469  
 2470  
 2471  
 2472  
 2473  
 2474  
 2475  
 2476  
 2477  
 2478  
 2479  
 2480  
 2481  
 2482  
 2483  
 2484  
 2485  
 2486  
 2487  
 2488  
 2489  
 2490  
 2491  
 2492  
 2493  
 2494  
 2495  
 2496  
 2497  
 2498  
 2499  
 2500  
 2501  
 2502  
 2503  
 2504  
 2505  
 2506  
 2507  
 2508  
 2509  
 2510  
 2511  
 2512  
 2513  
 2514  
 2515  
 2516  
 2517  
 2518  
 2519  
 2520  
 2521  
 2522  
 2523  
 2524  
 2525  
 2526  
 2527  
 2528  
 2529  
 2530  
 2531  
 2532  
 2533  
 2534  
 2535  
 2536  
 2537  
 2538  
 2539  
 2540  
 2541  
 2542  
 2543  
 2544  
 2545  
 2546  
 2547  
 2548  
 2549  
 2550  
 2551  
 2552  
 2553  
 2554  
 2555  
 2556  
 2557  
 2558  
 2559  
 2560  
 2561  
 2562  
 2563  
 2564  
 2565  
 2566  
 2567  
 2568  
 2569  
 2570  
 2571  
 2572  
 2573  
 2574  
 2575  
 2576  
 2577  
 2578  
 2579  
 2580  
 2581  
 2582  
 2583  
 2584  
 2585  
 2586  
 2587  
 2588  
 2589  
 2590  
 2591  
 2592  
 2593  
 2594  
 2595  
 2596  
 2597  
 2598  
 2599  
 2600  
 2601  
 2602  
 2603  
 2604  
 2605  
 2606  
 2607  
 2608  
 2609  
 2610  
 2611  
 2612  
 2613  
 2614  
 2615  
 2616  
 2617  
 2618  
 2619  
 2620  
 2621  
 2622  
 2623  
 2624  
 2625  
 2626  
 2627  
 2628  
 2629  
 2630  
 2631  
 2632  
 2633  
 2634  
 2635  
 2636  
 2637  
 2638  
 2639  
 2640  
 2641  
 2642  
 2643  
 2644  
 2645  
 2646  
 2647  
 2648  
 2649  
 2650  
 2651  
 2652  
 2653  
 2654  
 2655  
 2656  
 2657  
 2658  
 2659  
 2660  
 2661  
 2662  
 2663  
 2664  
 2665  
 2666  
 2667  
 2668  
 2669  
 2670  
 2671  
 2672  
 2673  
 2674  
 2675  
 2676  
 2677  
 2678  
 2679  
 2680  
 2681  
 2682  
 2683  
 2684  
 2685  
 2686  
 2687  
 2688  
 2689  
 2690  
 2691  
 2692  
 2693  
 2694  
 2695  
 2696  
 2697  
 2698  
 2699  
 2700  
 2701  
 2702  
 2703  
 2704  
 2705  
 2706  
 2707  
 2708  
 2709  
 2710  
 2711  
 2712  
 2713  
 2714  
 2715  
 2716  
 2717  
 2718  
 2719  
 2720  
 2721  
 2722  
 2723  
 2724  
 2725  
 2726  
 2727  
 2728  
 2729  
 2730  
 2731  
 2732  
 2733  
 2734  
 2735  
 2736  
 2737  
 2738  
 2739  
 2740  
 2741  
 2742  
 2743  
 2744  
 2745  
 2746  
 2747  
 2748  
 2749  
 2750  
 2751  
 2752  
 2753  
 2754  
 2755  
 2756  
 2757  
 2758  
 2759  
 2760  
 2761  
 2762  
 2763  
 2764  
 2765  
 2766  
 2767  
 2768  
 2769  
 2770  
 2771  
 2772  
 2773  
 2774  
 2775  
 2776  
 2777  
 2778  
 2779  
 2780  
 2781  
 2782  
 2783  
 2784  
 2785  
 2786  
 2787  
 2788  
 2789  
 2790  
 2791  
 2792  
 2793  
 2794  
 2795  
 2796  
 2797  
 2798  
 2799  
 2800  
 2801  
 2802  
 2803  
 2804  
 2805  
 2806  
 2807  
 2808  
 2809  
 2810  
 2811  
 2812  
 2813  
 2814  
 2815  
 2816  
 2817  
 2818  
 2819  
 2820  
 2821  
 2822  
 2823  
 2824  
 2825  
 2826  
 2827  
 2828  
 2829  
 2830  
 2831  
 2832  
 2833  
 2834  
 2835  
 2836  
 2837  
 2838  
 2839  
 2840  
 2841  
 2842  
 2843  
 2844  
 2845  
 2846  
 2847  
 2848  
 2849  
 2850  
 2851  
 2852  
 2853  
 2854  
 2855  
 2856  
 2857  
 2858  
 2859  
 2860  
 2861  
 2862  
 2863  
 2864  
 2865  
 2866  
 2867  
 2868  
 2869  
 2870  
 2871  
 2872  
 2873  
 2874  
 2875  
 2876  
 2877  
 2878  
 2879  
 2880  
 2881  
 2882  
 2883  
 2884  
 2885  
 2886  
 2887  
 2888  
 2889  
 2890  
 2891  
 2892  
 2893  
 2894  
 2895  
 2896  
 2897  
 2898  
 2899  
 2900  
 2901  
 2902  
 2903  
 2904  
 2905  
 2906  
 2907  
 2908  
 2909  
 2910  
 2911

APPENDIX C. NUCLEAR SPECTROSCOPY STANDARDS

1. Gamma-ray Energy and Intensity Standards

Table 1 lists some  $\gamma$ -ray energy standards, from the evaluation of Helmer *et al.*<sup>1</sup>, and intensity standards, recommended by the IAEA Co-ordinated Research Programme<sup>2,3</sup> (CRP), for calibration of  $\gamma$ -ray measurements. Most of the isotopes given here have half-lives of more than 30 days, and many are commercially available. The  $\gamma$ -ray energies are based on the *gold standard*, the 411.80205 17 keV transition from <sup>198</sup>Au decay. Uncertainties are intended to represent one standard deviation, and include the 0.3 ppm uncertainty in the definition of the electron volt relative to wavelength. The  $\gamma$ -ray energies reported in Table 1 are from absolute wavelength or curved-crystal spectrometer measurements, which are tied directly to the *gold standard*, and from the measurements of small  $\gamma$ -ray energy differences using Ge detectors. Energies that are rounded to the nearest 0.1-keV and tabulated without uncertainty are not recommended values; however, they have been included because these transitions are useful intensity calibration standards. Other, apparently precise, transition energies and intensities have been tabulated in the *Table of Isotopes*, but the reader should use these values with great caution because of unknown systematic uncertainties which may not have been included. Columns 1 and 2 show the isotope names and half-lives from the *Table of Isotopes*, respectively. Columns 3 and 4 list the  $\gamma$ -ray energies and intensities with their corresponding uncertainties (in italics) in the least significant digit(s).

<sup>1</sup> R.G. Helmer and C. van der Leun, private communication, draft of a paper to be submitted to *Nucl. Instr. Meth.*, 1999.

<sup>2</sup> *X-ray and Gamma-ray Standards for Detector Calibration*, report by the Co-ordinated Research IAEA Programme, IAEA-TECDOC-619 (1991).

<sup>3</sup> R. Vaninbrouckx, *Emission Probabilities of Selected Gamma Rays for Radionuclides Used as Detector-Calibration Standards*, report presented at the Advisory Group Meeting of the International Atomic Energy Agency (IAEA), Vienna (1985).

Table 1. Gamma-ray Energies and Absolute Intensities for Some Standard Sources

Source	Half-life	$E_{\gamma}$ (keV) #	$I_{\gamma}$ (%) &	Source	Half-life	$E_{\gamma}$ (keV) #	$I_{\gamma}$ (%) &
<sup>7</sup> Be	53.12 d	477.6035 <sup>20</sup>	10.45 <sup>10</sup> †	<sup>59</sup> Fe	44.503 d	142.651 <sup>2</sup>	
<sup>22</sup> Na	2.6019 y	1274.537 <sup>7</sup>	99.935 <sup>15</sup>			192.349 <sup>5</sup>	
<sup>24</sup> Na	14.9590 h	1368.625 <sup>5</sup>	99.9936 <sup>15</sup>			1099.245 <sup>3</sup>	
		2754.008 <sup>11</sup>	99.855 <sup>5</sup>			1291.590 <sup>6</sup>	
<sup>35</sup> Cl(n, $\gamma$ )		517.1	0.227 <sup>20</sup>	<sup>56</sup> Co	77.27 d	846.7638 <sup>19</sup>	99.933 <sup>7</sup>
		786.3	0.096 <sup>9</sup>			1037.8333 <sup>24</sup>	14.13 <sup>5</sup>
		788.4	0.150 <sup>12</sup>			1175.0878 <sup>22</sup>	2.239 <sup>11</sup>
		1164.9	0.257 <sup>22</sup>			1238.2736 <sup>22</sup>	66.07 <sup>19</sup>
		1600.8	0.034 <sup>3</sup>			1360.196 <sup>4</sup>	4.256 <sup>15</sup>
		1951.1	0.187 <sup>15</sup>			1771.327 <sup>3</sup>	15.49 <sup>5</sup>
		1959.3	0.121 <sup>10</sup>			2015.176 <sup>5</sup>	3.029 <sup>13</sup>
		2863.9	0.060 <sup>5</sup>			2034.752 <sup>5</sup>	7.771 <sup>27</sup>
		3061.7	0.035 <sup>3</sup>			2113.092 <sup>6</sup>	0.366 <sup>6</sup>
		5715.2	0.051 <sup>4</sup>			2212.898 <sup>3</sup>	0.390 <sup>7</sup>
		6110.8	0.197 <sup>16</sup>			2598.438 <sup>4</sup>	16.96 <sup>6</sup>
		6619.4	0.081 <sup>7</sup>			3009.559 <sup>4</sup>	0.995 <sup>21</sup>
		6627.5	0.046 <sup>4</sup>			3201.930 <sup>11</sup>	3.13 <sup>9</sup>
		6977.6	0.0223 <sup>20</sup>			3253.402 <sup>5</sup>	7.62 <sup>24</sup>
		7413.7	0.100 <sup>8</sup>			3272.978 <sup>5</sup>	1.78 <sup>6</sup>
		7790.0	0.086 <sup>7</sup>			3451.119 <sup>4</sup>	0.93 <sup>4</sup>
		8576.2	0.0294 <sup>24</sup>			3548.3	0.178 <sup>9</sup>
<sup>46</sup> Sc	83.79 d	889.271 <sup>2</sup>	99.9844 <sup>16</sup>	<sup>57</sup> Co	271.79 d	14.4130 <sup>4</sup>	9.16 <sup>15</sup>
		1120.537 <sup>3</sup>	99.9874 <sup>11</sup>			122.06065 <sup>12</sup>	85.60 <sup>17</sup>
<sup>44</sup> Ti	63 y	67.8688 <sup>17</sup>				136.47356 <sup>29</sup>	10.68 <sup>8</sup>
		78.3236 <sup>17</sup>		<sup>58</sup> Co	70.86 d	810.7593 <sup>20</sup>	99.45 <sup>1</sup>
<sup>51</sup> Cr	27.7025 d	320.0824 <sup>4</sup>	9.86 <sup>5</sup>			863.951 <sup>6</sup>	0.69 <sup>3</sup>
<sup>54</sup> Mn	312.3 d	834.838 <sup>5</sup>	99.9758 <sup>24</sup>			1674.725 <sup>7</sup>	0.519 <sup>10</sup>
<sup>56</sup> Mn	2.5785 h	846.8	98.87 <sup>3</sup> †	<sup>60</sup> Co	5.2714 y	1173.228 <sup>3</sup>	99.857 <sup>22</sup>
		1810.7	27.2 <sup>8</sup> †			1332.492 <sup>4</sup>	99.983 <sup>6</sup>
		2113.0	14.3 <sup>4</sup> †	<sup>65</sup> Zn	244.26 d	1115.539 <sup>2</sup>	50.60 <sup>24</sup>

Table 1. Gamma-ray Energies and Absolute Intensities (continued)

Source	Half-life	$E_{\gamma}$ (keV) <sup>#</sup>	$I_{\gamma}$ (%) <sup>&amp;</sup>	Source	Half-life	$E_{\gamma}$ (keV) <sup>#</sup>	$I_{\gamma}$ (%) <sup>&amp;</sup>										
<sup>66</sup> Ga	9.49 h	833.5324 <sup>21</sup>	6.03 <sup>23</sup>	<sup>108m</sup> Ag	418 y	433.937 <sup>4</sup>											
		1039.220 <sup>3</sup>	37.9 <sup>12</sup>			614.276 <sup>4</sup>											
		1333.112 <sup>5</sup>	1.23 <sup>5</sup>			722.907 <sup>10</sup>											
		1418.754 <sup>5</sup>				<sup>110m</sup> Ag	249.79 d	446.812 <sup>3</sup>	3.72 <sup>3†</sup>								
		1508.158 <sup>7</sup>						620.3553 <sup>17</sup>									
		1918.329 <sup>5</sup>	2.14 <sup>8</sup>					657.7600 <sup>11</sup>	94.4 <sup>1†</sup>								
		2189.616 <sup>6</sup>	5.71 <sup>21</sup>					677.6217 <sup>12</sup>	10.40 <sup>8†</sup>								
		2422.525 <sup>7</sup>	1.96 <sup>7</sup>					687.0091 <sup>18</sup>	6.44 <sup>3†</sup>								
		2751.835 <sup>5</sup>	23.2 <sup>11</sup>					706.6760 <sup>15</sup>	16.6 <sup>1†</sup>								
		3228.800 <sup>6</sup>	1.48 <sup>12</sup>					744.2755 <sup>18</sup>	4.70 <sup>4†</sup>								
		3380.850 <sup>6</sup>	1.40 <sup>12</sup>					763.9424 <sup>17</sup>	22.39 <sup>8†</sup>								
		3422.040 <sup>8</sup>						818.0244 <sup>18</sup>	7.32 <sup>4†</sup>								
		3791.009 <sup>6</sup>	1.02 <sup>11</sup>					884.6781 <sup>13</sup>	72.7 <sup>3†</sup>								
		4085.853 <sup>9</sup>	1.14 <sup>19</sup>					937.485 <sup>3</sup>	34.31 <sup>12†</sup>								
		4295.7	3.5 <sup>7</sup>					1384.2931 <sup>20</sup>	24.25 <sup>8†</sup>								
4461.202 <sup>9</sup>		1475.7792 <sup>23</sup>	3.99 <sup>2†</sup>														
4806.007 <sup>10</sup>	1.5 <sup>4</sup>	1505.0280 <sup>20</sup>	13.04 <sup>4†</sup>														
1562.2940 <sup>18</sup>																	
<sup>75</sup> Se	119.779 d	66.0518 <sup>8</sup>	1.10 <sup>2</sup>	<sup>109</sup> Cd	462.6 d	88.03360 <sup>10</sup>	3.63 <sup>2</sup>										
		96.7340 <sup>9</sup>	3.41 <sup>4</sup>			<sup>111</sup> In	2.8047 d	171.3	90.78 <sup>10</sup>								
		121.1155 <sup>11</sup>	17.1 <sup>1</sup>	245.4	94.16 <sup>3</sup>												
		136.0001 <sup>6</sup>	58.8 <sup>3</sup>	<sup>115m</sup> In	4.486 h			336.2	45.9 <sup>2†</sup>								
		198.6060 <sup>12</sup>	1.49 <sup>1</sup>					<sup>113</sup> Sn	115.09 d	391.698 <sup>3</sup>	64.89 <sup>13</sup>						
		264.6576 <sup>9</sup>	59.0 <sup>2</sup>							<sup>125</sup> Sn	9.64 d	1806.690 <sup>16</sup>					
		279.5422 <sup>10</sup>	25.0 <sup>1</sup>									1889.884 <sup>16</sup>					
		303.9236 <sup>10</sup>	1.31 <sup>1</sup>									2002.134 <sup>12</sup>					
		400.6572 <sup>6</sup>	11.5 <sup>1</sup>									2201.002 <sup>12</sup>					
		<sup>82</sup> Br	35.30 h									221.4788 <sup>18</sup>		2275.748 <sup>10</sup>		<sup>124</sup> Sb	60.20 d
554.346 <sup>3</sup>														645.8520 <sup>19</sup>	7.3 <sup>1†</sup>		
619.104 <sup>3</sup>												713.776 <sup>4</sup>					
698.368 <sup>3</sup>												722.782 <sup>3</sup>	11.3 <sup>2†</sup>				
776.513 <sup>4</sup>						790.706 <sup>7</sup>											
827.820 <sup>5</sup>						968.195 <sup>4</sup>											
1043.993 <sup>5</sup>						1045.125 <sup>4</sup>											
1317.466 <sup>4</sup>						1325.504 <sup>4</sup>											
1474.874 <sup>5</sup>						1368.157 <sup>5</sup>											
1650.328 <sup>5</sup>						1436.554 <sup>7</sup>											
<sup>84</sup> Rb	32.77 d			881.6041 <sup>16</sup>		1690.971 <sup>4</sup>	48.5 <sup>3†</sup>	<sup>125</sup> Sb	2.7582 y	176.314 <sup>2</sup>	6.85 <sup>7</sup>						
				1016.158 <sup>11</sup>		2090.930 <sup>7</sup>	5.66 <sup>9†</sup>										
				1897.751 <sup>11</sup>		380.5	1.518 <sup>16</sup>										
<sup>85</sup> Sr	64.84 d			514.0048 <sup>22</sup>	98.4 <sup>4</sup>	427.874 <sup>4</sup>	29.7 <sup>3</sup>			<sup>125</sup> I	59.408 d	35.5	6.58 <sup>8</sup>				
				898.036 <sup>4</sup>	94.0 <sup>3</sup>	463.365 <sup>4</sup>	10.48 <sup>11</sup>										
<sup>88</sup> Y	106.65 d	1836.052 <sup>13</sup>	99.36 <sup>3</sup>	600.597 <sup>2</sup>	17.73 <sup>18</sup>	<sup>132</sup> Cs	6.479 d					667.714 <sup>2</sup>					
		724.193 <sup>3</sup>	44.15 <sup>20†</sup>	606.713 <sup>3</sup>	5.00 <sup>5</sup>												
<sup>95</sup> Zr	64.02 d	756.7	54.50 <sup>25†</sup>	635.950 <sup>3</sup>	11.21 <sup>12</sup>							1317.918 <sup>6</sup>					
		702.639 <sup>4</sup>	99.79 <sup>5</sup>	671.441 <sup>6</sup>	1.80 <sup>2</sup>												
<sup>94</sup> Nb	2.03×10 <sup>4</sup> y	871.114 <sup>3</sup>	99.86 <sup>5</sup>	1985.625 <sup>6</sup>													
		765.803 <sup>6</sup>	99.81 <sup>3</sup>														
<sup>95</sup> Nb	34.975 d	765.803 <sup>6</sup>	99.81 <sup>3</sup>														
		<sup>99</sup> Mo	65.94 h	40.58323 <sup>17</sup>													
				140.511 <sup>1</sup>													
				204.1161 <sup>17</sup>													
				582.0775 <sup>21</sup>													
786.1922 <sup>27</sup>																	
<sup>95m</sup> Tc	61 d	820.622 <sup>7</sup>															
		835.146 <sup>6</sup>															
		1039.260 <sup>6</sup>															
		140.511 <sup>1</sup>	89.0 <sup>2†</sup>														
		511.8534 <sup>23</sup>															
<sup>99m</sup> Tc	6.01 h	140.511 <sup>1</sup>	89.0 <sup>2†</sup>														
		<sup>106</sup> Ru	373.59 d	511.8534 <sup>23</sup>													

Table 1. Gamma-ray Energies and Absolute Intensities (continued)

Source	Half-life	$E_{\gamma}$ (keV) <sup>#</sup>	$I_{\gamma}$ (%) <sup>&amp;</sup>	Source	Half-life	$E_{\gamma}$ (keV) <sup>#</sup>	$I_{\gamma}$ (%) <sup>&amp;</sup>				
<sup>134</sup> Cs	2.0648 y	475.4	1.49 <sup>2</sup>	<sup>160</sup> Tb	72.3 d	86.7877 <sup>3</sup>					
		563.2	8.36 <sup>3</sup>			197.0341 <sup>10</sup>					
		569.3	15.39 <sup>6</sup>			215.6452 <sup>11</sup>					
		604.7	97.63 <sup>6</sup>			298.5783 <sup>17</sup>					
		795.8	85.4 <sup>3</sup>			879.378 <sup>2</sup>					
		801.9	8.69 <sup>3</sup>			962.311 <sup>3</sup>					
		1038.6	0.990 <sup>5</sup>			966.166 <sup>2</sup>					
		1168.0	1.792 <sup>7</sup>			1177.954 <sup>3</sup>					
<sup>137</sup> Cs	30.07 y	1365.2	3.016 <sup>11</sup>	1271.873 <sup>5</sup>							
		<sup>133</sup> Ba	10.51 y	661.657 <sup>3</sup>	85.1 <sup>2</sup>	<sup>161</sup> Tb	6.88 d	25.65135 <sup>3</sup>			
				53.1622 <sup>6</sup>				48.91533 <sup>5</sup>			
				79.6142 <sup>12</sup>				57.1917 <sup>3</sup>			
				80.9979 <sup>11</sup>	34.11 <sup>28</sup>			74.56669 <sup>6</sup>			
				160.6120 <sup>16</sup>				84.25474 <sup>8</sup>			
				223.2368 <sup>13</sup>				63.12044 <sup>4</sup>			
				276.3989 <sup>12</sup>	7.147 <sup>30</sup>			93.61447 <sup>8</sup>			
302.8508 <sup>5</sup>	18.30 <sup>6</sup>	109.77924 <sup>4</sup>									
<sup>139</sup> Ce	137.640 d	356.0129 <sup>7</sup>	61.94 <sup>14</sup>	118.18940 <sup>14</sup>							
		383.8485 <sup>12</sup>	8.905 <sup>29</sup>	130.52293 <sup>6</sup>							
		<sup>141</sup> Ce	32.501 d	165.857 <sup>3</sup>	79.87 <sup>6</sup>	177.21307 <sup>6</sup>					
				145.4433 <sup>14</sup>	48.6 <sup>4</sup> <sup>†</sup>	197.95675 <sup>7</sup>					
				<sup>144</sup> Ce	284.893 d	696.505 <sup>4</sup>		261.07712 <sup>9</sup>			
						1489.148 <sup>3</sup>		307.73586 <sup>10</sup>			
						2185.645 <sup>5</sup>		23.9330 <sup>2</sup>			
						<sup>152</sup> Eu	13.537 y	121.7817 <sup>3</sup>	28.37 <sup>13</sup>	78.7422 <sup>6</sup> <sup>†</sup>	
244.6974 <sup>8</sup>	7.53 <sup>4</sup>							81.7509 <sup>5</sup> <sup>†</sup>			
295.9387 <sup>17</sup>		90.6434 <sup>19</sup>									
344.2785 <sup>12</sup>	26.57 <sup>11</sup>	65.72215 <sup>15</sup>									
367.7891 <sup>20</sup>		67.74970 <sup>10</sup>									
411.1165 <sup>12</sup>	2.238 <sup>10</sup>	84.68024 <sup>26</sup>									
444.0	3.125 <sup>14</sup>	100.10595 <sup>7</sup>	14.23 <sup>25</sup> <sup>†</sup>								
778.9045 <sup>24</sup>	12.97 <sup>6</sup>	113.67170 <sup>22</sup>									
867.380 <sup>3</sup>	4.214 <sup>25</sup>	116.4179 <sup>6</sup>									
964.1	14.63 <sup>6</sup>	152.42991 <sup>26</sup>	7.02 <sup>8</sup> <sup>†</sup>								
1085.837 <sup>10</sup>	10.13 <sup>5</sup>	156.3864 <sup>3</sup>									
1089.737 <sup>5</sup>	1.731 <sup>9</sup>	179.39381 <sup>25</sup>									
1112.076 <sup>3</sup>	13.54 <sup>6</sup>	198.35187 <sup>29</sup>									
1212.948 <sup>11</sup>	1.412 <sup>8</sup>	222.1085 <sup>3</sup>	7.57 <sup>8</sup> <sup>†</sup>								
1299.142 <sup>8</sup>	1.626 <sup>11</sup>	229.3207 <sup>6</sup>									
1408.013 <sup>3</sup>	20.85 <sup>9</sup>	264.0740 <sup>3</sup>									
1457.643 <sup>11</sup>		1121.290 <sup>3</sup>	35.3 <sup>2</sup> <sup>†</sup>								
<sup>154</sup> Eu	8.593 y	123.0706 <sup>9</sup>	41.2 <sup>5</sup>	1157.302 <sup>3</sup>							
		247.9288 <sup>7</sup>	6.95 <sup>9</sup>	1189.040 <sup>3</sup>	16.42 <sup>10</sup> <sup>†</sup>						
		591.755 <sup>3</sup>	4.99 <sup>6</sup>	1221.395 <sup>3</sup>	27.20 <sup>22</sup> <sup>†</sup>						
		723.3014 <sup>22</sup>	20.2 <sup>2</sup>	1231.004 <sup>3</sup>	11.57 <sup>8</sup> <sup>†</sup>						
		756.8020 <sup>23</sup>	4.58 <sup>6</sup>	1257.407 <sup>3</sup>							
		873.1834 <sup>23</sup>	12.24 <sup>15</sup>	1273.719 <sup>3</sup>							
		996.3	10.48 <sup>13</sup>	1289.145 <sup>3</sup>							
		1004.7	18.2 <sup>2</sup>	1373.824 <sup>3</sup>							
		1274.429 <sup>4</sup>	35.0 <sup>4</sup>	1387.390 <sup>3</sup>							
		1494.048 <sup>5</sup>	0.71 <sup>2</sup>	<sup>185</sup> Os	93.6 d	125.3581 <sup>9</sup>					
		1596.4804 <sup>29</sup>	1.81 <sup>2</sup>			162.852 <sup>3</sup>					
<sup>153</sup> Gd	240.4 d	69.67300 <sup>13</sup>		234.156 <sup>4</sup>							
		75.42213 <sup>23</sup>		592.0722 <sup>22</sup>							
		83.36717 <sup>21</sup>		646.127 <sup>4</sup>							
		89.48595 <sup>22</sup>		717.4298 <sup>24</sup>							
		97.43100 <sup>21</sup>		874.826 <sup>4</sup>							
		103.18012 <sup>17</sup>		880.2816 <sup>27</sup>							
		172.85307 <sup>19</sup>									

Table 1. Gamma-ray Energies and Absolute Intensities (continued)

Source	Half-life	$E_{\gamma}$ (keV) <sup>#</sup>	$I_{\gamma}$ (%) <sup>&amp;</sup>	Source	Half-life	$E_{\gamma}$ (keV) <sup>#</sup>	$I_{\gamma}$ (%) <sup>&amp;</sup>		
<sup>192</sup> Ir	73.831 d	136.34257 <sup>26</sup>		<sup>210</sup> Pb	22.3 y	46.539 <sup>1</sup>			
		205.79430 <sup>9</sup>		<sup>207</sup> Bi	31.55 y	569.698 <sup>2</sup>	97.74 <sup>3</sup>		
		295.95650 <sup>15</sup>	28.7 <sup>1†</sup>			1063.656 <sup>3</sup>	74.5 <sup>2</sup>		
		308.45507 <sup>17</sup>	29.8 <sup>1†</sup>			1770.228 <sup>9</sup>	6.87 <sup>4</sup>		
		316.50618 <sup>17</sup>	83.0 <sup>3†</sup>	<sup>228</sup> Th <sup>@</sup>	1.9131 y	84.4	1.22 <sup>2</sup>		
		416.4688 <sup>7</sup>				238.6	43.5 <sup>4</sup>		
		468.06885 <sup>26</sup>	47.7 <sup>2†</sup>			241.0	4.10 <sup>5</sup>		
		484.5751 <sup>4</sup>				277.4	2.30 <sup>3</sup>		
		588.5810 <sup>7</sup>	4.49 <sup>2†</sup>			300.1	3.25 <sup>3</sup>		
		604.41105 <sup>25</sup>	8.11 <sup>4†</sup>			510.8	8.18 <sup>10</sup>		
		612.46215 <sup>26</sup>	5.28 <sup>3†</sup>			583.187 <sup>2</sup>	30.6 <sup>2</sup>		
884.5365 <sup>7</sup>		727.3	6.69 <sup>9</sup>						
		860.6	4.50 <sup>4</sup>						
		1620.7	1.49 <sup>5</sup>						
<sup>198</sup> Au	2.69517 d	411.80205 <sup>17</sup>	95.6 <sup>5</sup>	<sup>239</sup> Np	2.3565 d	106.1	26.7 <sup>4</sup>		
		675.8836 <sup>7</sup>	0.806 <sup>7</sup>			228.2	11.12 <sup>15</sup>		
		1087.6842 <sup>7</sup>	0.159 <sup>3</sup>			277.6	14.31 <sup>20</sup>		
						26.3446 <sup>2</sup>	2.4 <sup>1</sup>		
<sup>199</sup> Au	3.139 d	49.82635 <sup>12</sup>		<sup>241</sup> Am	432.2 y	59.5409 <sup>2</sup>	36.0 <sup>4</sup>		
		158.37851 <sup>10</sup>				<sup>243</sup> Am	7370 y	43.5	5.94 <sup>11</sup>
		208.20481 <sup>12</sup>						74.7	67.4 <sup>10</sup>
<sup>203</sup> Hg	46.612 d	279.1952 <sup>10</sup>	81.48 <sup>8</sup>						
		<sup>203</sup> Pb	51.873 h	279.1952 <sup>10</sup>					
401.320 <sup>4</sup>									
		680.515 <sup>3</sup>							

<sup>#</sup> From reference 1 when listed with uncertainty. Otherwise rounded to the nearest 0.1 keV.

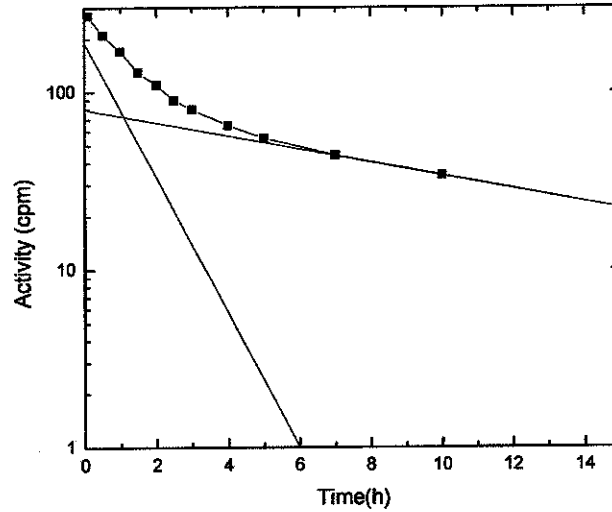
<sup>&</sup> From reference 2, except where indicated.

<sup>†</sup> From reference 3.

<sup>‡</sup> In equilibrium with <sup>172</sup>Lu (6.70 d).

<sup>@</sup> In equilibrium with decay daughter isotopes.

4	65
5	55
7	44
10	34
15	22



From the graph, we see:

$$\begin{array}{ll}
 t_{1/2}(B) = 8.0 \text{ h} & A_0(B) = 80 \text{ cpm} \\
 t_{1/2}(C) = 0.8 \text{ h} & A_0(C) = 190 \text{ cpm}
 \end{array}$$

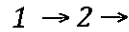
### 3.3 Radioactive Decay Equilibrium

When a radionuclide decays, it does not disappear, but is transformed into a new nuclear species of lower energy and often differing  $Z$ ,  $A$ ,  $J$ ,  $\pi$ , etc. The equations of radioactive decay discussed so far have focused on the decrease of the parent radionuclides but have ignored the formation (and possible decay) of daughter, granddaughter, etc., species. It is the formation and decay of these "children" that is the focus of this section.



Let us begin by considering the case when a radionuclide 1 decays with decay constant  $\lambda_1$ , forming a daughter nucleus 2 which in turn decays with decay constant  $\lambda_2$ .

Schematically we have



We can write terms for the production and depletion of 2, i.e.,

rate of change of 2 nuclei present at time t = rate of production of 2 - rate of decay of 2

$$\frac{dN_2}{dt} = \lambda_1 N_1 - \lambda_2 N_2 \quad (3-13)$$

where  $N_1$  and  $N_2$  are the numbers of (1) and (2) present at time  $t$ .

Rearranging and collecting similar terms

$$dN_2 + \lambda_2 N_2 dt = \lambda_1 N_1 dt \quad (3-14)$$

Remembering that

$$N_1 = N_1^0 e^{-\lambda_1 t} \quad (3-15)$$

we have

$$dN_2 + \lambda_2 N_2 dt = \lambda_1 N_1^0 e^{-\lambda_1 t} dt \quad (3-16)$$

This is a first order linear differential equation and can be solved using the method of integrating factors which we show below. Multiplying both sides by  $e^{\lambda_2 t}$ , we have

$$e^{\lambda_2 t} dN_2 + \lambda_2 N_2 e^{\lambda_2 t} dt = \lambda_1 N_1^0 e^{(\lambda_2 - \lambda_1)t} dt \quad (3-17)$$

The left hand side is now a perfect differential

$$d(N_2 e^{\lambda_2 t}) = \lambda_1 N_1^0 e^{(\lambda_2 - \lambda_1)t} dt \quad (3-18)$$

Integrating from  $t=0$  to  $t=t$ , we have

$$N_2 e^{\lambda_2 t} \Big|_0^t = \frac{\lambda_1 N_1^0 e^{(\lambda_2 - \lambda_1)t}}{\lambda_2 - \lambda_1} \Big|_0^t \quad (3-19)$$

$$N_2 e^{\lambda_2 t} - N_2^0 = \frac{\lambda_1}{\lambda_2 - \lambda_1} N_1^0 (e^{(\lambda_2 - \lambda_1)t} - 1) \quad (3-20)$$

Multiplying by  $e^{-\lambda_2 t}$  and rearranging gives

$$N_2(t) = \frac{\lambda_1}{\lambda_2 - \lambda_1} N_1^0 (e^{-\lambda_1 t} - e^{-\lambda_2 t}) + N_2^0 e^{-\lambda_2 t} \quad (3-21)$$

where  $N_2^0$  is the number of species (2) present at  $t=0$ . The first term in Equation (3-21) represents the growth of the daughter due to the decay of the parent while the second term represents the decay of any daughter nuclei that were present initially. Remembering that  $A_2 = \lambda_2 N_2$ , we can write an expression for the activity of 2 as

$$A_2 = \frac{\lambda_1 \lambda_2}{\lambda_2 - \lambda_1} N_1^0 (e^{-\lambda_1 t} - e^{-\lambda_2 t}) + A_2^0 e^{-\lambda_2 t} \quad (3-22)$$

These two equations, (3-21) and (3-22) are the general expressions for the number of daughter nuclei and the daughter activity as a function of time, respectively.

The general behavior of the activity of parent and daughter species, as predicted by Equation (3-22), is shown in Figure 3-6. As one expects qualitatively for  $N_2^0 = 0$ , the initial activity of the daughter is zero, rises to a maximum, and if one waits long enough, eventually decays.

Thus there must be a time when the daughter activity is the maximum. We can calculate this by noting the condition for a maximum in the activity of (2) is

$$\frac{dN_2}{dt} = 0 \tag{3-23}$$

Taking the derivative of Equation (3-21) and simplifying,

$$\lambda_1 e^{-\lambda_1 t} = \lambda_2 e^{-\lambda_2 t} \tag{3-24}$$

Solving for t

$$t_{\max} = \frac{\ln\left(\frac{\lambda_2}{\lambda_1}\right)}{(\lambda_2 - \lambda_1)} \tag{3-25}$$

All of this development may seem like something that would be best handled by a computer program or just represents a chance to practice one's skill with differential equations. But that is not true. It is important to understand the mathematical foundation of this development to gain insight into practical situations that such insight offers. Let us consider some cases that illustrate this point.

Consider the special case where  $\lambda_1 = \lambda_2$ . Plugging into Equations (3-21) or (3-22), or a computer program based upon them leads to a division by zero. Does nature therefore forbid  $\lambda_1$  from equaling  $\lambda_2$  in a chain of decays? Nonsense! One simply understands that one must redo the derivation (Equations (3-13) through (3-21)) of Equations (3-21) and (3-22) for this special case (see homework).

Let us now consider a number of other special cases of Equations (3-21) and (3-22) that are of practical importance. *Suppose the daughter nucleus is stable ( $\lambda_2 = 0$ ).* Then we have

$$\frac{dN_2}{dt} = \lambda_1 N_1 \tag{3-26}$$

$$dN_2 = \lambda_1 N_1 dt = \lambda_1 N_1^0 e^{-\lambda_1 t} dt \tag{3-27}$$

$$N_2 = \frac{\lambda_1 N_1^0}{-\lambda_1} (e^{-\lambda_1 t}) \Big|_0^t = N_1^0 (1 - e^{-\lambda_1 t}) \quad (3-28)$$

These relations are shown in Figure 3-7. They represent the typical decay of many radionuclides prepared by neutron capture reactions, the type of reaction that commonly occurs in a nuclear reactor.

In Figure 3-8, we show the activity relationships for parent and daughter (as predicted by Equation (3-22)) for various choices of the relative values of the half-lives of the parent and daughter nuclides. In the first of these cases, we have  $t_{1/2}$  (parent) <  $t_{1/2}$  (daughter), *i.e.*, the parent is shorter lived than the daughter. This is called the “*no equilibrium*” case because the daughter buildup (due to the decay of the parent) is faster than its loss due to decay. Essentially all of the parent nuclides are converted to daughter nuclides and the subsequent activity is due to the decay of the daughters only. Thus the name “no equilibrium” is used. Practical examples of this decay type are  $^{131}\text{Te} \rightarrow ^{131}\text{I}$ ,  $^{210}\text{Bi} \rightarrow ^{210}\text{Po}$ ,  $^{92}\text{Sr} \rightarrow ^{92}\text{Y}$ . This situation typically occurs when one is very far from stability and the nuclei decay by  $\beta$  decay towards stability.

A second special case of Equations (3-21) and (3-22) is called *transient equilibrium* (Figures 3-8b and 3-9a). In this case, the parent is significantly ( $\sim 10x$ ) longer-lived than the daughter and thus controls the decay chain. Thus

$$\lambda_2 > \lambda_1 \quad (3-29)$$

In Equation (3-21), as  $t \rightarrow \infty$ ,

$$e^{-\lambda_2 t} \ll e^{-\lambda_1 t} \quad (3-30)$$

$$N_2^0 e^{-\lambda_2 t} \rightarrow 0$$

and we have

$$N_2 \approx \frac{\lambda_1}{\lambda_2 - \lambda_1} N_1^0 e^{-\lambda_1 t} \quad (3-31)$$

Substituting

$$N_1 = N_1^0 e^{-\lambda_1 t} \quad (3-32)$$

we have

$$\frac{N_1}{N_2} = \frac{\lambda_2 - \lambda_1}{\lambda_1} \quad (3-33)$$

At long times, the ratio of daughter to parent activity becomes constant, and both species disappear with the effective half-life of the parent. The classic examples of this decay equilibrium are the decay of  $^{140}\text{Ba}$  ( $t_{1/2} = 12.8$  d) to  $^{140}\text{La}$  ( $t_{1/2} = 40$  hr) or the equilibrium between  $^{222}\text{Rn}$  ( $t_{1/2} = 3.8$  d) and its short-lived decay products.

A third special case of Equations (3-21) and (3-22) is called *secular equilibrium* (Figure 3-8 (c+d), 3-9b). In this case, the parent is very much longer lived ( $\sim 10^4 \times$ ) than the daughter or the parent is constantly being replenished through some other process. During the time of observation, there is no significant change in the number of parent nuclei present, although several half-lives of the daughter may occur. In the previous case of transient equilibrium, we had

$$\frac{N_1}{N_2} = \frac{\lambda_2 - \lambda_1}{\lambda_1} \quad (3-34)$$

Since we now also have

$$\lambda_1 \ll \lambda_2 \quad (3-35)$$

we can simplify even more to give

$$\frac{N_1}{N_2} = \frac{\lambda_2}{\lambda_1} \quad (3-36)$$

$$\lambda_1 N_1 = \lambda_2 N_2 \quad (3-37)$$

$$A_1 = A_2$$

In short, the activity of the parent and daughter are the same and the total activity of the sample remains effectively constant during the period of observation.

The naturally occurring heavy element decay chains (see below) where  $^{238}\text{U} \rightarrow ^{206}\text{Pb}$ ,  $^{235}\text{U} \rightarrow ^{207}\text{Pb}$ ,  $^{232}\text{Th} \rightarrow ^{208}\text{Pb}$  and the extinct heavy element decay series  $^{237}\text{Np} \rightarrow ^{209}\text{Bi}$  are examples of secular equilibrium because of the long half-lives of the parents. Perhaps the most important cases of secular equilibrium are the production of radionuclides by a nuclear reaction in an accelerator, a reactor, a star or the upper atmosphere. In this case, we have

$$\text{Nuclear Reaction} \rightarrow (2) \rightarrow \quad (3-38)$$

which produces the radionuclide 2 with rate R. If the reaction is simply the decay of a long-lived nuclide, then  $R = \lambda_1 N_1^0$  and  $N_2^0 = 0$ . Substitution into 3-21 gives the expression

$$N_2 = \frac{\lambda_1}{\lambda_2 - \lambda_1} N_1^0 (e^{-\lambda_1 t} - e^{-\lambda_2 t}) \quad (3-39)$$

If the reaction is slower than the decay or

$$\lambda_1 \ll \lambda_2 \quad (3-40)$$

It is most appropriate to say (since  $\lambda_1 \approx 0$ )

$$N_2 \approx \frac{\lambda_1}{\lambda_2} N_1^0 (1 - e^{-\lambda_2 t}) \quad (3-41)$$

or in terms of the activities

$$A_2 = \lambda_2 N_2 = R (1 - e^{-\lambda_2 t}) \quad (3-42)$$

Equation (3-42) is known as the activation equation and is shown in Figure 3-10.

Initially the growth of the product radionuclide activity is nearly linear (due to the behavior of  $(1 - e^{-\lambda_2 t})$  for small values of  $\lambda t$ ) but eventually the product activity becomes “saturated” or constant, decaying as fast as it is produced. At an irradiation time of one half-life, half the maximum activity is formed; after 2 half-lives, 3/4 of the maximum activity is formed, etc. This situation gives rise to the rough rule that irradiations that extend for periods that are greater than twice  $t_{1/2}$  of the desired radionuclide are usually not worthwhile.

Equation (3-21) may be generalized to a chain of decaying nuclei of arbitrary length in using the Bateman equations (Bateman, 1910). If we assume that at  $t=0$ , none of the daughter nuclei are present,  $N_2^0 = N_3^0 = \dots = N_n^0 = 0$ , we get

$$(1) \rightarrow (2) \rightarrow (3), \dots, (n) \rightarrow$$

$$N_n = C_1 e^{-\lambda_1 t} + C_2 e^{-\lambda_2 t} + C_3 e^{-\lambda_3 t} + \dots + C_n e^{-\lambda_n t}$$

where

$$C_1 = \frac{\lambda_1 \lambda_2 \dots \lambda_{n-1}}{(\lambda_2 - \lambda_1)(\lambda_3 - \lambda_1) \dots (\lambda_n - \lambda_1)} N_1^0 \quad (3-43)$$

$$C_2 = \frac{\lambda_1 \lambda_2 \dots \lambda_{n-1}}{(\lambda_1 - \lambda_2)(\lambda_3 - \lambda_2) \dots (\lambda_n - \lambda_2)} N_1^0$$

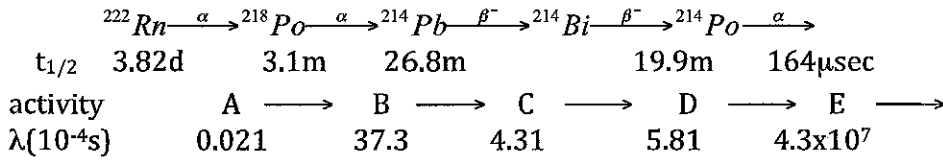
$$C_n = \frac{\lambda_1 \lambda_2 \dots \lambda_{n-1}}{(\lambda_1 - \lambda_n)(\lambda_2 - \lambda_n) \dots (\lambda_{n-1} - \lambda_n)} N_1^0$$

These equations describe the activities produced in new fuel in a nuclear reactor. No fission or activation products are present when the fuel is loaded and they grow in as the reactions take place.

**Example**

Consider the decay of a 1  $\mu\text{Ci}$  sample of pure  $^{222}\text{Rn}$  ( $t_{1/2} = 3.82$  days). Use the Bateman equations to estimate the activity of its daughters ( $^{218}\text{Po}$ ,  $^{214}\text{Pb}$ ,  $^{214}\text{Bi}$  and  $^{214}\text{Po}$ ) after a decay time of 4 hours.

The decay sequence is



$$A = A_0 e^{-\lambda_A t} = 1 \mu\text{Ci} \left( e^{-\frac{\ln 2 \cdot 4}{24 \cdot 3.82}} \right)$$

$$A = 0.97 \mu\text{Ci}$$

$$B = \lambda_B (C_1 e^{-\lambda_A t} + C_2 e^{-\lambda_2 t})$$

$$C_1 = \frac{\lambda_A N_A^0}{\lambda_B - \lambda_A} = \frac{A_0}{\lambda_B - \lambda_A} \quad C_2 = \frac{\lambda_A N_A^0}{\lambda_A - \lambda_B} = \frac{A_0}{\lambda_A - \lambda_B}$$

$$B = \lambda_B \left( \frac{A_0 e^{-\lambda_A t}}{\lambda_B - \lambda_A} + \frac{A_0 e^{-\lambda_B t}}{\lambda_A - \lambda_B} \right)$$

$$B = 37.3 \left( \frac{0.97}{37.3 - 0.021} + \frac{e^{-\frac{\ln 2 \cdot 4}{3.1/60}}}{0.021 - 37.3} \right)$$

$$B = 0.97 \mu\text{Ci}$$

(Actually B/A = 1.00056)

The reader should verify that for C, D and E, the only significant term is the term multiplying  $e^{-\lambda_A t}$  as it was for B. Thus for D/A, we have



$$\frac{D}{A} = \frac{\lambda_B}{\lambda_B - \lambda_A} \cdot \frac{\lambda_C}{\lambda_C - \lambda_A} \cdot \frac{\lambda_D}{\lambda_D - \lambda_A} = 1.0091$$

The reader should, as an exercise, compute the quantities of C and E present.

### 3.4 Branching Decay

Some nuclides decay by more than one mode. Some nuclei may decay by either  $\beta^+$  decay or electron capture; others by  $\alpha$ -decay or spontaneous fission; still others by  $\gamma$ -ray emission or internal conversion, etc. In these cases, we can characterize each competing mode of decay by a separate decay constant  $\lambda_i$  for each type of decay where the total decay constant,  $\lambda$ , is given by the sum

$$\lambda = \lambda_1 + \lambda_2 + \dots = \sum_{i=1}^N \lambda_i \quad (3-44)$$

Corresponding to each partial decay constant  $\lambda_i$ , there is a partial half-life  $t_{1/2}^i$  where

$$t_{1/2}^i = \frac{0.693}{\lambda_i} \quad (3-45)$$

and the total half-life,  $t_{1/2}$ , is the sum of the reciprocals

$$\frac{1}{t_{1/2}} = \frac{1}{t_{1/2}^1} + \frac{1}{t_{1/2}^2} + \dots = \sum_{i=1}^N \frac{1}{t_{1/2}^i} \quad (3-46)$$

The fraction of decays proceeding by the  $i^{\text{th}}$  mode is given by the obvious expression

$$f_i = \frac{\lambda_i}{\sum \lambda_i} = \frac{\lambda_i}{\lambda} \quad (3-47)$$

By analogy, the energy uncertainty associated with a given state,  $\Delta E$ , through the Heisenberg uncertainty principle can be obtained from the lifetime contributed by each

### Equipment Required

- |  |  |
|--|--|
| <ul style="list-style-type: none"><li>• <b>SPA38</b> Integral Assembly consisting of a 38 mm x 38 mm NaI(Tl) Scintillator, Photomultiplier Tube, and PMT Base with Stand</li><li>• <b>4001A/4002D</b> NIM Bin and Power Supply</li><li>• <b>556</b> High Voltage Bias Supply</li><li>• <b>113</b> Scintillation Preamplifier</li><li>• <b>575A</b> Spectroscopy Amplifier</li><li>• <b>EASY-MCA-2K</b> including USB cable and MAESTRO software (other ORTEC MCAs may be substituted)</li><li>• Personal Computer with a USB port and a recent, supportable version of the Windows operating system.</li><li>• <b>TDS3032C</b> Oscilloscope with a bandwidth <math>\geq 150</math> MHz.</li><li>• <b>C-34-12</b> RG-59A/U 75-<math>\Omega</math> Cable with one SHV female plug and one MHV male plug, 3.7-m (12-ft.) length.</li><li>• Five <b>C-24-1</b> RG-62A/U 93-<math>\Omega</math> Coaxial Cables with BNC plugs, 30-cm (1-ft.) length.</li><li>• <b>C-24-12</b> RG-62A/U 93-<math>\Omega</math> Coaxial Cable with BNC plugs, 3.7-m (12-ft.) length.</li><li>• Three <b>C-24-4</b> RG-62A/U 93-<math>\Omega</math> Coaxial Cables with BNC plugs, 1.2-m (4-ft.) length</li><li>• <b>C-29</b> BNC Tee Connector</li><li>• <b>C-27</b> 100 <math>\Omega</math> Terminator (BNC male plug)</li></ul> | <ul style="list-style-type: none"><li>• <b>RSS8*</b> Gamma Source Set. Includes <math>\sim 1</math> <math>\mu\text{Ci}</math> each of: <math>^{60}\text{Co}</math>, <math>^{137}\text{Cs}</math>, <math>^{22}\text{Na}</math>, <math>^{54}\text{Mn}</math>, <math>^{133}\text{Ba}</math>, <math>^{109}\text{Cd}</math>, <math>^{57}\text{Co}</math>, and a mixed Cs/Zn source (<math>\sim 0.5</math> <math>\mu\text{Ci}</math> <math>^{137}\text{Cs}</math>, <math>\sim 1</math> <math>\mu\text{Ci}</math> <math>^{65}\text{Zn}</math>). The first three are required in this experiment. An unknown for Experiment 3.2 can be selected from the remaining sources.</li><li>• <b>GF-137-M-5*</b> 5 <math>\mu\text{Ci} \pm 5\%</math> <math>^{137}\text{Cs}</math> Gamma Source (used as a reference standard for activity in Experiment 3.5).</li><li>• <b>GF-057-M-20*</b> 20 <math>\mu\text{Ci}</math> <math>^{57}\text{Co}</math> Source (for Experiment 3.9).</li><li>• One each of pure metal foil absorber sets: <b>FOIL-AL-30</b>, <b>FOIL-FE-5</b>, <b>FOIL-CU-10</b>, <b>FOIL-MO-3</b>, <b>FOIL-SN-4</b>, and <b>FOIL-TA-5</b>. Each set contains 10 identical foils of the designated pure element and thickness in thousandths of an inch (Foil-Element-Thickness).</li><li>• <b>RAS20</b> Absorber Foil Kit containing 5 lead absorbers from 1100 to 7400 <math>\text{mg}/\text{cm}^2</math>. The 10 aluminum absorbers from 140 to 840 <math>\text{mg}/\text{cm}^2</math> also included in this kit are not used in this experiment.</li><li>• Small, flat-blade screwdriver for tuning screwdriver-adjustable controls</li><li>• Additional Equipment Needed for Experiment 3.10</li><li>• <b>427A</b> Delay Amplifier</li><li>• <b>551</b> Timing Single-Channel Analyzer</li><li>• <b>426</b> Linear Gate</li><li>• <b>416A</b> Gate and Delay Generator</li></ul> |
|--|--|

\*Sources are available direct from supplier. See the ORTEC website at [www.ortec-online.com/Service-Support/Library/Experiments-Radioactive-Source-Suppliers.aspx](http://www.ortec-online.com/Service-Support/Library/Experiments-Radioactive-Source-Suppliers.aspx)

### Purpose

The purpose of this experiment is to acquaint the student with some of the basic techniques used for measuring gamma rays. It is based on the use of a thallium-activated sodium iodide detector. The written name of this type of detector is usually shortened to NaI(Tl). In verbal conversations, it is typically simply called a sodium iodide detector.

### Gamma Emission

Most isotopes used for gamma-ray measurements also have beta-emissions in their decay schemes. The decay scheme for the isotope typically includes beta decay to a particular level, followed by gamma emission to the ground state of the final isotope. The beta particles will usually be absorbed in the surrounding material and not enter the scintillation detector. This absorption can be assured with aluminum absorbers (ref. 10). For this experiment, the beta emissions cause negligible interference, so absorbers are not specified. There is always some beta absorption by the light shield encapsulating the detector. The gammas, however, are quite penetrating, and will easily pass through the aluminum light shield.

Generally there are two unknowns that we would like to investigate about a gamma source. One is measuring the energies of the gamma rays from the source. The other is counting the number of gamma-ray photons that leave the source per unit of time. In this experiment the student will become familiar with some of the basic NaI(Tl) measurements associated with identifying a gamma-emitting radioisotope. A total time of  $\sim 6$  hours is required to complete all the parts of Experiment 3 (3.1 through 3.10). Since each part is written to be fairly independent of the others, the complete series can be done in two 3-hour lab periods.

## Experiment 3 Gamma-Ray Spectroscopy Using NaI(Tl)

### The NaI(Tl) Detector

The structure of the NaI(Tl) detector is illustrated in Figure 3.1. It consists of a single crystal of thallium activated sodium iodide optically coupled to the photocathode of a photomultiplier tube. When a gamma ray enters the detector, it interacts by causing ionization of the sodium iodide. This creates excited states in the crystal that decay by emitting visible light photons. This emission is called a scintillation, which is why this type of sensor is known as a scintillation detector. The thallium doping of the crystal is critical for shifting the wavelength of the light photons into the sensitive range of the photocathode. Fortunately, the number of visible-light photons is proportional to the energy deposited in the crystal by the gamma ray. After the onset of the flash of light, the intensity of the scintillation decays approximately exponentially in time, with a decay time constant of 250 ns. Surrounding the scintillation crystal is a thin aluminum enclosure, with a glass window at the interface with the photocathode, to provide a hermetic seal that protects the hygroscopic NaI against moisture absorption. The inside of the aluminum is lined with a coating that reflects light to improve the fraction of the light that reaches the photocathode.

At the photocathode, the scintillation photons release electrons via the photoelectric effect. The number of photoelectrons produced is proportional to the number of scintillation photons, which, in turn, is proportional to the energy deposited in the crystal by the gamma ray.

The remainder of the photomultiplier tube consists of a series of dynodes enclosed in the evacuated glass tube. Each dynode is biased to a higher voltage than the preceding dynode by a high voltage supply and resistive biasing ladder in the photomultiplier tube base. Because the first dynode is biased at a considerably more positive voltage than the photocathode, the photoelectrons are accelerated to the first dynode. As each electron strikes the first dynode the electron has acquired sufficient kinetic energy to knock out 2 to 5 secondary electrons. Thus, the dynode multiplies the number of electrons in the pulse of charge. The secondary electrons from each dynode are attracted to the next dynode by the more positive voltage on the next dynode. This multiplication process is repeated at each dynode, until the output of the last dynode is collected at the anode. By the time the avalanche of charge arrives at the anode, the number of electrons has been multiplied by a factor ranging from  $10^4$  to  $10^6$ , with higher applied voltages yielding larger multiplication factors. For the selected bias voltage, the charge arriving at the anode is proportional to the energy deposited by the gamma ray in the scintillator.

The preamplifier collects the charge from the anode on a capacitor, turning the charge into a voltage pulse. Subsequently, it transmits the voltage pulse over the long distance to the supporting amplifier. At the output of the preamplifier and at the output of the linear amplifier, the pulse height is proportional to the energy deposited in the scintillator by the detected gamma ray. The Multichannel Analyzer (MCA) measures the pulse heights delivered by the amplifier, and sorts them into a histogram to record the energy spectrum produced by the NaI(Tl) detector. See Figure 3.2 for the modular electronics used with the NaI(Tl) detector.

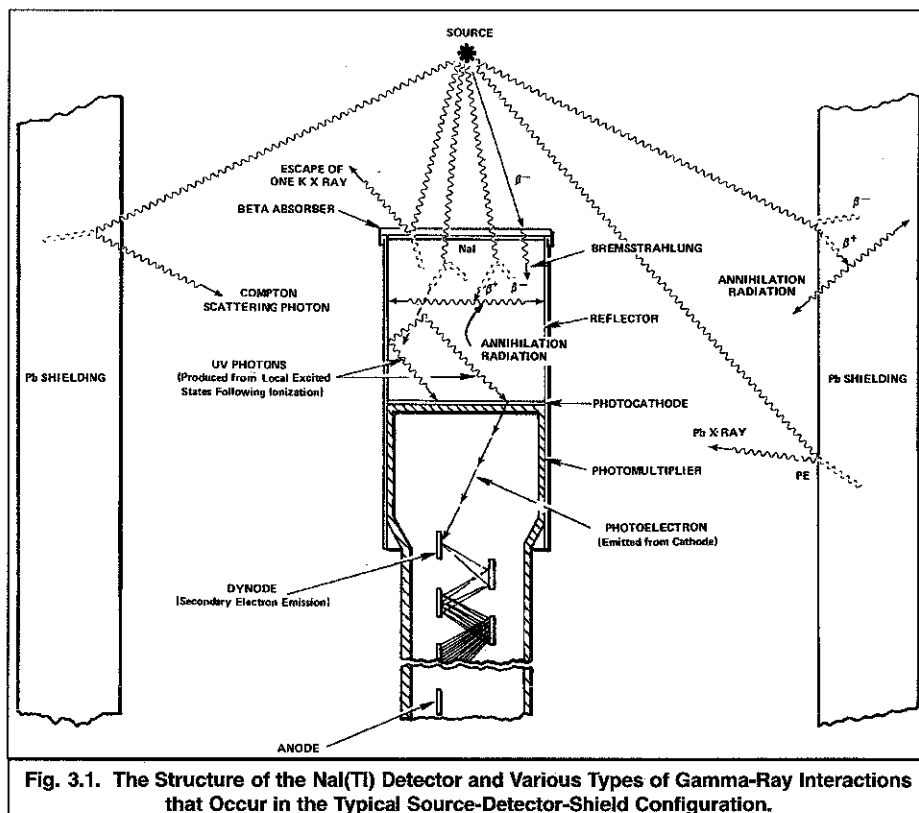


Fig. 3.1. The Structure of the NaI(Tl) Detector and Various Types of Gamma-Ray Interactions that Occur in the Typical Source-Detector-Shield Configuration.

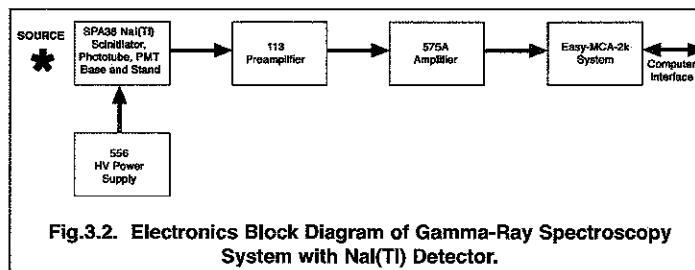


Fig.3.2. Electronics Block Diagram of Gamma-Ray Spectroscopy System with NaI(Tl) Detector.

## Experiment 3

### Gamma-Ray Spectroscopy Using NaI(Tl)

For an ideal detector and supporting pulse processing electronics, the spectrum of 662-keV gamma rays from a  $^{137}\text{Cs}$  radioactive source would exhibit a peak in the spectrum whose width is determined only by the natural variation in the gamma-ray energy. The NaI(Tl) detector is far from ideal, and the width of the peak it generates is typically 7% to 10% of the 662-keV gamma-ray energy. The major source of this peak broadening is the number of photoelectrons emitted from the photocathode for a 662-keV gamma-ray. For a high-quality detector this is on the order of 1,000 photoelectrons. Applying Poisson statistics (ref. 1 and 11), 1,000 photoelectrons limit the full width of the peak at half its maximum height (FWHM) to no less than 7.4%. Statistical fluctuations in the secondary electron yield at the first dynode and fluctuations in the light collected from the scintillator also make a small contribution to broadening the width of the peak in the energy spectrum. Because the broadening is dominated by the number of photoelectrons, and that number is proportional to the gamma-ray energy, the FWHM of a peak at energy  $E$  is approximately described by

$$\% \text{ Resolution (FWHM)} = \frac{\delta E}{E} \times 100\% \approx \frac{k \times 100\%}{\sqrt{E}} \quad (1)$$

Where

$E$  is the energy of the peak,

$\delta E$  is the FWHM of the peak in energy units, and

$k$  is a proportionality constant characteristic of the particular detector.

Equation (1) indicates that the percent energy resolution of the NaI(Tl) detector improves as the gamma-ray energy increases.

Because the scintillation has a 250-ns decay time constant, it is important to collect the resulting charge pulse from the photomultiplier tube for at least four time constants (i.e.,  $1 \mu\text{s}$ ). This collection time ensures that 98% of the light will contribute to the analyzed pulse height, thus assuring that the best possible energy resolution can be achieved. If a  $0.5\text{-}\mu\text{s}$  shaping time constant is chosen on the linear amplifier, the amplifier output pulse will reach its maximum amplitude in approximately  $1.1 \mu\text{s}$ . Hence this is the minimum shaping time constant that can be employed. If high counting rates are not expected, and the dead time caused by the pulse width is not a problem, a  $1\text{-}\mu\text{s}$  shaping time constant can be selected. The latter choice delivers a pulse that reaches peak amplitude in approximately  $2.2 \mu\text{s}$ .

For an MCA having a conversion time  $<2 \mu\text{s}$ , the dominant source of dead time is the duration of the amplifier output pulse. The dead time comprises the sum of the time to reach peak amplitude and the width of the pulse at the baseline. For the  $0.5 \mu\text{s}$  shaping time constant, the dead time amounts to about  $5 \mu\text{s}$ , and for the  $1 \mu\text{s}$  time constant, the dead time is approximately  $10 \mu\text{s}$ . Consequently, the NaI(Tl) system will experience a 10% dead time loss in the range of 10,000 to 20,000 counts/second, depending on the choice of amplifier shaping time constant. Above 20,000 counts/second, the gain of the photomultiplier tube can be affected by the counting rate. Consequently, 20,000 counts/second is a reasonable upper limit for normal operation. For more information on pulse shaping and the relevant dead time, see references 1, 11, 12, 13 and 14.

### The Multichannel Pulse-Height Analyzer

The other major concept introduced in this experiment is the Multichannel Analyzer (MCA). It is responsible for measuring the height of each pulse delivered by the linear amplifier. Over the period of time the gamma rays are counted, the MCA sorts the pulses, according to pulse height, into a histogram that represents the spectrum of gamma-ray energies intercepted by the NaI(Tl) detector. The MCA is the central analyzer for many of the experiments in this series. Rather than including a complete description of its function in each experiment, the student is referred to the document entitled, The Multichannel Pulse-Height Analyzer which can be found on the Library page at [www.ortec-online.com/solutions/educational.aspx](http://www.ortec-online.com/solutions/educational.aspx).

The MCA listed in the Equipment Required for this experiment uses software in a supporting personal computer to operate the instrument and display the spectrum. The MCA connects to the computer via a USB cable. It is important to become familiar with the controls that are accessible via the MAESTRO software. The most efficient approach may be to have the laboratory instructor provide a quick demonstration. You will need to know how to start/stop data acquisition, clear the contents of the memory, select the digital resolution, adjust the upper and lower discriminator thresholds, set the preset live time, monitor the percent dead time, read the peak positions with the mouse pointer, set regions of interest, and calibrate the horizontal scale to read in keV (energy).

One of the benefits of the MCA is the incorporation of a live time clock. This feature automatically corrects for dead time losses by measuring elapsed time only when the spectrometer is not busy processing a pulse. See references 1, 11, 13 and 14 for more information.

## Experiment 3

### Gamma-Ray Spectroscopy Using NaI(Tl)

---

#### EXPERIMENT 3.1. Energy Calibration

##### 3.1.1. Equipment Setup

Set up the electronics as shown in Fig. 3.2.

1. Turn off power to the NIM Bin and Power Supply and the 556 HV Power Supply.
2. Check that the front-panel controls on the 556 HV Power Supply are set to their minimum values. Confirm that POSITIVE POLARITY has been selected on the rear panel, and the CONTROL toggle switch has been set to INTERNAL. The 556 derives its primary power from an AC power outlet. But, for convenience, it can be inserted into a vacant location in the NIM Bin.
3. Ensure that the NaI(Tl) detector assembly is properly mounted in the stand. Connect the MHV High Voltage (Bias) connector on the detector to the SHV High Voltage OUTPUT on the rear of the 556 using the C-34-12 coaxial cable. Note that the connectors are different on each end of this high voltage cable. One connector is specific to the MHV connector used on the detector, and the other is matched to the SHV connector on the rear of the 556 HV Supply.
4. Using the C-24-1 coaxial cable, connect the anode output of the NaI(Tl) detector assembly (BNC connector) to the INPUT of the 113 Preamplifier. Set the 113 INPUT CAPACITANCE to 200 pF. The polarities of the anode output of the photomultiplier tube and the preamplifier are both negative.
5. Remove the 575A Amplifier from the NIM Bin and check that the slide switches accessible through the side panel are all set to 0.5  $\mu$ s. That selection ensures that the shaping time constant is set to 0.5  $\mu$ s. Insert the amplifier back into the NIM Bin.
6. Connect the power cable from the 113 Preamplifier to the PREAMP. POWER connector on the rear of the 575A Amplifier.
7. Using a C-24-12 coaxial cable, connect the OUTPUT of the 113 Preamplifier to the INPUT of the 575A Amplifier.
8. Select the NEGATIVE input polarity on the 575A Amplifier.
9. Using a C-24-4 coaxial cable, connect the UNIPOLAR OUTPUT of the 575A Amplifier to the analog INPUT of the EASY-MCA. Using the USB cable, connect the USB port on the rear of the EASY-MCA to the USB port on the supporting computer. Ensure that the MAESTRO software that operates the EASY-MCA has been installed on the computer.
10. Turn on the power to the computer and the NIM Bin and Power Supply.

There are two parameters that ultimately determine the overall gain of the system: the high voltage furnished to the phototube and the gain of the spectroscopy amplifier. The gain of the photomultiplier tube is quite dependent upon its high voltage. A rule of thumb for most phototubes is that, near the desired operating voltage, a 10% change in the high voltage will change the gain by a factor of 2. The desired high voltage value depends on the phototube being used. Consult your instruction manual for the phototube and select a value in the middle of its normal operating range. Sometimes, the detector will have a stick-on label that lists the percent resolution and the voltage at which that resolution was measured. In that case, use the high voltage value on that label. Lacking those sources to specify the operating voltage, check with the laboratory instructor for the recommended value. The operating voltage will likely fall in the range of +800 to +1300 Volts.

11. Set the voltage controls on the 556 High Voltage Power Supply to the operating voltage recommended for the detector. Turn on the POWER switch on the 556.
12. Using the MCB Properties menu in the MAESTRO software, set up the acquisition conditions for the EASY-MCA. Select a conversion gain of 1024 channels for the pulse-height range of 0 to +10 Volts. Turn the GATE to Off. For a starting value, the lower level discriminator threshold can be set to about 100 mV (10 channels). Set the upper level discriminator to full scale, or slightly higher. Initially, the preset time limit can be turned off. Your laboratory instructor may have additional recommendations for the set-up of the EASY-MCA.

##### 3.1.2. Pole Zero Cancellation Adjustment

The NaI(Tl) detector produces a pulse of charge that lasts for about 1  $\mu$ s at the anode output of the photomultiplier tube. The preamplifier collects that charge on the input capacitance and turns it into a voltage pulse at the preamplifier output. Because the anode pulse has a negative polarity, and the 113 Preamplifier is non-inverting, the voltage pulse at the preamplifier output has a negative polarity. The decay time of the scintillation controls the shape of the leading-edge response of the preamplifier output pulse. For the 250-ns decay time constant of the NaI(Tl) scintillator, the fall time (10% to 90% of the pulse height) on the leading edge of the voltage pulse will be approximately 0.55  $\mu$ s. Within about 1  $\mu$ s, the absolute value of the pulse amplitude reaches its maximum excursion. Subsequently, the voltage pulse decays back towards zero Volts with an exponential decay that is characterized by a 50  $\mu$ s time constant. That decay time constant is nominal, and could lie anywhere in the range of 30 to 80  $\mu$ s.

## Experiment 3

### Gamma-Ray Spectroscopy Using NaI(Tl)

In the amplifier, the long exponential decay of the preamplifier must be replaced by the shorter exponential decay selected by the shaping time constant switches on the amplifier. This is the function of the Pole-Zero Cancellation circuit near the input of the amplifier. The adjustment of the Pole-Zero Cancellation to achieve exact replacement will be implemented in the next series of steps. For more information on pole-zero cancellation, consult references 1, 11 and 12.

1. Disconnect the Amplifier UNipolar OUTput from the EASY-MCA and connect it instead to the Channel 1 (CH1) input of the oscilloscope. Select Auto triggering on CH1 in the oscilloscope, a vertical scale of 5 V per major division and 1  $\mu$ s per major horizontal division. Adjust the vertical position of the baseline in the display to the centerline of the display. Make sure the input impedance of channel 1 is set to 1 M $\Omega$ .
2. Place the  $^{137}\text{Cs}$  source from the gamma source kit ( $E_\gamma = 0.662$  MeV) in the stand  $\sim 2$  cm below the front surface of the NaI(Tl) crystal.
3. Observe the signal on the oscilloscope. It should look approximately like the yellow signal in Figure 3.3, except the vertical and horizontal scales will be different. There should be an intense signal at the top of the range of pulse heights, and a distribution of less intense pulses at lower amplitudes. The intense signal at the top of distribution is the full-energy signal from the 662-keV gamma ray. If no signals are observed, try adjusting the oscilloscope triggering and the vertical scale to find the signals.
4. Once you are able to display the signals, adjust the amplifier coarse and fine gain controls to make the amplitude of the full-energy signal from the 662-keV gamma rays approximately 10 Volts. It may be useful to change the oscilloscope triggering mode from Auto to Normal at this point.
5. Change the oscilloscope horizontal scale to 50  $\mu$ s per major division.
6. Change the vertical scale to 100 mV per major division. Re-adjust the triggering and vertical position so that the baseline before and after the pulses aligns with the main horizontal scale line across the middle of the display.
7. Turn the PZ ADJ screwdriver adjustment on the front panel of the 575A Amplifier clockwise and/or counter-clockwise, as needed, to make the observed pulses return to baseline as quickly as possible after each pulse without any undershoot. Consult references 1, 11 and 12 for more guidance.

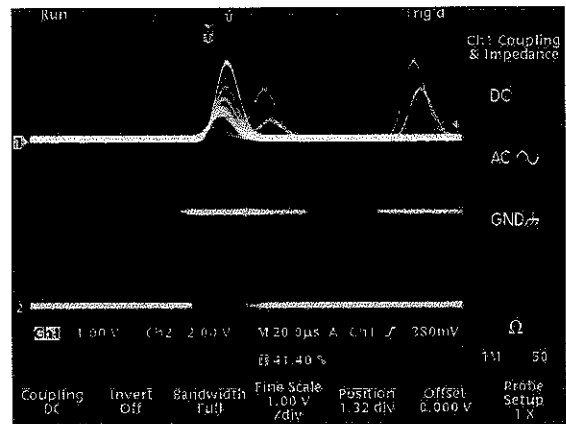


Fig. 3.3. Oscilloscope Signal.

**CAUTION:** On some oscilloscopes, the 10-V pulse amplitude may cause an overload of the oscilloscope amplifiers on the more sensitive vertical scales. When this happens the recovery of the trailing edge of the pulse will appear distorted, making it impossible to make a valid PZ adjustment. If this problem is suspected, start with the 5 V per major division scale and increase the vertical scale sensitivity one step at a time. For each increase in vertical sensitivity verify that the shape of the trailing edge differs from the shape on the previous scale setting in proportion to the change in the scale factor. When abrupt distortion is encountered on the more sensitive vertical scale, return to the previous, less sensitive scale to make the PZ adjustment.

It may be useful to try different horizontal scales ranging from 10  $\mu$ s to 100  $\mu$ s per major division while making the pole-zero cancellation adjustment.

#### 3.1.3. Adjusting the Gain for Recording Spectra

1. Set the oscilloscope vertical scale to 1 Volt per major division, and the horizontal scale to 1  $\mu$ s per major division. Adjust the triggering and vertical position if needed to observe the signals.
2. Reduce the amplifier gain to set the 662-keV pulse height to approximately 2.4 Volts.
3. Disconnect the amplifier UNipolar OUTput from the oscilloscope and re-connect it to the analog INPUT of the EASY-MCA.
4. Acquire a spectrum on the EASY-MCA for at least 30 seconds, and no more than a couple of minutes. The spectrum should look like Figure 3.4.
5. Identify the 662-keV photopeak (full-energy peak). Click on the top of the peak, and note the channel number corresponding to the maximum value.
6. If the 662-keV photopeak position does not correspond to channel 238, adjust the amplifier fine gain and repeat the spectrum acquisition. Repeat this process until the peak position lies at channel 238. This adjustment ensures that the  $1.17 + 1.33$  MeV =

## Experiment 3 Gamma-Ray Spectroscopy Using NaI(Tl)

2.50 MeV sum peak from the  $^{60}\text{Co}$  source in Experiment 3.8 will be positioned at channel 900, well within the 1000-channel limit. (Note that the calibration in Fig. 3.4 places the peak at channel 280, which would shift the sum peak in Expt. 3.8 past the top end of the scale.)

### 3.1.4. Lower-Level Discriminator Adjustment

The optimum setting of the Lower-Level Discriminator threshold is slightly above the maximum noise amplitude. This prevents the MCA from wasting time analyzing the useless information in the noise surrounding the baseline between valid pulses. Setting the Lower-Level Discriminator threshold reasonably close to the noise improves the quality of the automatic dead time correction by measuring the full duration of the pulses at the noise threshold. To adjust the Lower-Level Discriminator use the following procedure.

1. Remove any radioactive sources from the vicinity of the NaI(Tl) detector, so that no gamma rays are being detected.
2. Start a data acquisition and observe the Percent Dead Time displayed for the MCA. It should be less than 1%. If the dead time is larger than 1% jump to step 5.
3. Using the MCB Properties menu, reduce the Lower-Level Discriminator threshold, start another acquisition and observe the percent dead time.
4. Keep repeating step 3 until the percent dead time abruptly increases.
5. Once the dead time increases significantly above 1%, gradually increase the Lower-Level Discriminator threshold until the percent dead time is less than 1%.
6. Repeat steps 3 through 5 until you are confident the threshold has been set reasonably close to the noise, with little risk of counting random noise excursions.

The absolute amplitude of the noise at the MCA input is dependent on the preamplifier characteristics and the gain setting on the amplifier. Consequently, the MCA Lower-Level Discriminator threshold should be adjusted any time the amplifier gain is changed, or the preamplifier is replaced with a different unit. Adjustment of this threshold is important whenever a detector system is assembled for initial set-up.

### 3.1.5. Energy Calibration with $^{137}\text{Cs}$ and $^{60}\text{Co}$

1. Return the  $^{137}\text{Cs}$  source to the counting position, and implement an acquisition for a time period long enough to form a well defined spectrum with minimal random scatter in the vertical direction. The amount of scatter is controlled by counting statistics. If the  $i^{\text{th}}$  channel contains  $N_i$  counts, the standard deviation in those counts is expected to be

$$\sigma_{N_i} = \sqrt{N_i} \quad (2)$$

And the percent standard deviation in the  $N_i$  counts is

$$\% \sigma_{N_i} = \frac{\sigma_{N_i}}{N_i} \times 100\% = \frac{100\%}{\sqrt{N_i}} \quad (3)$$

Note that 100 counts in a channel corresponds to a 10% standard deviation, 10,000 counts yield a 1% standard deviation, and 1 million counts are needed to achieve a 0.1% standard deviation. Consequently, the vertical scatter in the spectrum will begin to appear acceptable when the rather flat continuum at energies below the Compton edge has more than a few hundred counts per channel.

2. Plot the spectrum accumulated in step 1 with a linear vertical scale. Mark the photopeak, the Compton edge and the backscatter peak (if discernable) on the spectrum as indicated in Figure 3.4.

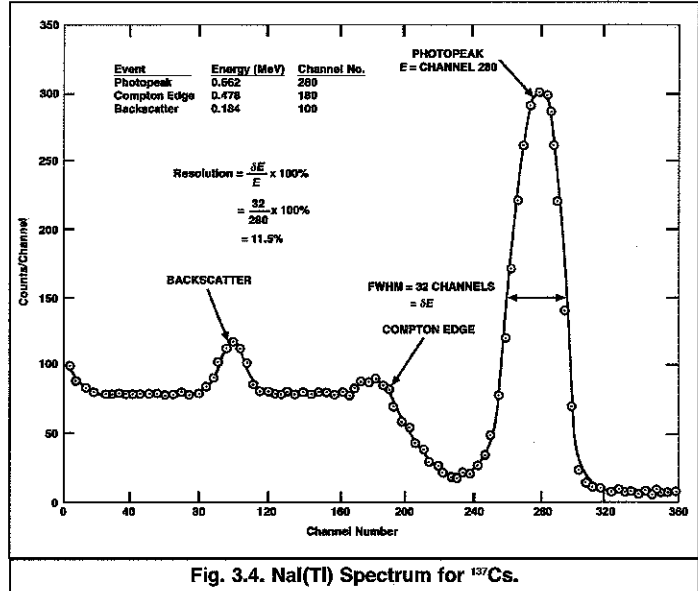
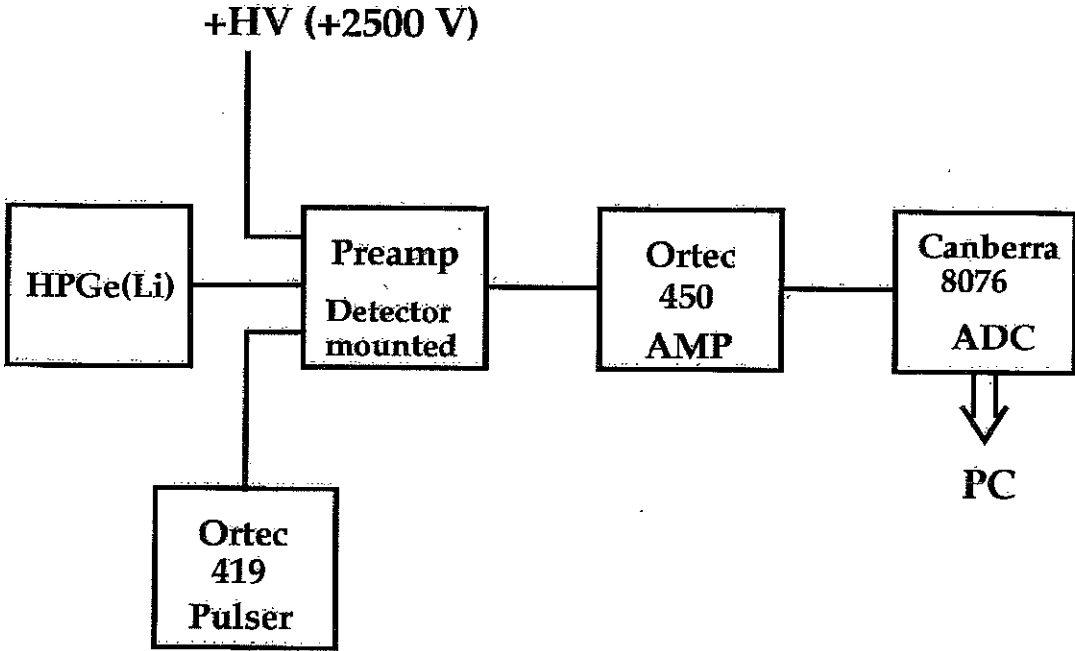
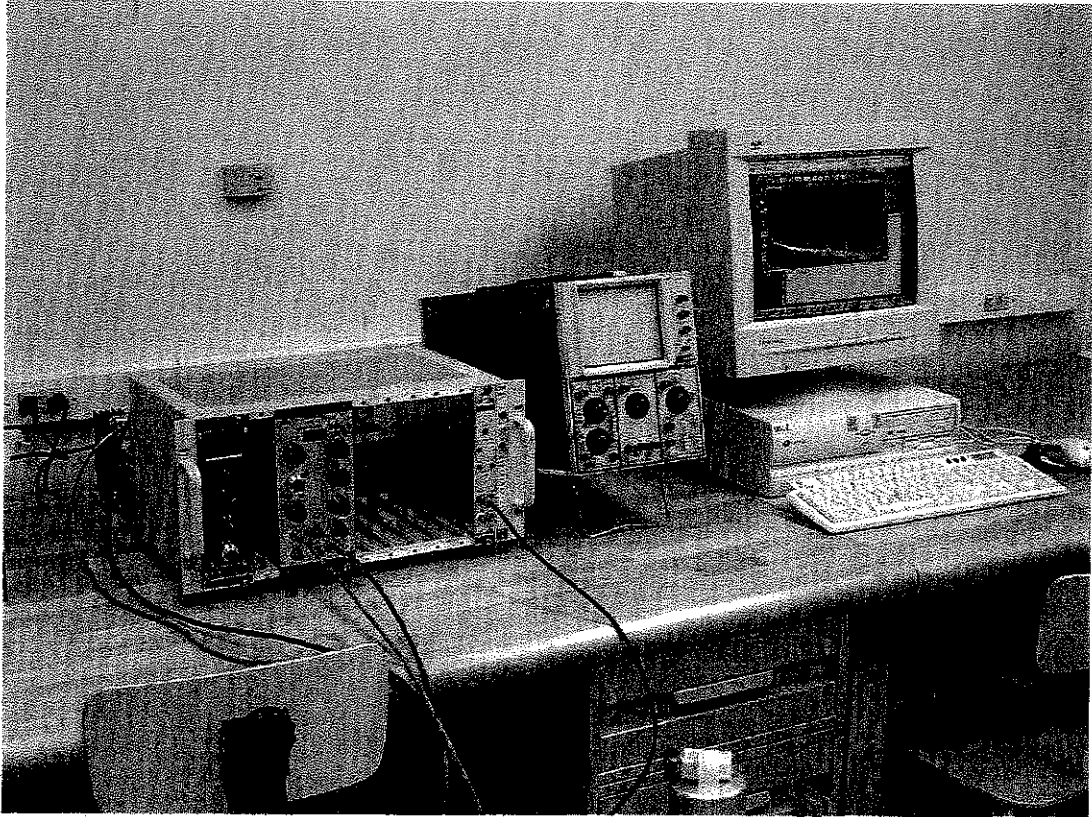


Fig. 3.4. NaI(Tl) Spectrum for  $^{137}\text{Cs}$ .

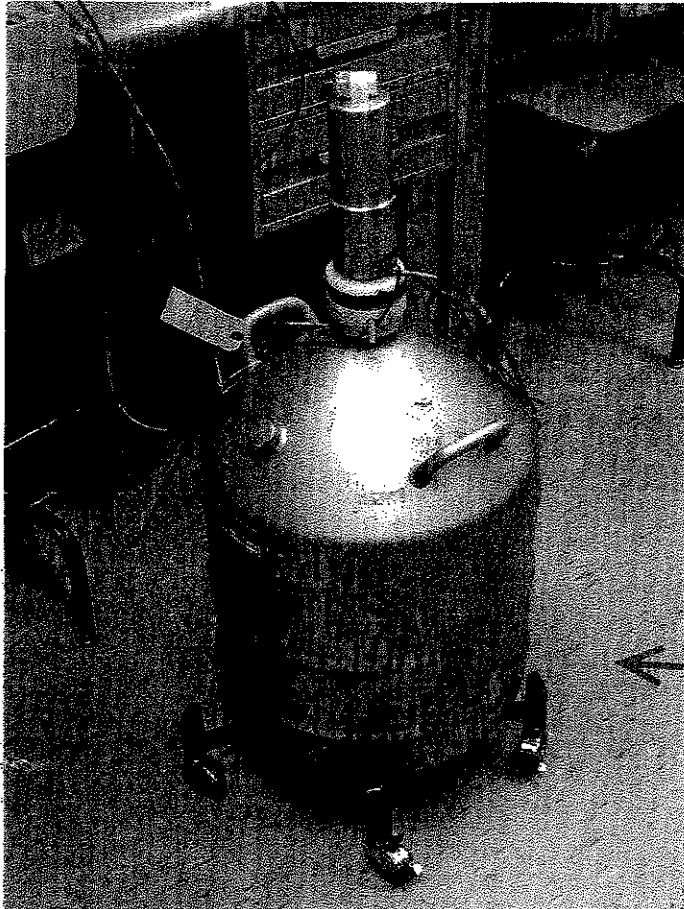
# Experiment Layout







Electronics and DAQ



Ge(Li) detector + dewar

## Section 6 Detector Specifications and Performance Data

### 6.1 SPECIFICATIONS

Model Number GR1020

Serial Number 5871624

The purchase specifications and therefore the warranted performance of this detector are as follows:

Rel. Efficiency - 10 %  
 Resolution - 2.0 keV (FWHM) @ 1.33 MeV  
                   - \_\_\_\_\_ keV (FWTM)  
                   - \_\_\_\_\_ keV (FWHM) @ \_\_\_\_\_  
                   - \_\_\_\_\_ keV (FWTM)  
 Peak/Compton - \_\_\_\_\_ :1

Cryostat Description or Drw. No. if special 7600

### 6.2 PHYSICAL/PERFORMANCE DATA

Actual performance of this detector when tested is given below.

Geometry Reverse electrode closed ended coaxial

Diameter 44.6 mm

Length 36 mm

Active area facing window 15.8 cm<sup>2</sup>

Distance from window 5 mm

#### Electrical Characteristics

Depletion Voltage (-)3000 V dc.

Recommended Bias Voltage (-) 4000 V dc.

Leakage Current at Recommended Bias 0.04 Na.

Preamplifier Test Point Voltage at Recommended Bias (-) 1.60 V dc.

Capacitance at Recommended Bias ~ 17 pf.

Resolution and Efficiency--with Amp Time Constant of 4 microseconds.

Isotope	Co <sup>57</sup>	Co <sup>60</sup>			Cd <sup>109</sup>
Energy (keV)	122	1332			Ratio 22/88keV
FWHM (keV)	0.72	1.73			
FWTM (keV)	1.32	3.21			
Peak/Compton		49:1			
Efficiency (%)		13.8			>23:1

## National Bureau of Standards

## Certificate

## Standard Reference Material 4275-B

MIXED-RADIONUCLIDE POINT-SOURCE STANDARD  
for the  
EFFICIENCY CALIBRATION OF GERMANIUM-SPECTROMETER SYSTEMS

Antimony-125-Tellurium-125m  
Europium-154  
Europium-155

Source identification	SRM 4275-B - 43
Source description	Point source on polyester tape (1)*
Reference time	1200 EST May 1, 1983

This standard is intended for use in measuring the full-energy-peak efficiencies of spectrometer systems for x and gamma rays from 27 to 1596 keV, provided that the responses to radiations approximately 5 keV apart can be resolved. Emission rates are specified at 19 energies for photon radiations from a mixture of antimony-125-tellurium-125m, europium-154, and europium-155. Uncertainties are estimated and combined at a level corresponding to a standard deviation of the mean, with the intent that the user can propagate this uncertainty along with the other uncertainties in the spectrometer calibration.

Table 1 gives the energies, emission rates, and uncertainties for selected radiations. A footnote indicates how emission rates will change with time. If there are any changes in measured emission rates that would correspond to an emission rate 0.5 percent different from that calculated from Table 1, or in measured half lives that would cause a corresponding difference after five years, notification will be sent to purchasers of the standard.

Table 2 lists the estimates of component uncertainties which have been combined in quadrature to give the total uncertainty in each emission rate.

Notes on the use of this standard are appended. One of the tables in the supplemental notes gives relative emission rates for radiations close in energy to the certified radiations; for spectrometer systems of poorer resolution, it may be necessary to use a combined emission rate for some multiple peaks.

This Standard Reference Material was prepared in the Center for Radiation Research, Nuclear Radiation Division, Radioactivity Group, Dale D. Hoppes, Group Leader.

Washington, D.C. 20234  
July, 1983

Stanley D. Rasberry, Chief  
Office of Standard Reference Materials

\*Footnotes on page 4

X-Ray and Gamma-Ray Energies, Emission Rates <sup>(2,3)</sup>,  
and Uncertainties for Standard Reference Material 4275-B

TABLE 1

Radionuclide	Photon Energy (keV)	Emission Rate ( $\times s^{-1}$ ) or ( $\gamma s^{-1}$ ) 1200 EST May 1, 1983	Total Estimated Uncertainty (%) <sup>*</sup>
<sup>125</sup> Sb - <sup>125m</sup> Te	K $\alpha$ , 27.4	$1.283 \times 10^4$	1.3
<sup>154</sup> Eu - <sup>155</sup> Eu	K $\alpha$ , 42.8	$9.537 \times 10^3$ (4)	1.3
1 <sup>155</sup> Eu	86.6	$5.471 \times 10^3$	0.8
2 <sup>155</sup> Eu	105.3	$3.779 \times 10^3$	1.1
3 <sup>154</sup> Eu	<del>123.1</del>	$1.307 \times 10^4$	0.7
4 <sup>125</sup> Sb	176.4	$1.408 \times 10^3$	0.6
5 <sup>154</sup> Eu	248.0	$2.215 \times 10^3$	0.6
6 <sup>125</sup> Sb	380.5	$3.120 \times 10^2$	0.8
7 <sup>125</sup> Sb	427.9	$6.118 \times 10^3$	0.7
8 <sup>125</sup> Sb	463.4	$2.151 \times 10^3$	0.7
9 <sup>154</sup> Eu	591.7	$1.585 \times 10^3$	0.6
10 <sup>125</sup> Sb	600.6	$3.634 \times 10^3$	0.6
11 <sup>125</sup> Sb	635.9	$2.322 \times 10^3$	0.6
12 <sup>154</sup> Eu	723.3	$6.434 \times 10^3$	0.6
13 <sup>154</sup> Eu	873.2	$3.905 \times 10^3$	0.7
14 <sup>154</sup> Eu	996.4	$3.343 \times 10^3$	1.0
15 <sup>154</sup> Eu	1004.8	$5.795 \times 10^3$	0.7
16 <sup>154</sup> Eu	<del>1274.4</del>	$1.117 \times 10^4$	0.6
17 <sup>154</sup> Eu	1596.5	$5.678 \times 10^2$	0.7

\* Estimated total uncertainties have the significance of one standard deviation of the mean. Components of these estimates are given in Table 2.

# Estimates of the Component Uncertainties for Photon-Emission-Rate Values for SRM 4275-B

## TYPICAL UNCERTAINTY COMPONENTS (%)

TABLE 2

Photon Energy (keV)	Number of Determinations	Std. Dev. of the Mean	Efficiency	Peak Analysis	Pile-up Compensation	Geometry	Other*	Overall Uncertainty**
27.4	6	0.3	1.0	0.7	0.3	0.1	0.2	1.31
42.8	6	0.06	1.0	0.7	0.1	0.1	0.5	1.3
86.6	6	0.12	0.65	0.3	0.1	0.1	0.05	0.74
105.3	6	0.09	1.0	0.3	0.1	0.1	0.05	1.1
123.1	6	0.08	0.6	0.4	0.1	0.08	0.05	0.74
176.4	6	0.09	0.5	0.2	0.2	0.1	0.05	0.59
248.0	6	0.04	0.5	0.3	0.1	0.08	0.05	0.60
380.5	6	0.36	0.7	0.2	0.2	0.08	0.05	0.84
427.9	6	0.23	0.7	0.2	0.2	0.08	0.05	0.79
463.4	7	0.22	0.58	0.2	0.2	0.08	0.05	0.69
591.7	6	0.12	0.45	0.3	0.1	0.08	0.05	0.57
600.6	7	0.20	0.42	0.4	0.2	0.08	0.05	0.65
635.9	6	0.19	0.42	0.2	0.2	0.08	0.05	0.55
723.3	6	0.05	0.54	0.2	0.1	0.08	0.05	0.59
873.2	5	0.12	0.63	0.3	0.1	0.08	0.05	0.72
996.4	5	0.11	0.54	0.75	0.1	0.08	0.05	0.94
1004.8	5	0.06	0.54	0.4	0.1	0.08	0.05	0.69
1274.4	5	0.06	0.45	0.1	0.1	0.08	0.05	0.46
1596.5	6	0.43	0.40	0.1	0.2	0.15	0.05	0.64

\* Includes contributions for the half lives for the Te x-ray, for the decay schemes for Gd x-ray, and for gravimetric factors in the source preparation.

\*\* Components of the uncertainty have been added in quadrature. This is the overall uncertainty for a typical detector, and some of the values are slightly greater than those given in the last column of Table 1.



UNITED STATES DEPARTMENT OF COMMERCE  
National Bureau of Standards  
Washington, D.C. 20234

NOTES ON THE USE OF STANDARD REFERENCE MATERIALS 4275-B AND 4276-B

MEASURING EFFICIENCIES OF GERMANIUM SPECTROMETER SYSTEMS  
WITH NBS LONG-LIVED MIXED-RADIONUCLIDE STANDARDS

1. Introduction

Careful measurements with many calibrated single-radionuclide sources may give the most accurate efficiency-energy relations for germanium spectrometers, but the use of one source with established photon (gamma-ray or x-ray) emission rates at many energies often suffices and is more convenient. There is a further convenience if the radionuclides involved are long-lived, for experience has shown that system efficiencies should be checked periodically.

Inevitably, there are compromises in the composition of such standards, especially if they are to have a sufficient density of photon energies to define the calibration relation without a strong dependence on an assumed analytic relation. In selecting the components for the present long-lived mixed radionuclide standard, we considered the balance of emission rates at significant energies, spectral conflicts, source attenuation, simplicity in use, correlated summing, calibration difficulties, and the cost and availability of the radionuclides.

The standard is composed of  $^{125}\text{Sb}$  (with  $^{125\text{m}}\text{Te}$  in equilibrium),  $^{154}\text{Eu}$ , and  $^{155}\text{Eu}$ . Photon-emission rates for the major radiations have been measured with four germanium spectrometer systems especially calibrated for the purpose. These emission rates are specified with total uncertainties of from 0.6 to 1.3 percent, estimated to correspond to one standard deviation of the mean. The goal was to provide the users of the standards with a "realistic" uncertainty (as opposed to one which is very conservative) that can be combined with others entering into detector calibrations (such as those from counting statistics, geometry and rate differences, correlated summing, and peak evaluation) to generate an overall uncertainty for their calibration curves.

New information will be supplied to purchasers whenever we have reason to believe that an emission-rate value is different from that stated by 0.5 percent, or when the accuracy has improved significantly.

These standards supply many useful calibration points between 27 and 1596 keV, with other long-lived NBS standards such as  $^{60}\text{Co}$ ,  $^{133}\text{Ba}$ ,  $^{152}\text{Eu}$ ,  $^{207}\text{Bi}$ , and  $^{228}\text{Th}$  (plus progeny) available to fill in sparse regions and extend the calibrations to higher energies, if that is required. Standards of  $^{22}\text{Na}$ ,  $^{54}\text{Mn}$ ,  $^{88}\text{Y}$ , and  $^{139}\text{Ce}$  are also often available.

We will now describe some points that should be considered in using the standards, and in applying gamma-ray spectrometry in general. A bibliography at the end of the report lists a few significant references, some of which describe the techniques used in the gamma-ray emission rate measurements for these standards.

## 2. Calculation of Emission Rates at Later Times

The half lives of only  $^{125}\text{Sb}$ ,  $^{154}\text{Eu}$ , and  $^{155}\text{Eu}$  are involved in the calculation. However, the gadolinium x rays, which supply a useful calibration point for good-resolution detectors, result from both  $^{154}\text{Eu}$  and  $^{155}\text{Eu}$  decays and hence the calculation involves the sum of two components, as shown on the certificate notes. The half lives and uncertainties (from an unweighted average of recent values from 2 or 3 laboratories) are:  $^{125}\text{Sb}$  -  $1008.7 \pm 1.0$  days;  $^{154}\text{Eu}$  -  $3127 \pm 8$  days; and  $^{155}\text{Eu}$  -  $1741 \pm 10$  days.

We will continue to monitor the emission rate of pure samples of each radionuclide, and report to the purchasers any change that would make a difference of greater than 0.5 percent after 5 years.

## 3. Spectral Conflicts

A complete list of the more than 200 gamma rays reported for this mixture would discourage any consideration of using such sources as efficiency-calibration standards, but an examination of spectra (as shown in Figures 1 and 2) shows that there are about 20 dominant peaks, with few serious energy conflicts for good resolution detectors and few background difficulties (Compton edges or backscatter peaks) that interfere with peak-area analyses to more than one percent. For poorer-resolution detectors, the contributions of weak peaks in the 176-keV region must be considered, and the analysis of the triad at about 600 keV and the doublet at 1 MeV will present a challenge if the peaks are analyzed separately. However, a simple summing of channel contents, after an interpolated or extrapolated background has been subtracted, can give areas accurate to about 2 percent, for energies of 87 keV or greater. For all systems, the challenge of constructing a consistent and smooth calibration curve, within the uncertainties shown on the emission-rate table, may prove informative about techniques and uncertainties. We are investigating better analysis techniques, and would be interested in non-abusive user comments if discrepancies are found.

Above 120 keV, the accuracy of some NBS emission-rate values appear to be limited by peak analysis uncertainties rather than efficiency uncertainties for our detectors. Below 120 keV, the converse is true for gamma rays, with the paucity of reliable efficiency points making interpolations less certain. For the x rays, the deviation of our measured  $K_{\alpha}$  to  $K_{\beta}$  ratios from literature values indicates that peak-area measurements are less reliable for these radiations at the present time, and this is reflected in the uncertainties quoted.

Table 1 lists the dominant photon energies, and suggests where conflicts may occur. The probability of interfering gamma rays, relative to the probability of the dominant gamma ray, are from NBS measurements, or literature values for some very small contributions. Users can judge if conflicts are significant for their system resolution and their required uncertainties, and make corrections (some of which change with time) if necessary.

#### 4. Pulse-Summing Corrections

When two radiations strike a germanium detector within the shaping time of the amplifier, one or both can fail to be recorded in channels where they would have been otherwise. This time coincidence may occur because of an accidental overlap of pulses resulting from the decay of two separate nuclei, or it may arise from the detection of nearly simultaneous cascade radiations in the decay of the same nucleus.

In the former case of the accidental pile-up of pulses, the rate-dependent losses can be monitored with a constant-rate-pulsar peak or almost accounted for with a pile-up rejector and live-time circuit. The live timer of a slow multi-channel analyzer may provide a partial compensation, but this should not be assumed for total rates, above amplifier noise, of more than a few hundred counts per second.

The effect of correlated or cascade summing due to cascade radiations is not rate-dependent but depends on the efficiencies of the detector for the radiations involved, and can result in either the gain or loss of peak counts, depending on the decay scheme of a particular radionuclide.

If a gamma-ray transition competes with two cascade lower-energy gamma rays connecting the same two levels, the peak due to the "crossover" gamma ray may be enhanced by the "summing in" of counts due to correlated gamma-ray pairs which deposit the same energy in the detector. In general the effect is small because the product of peak efficiencies is small compared with the peak efficiency of the crossover gamma ray. (The peak efficiency,  $\epsilon_p$ , is defined here as the fraction of all emitted gamma rays which are recorded in a full-energy spectral peak.) But, if the crossover gamma-ray probability is much lower than that of those summing, the effect can be significant. This is true for the 1596-keV gamma ray in the decay of  $^{154}\text{Eu}$ , and corrections will have to be applied for accurate efficiency determinations even with moderate separations between detector and source.

If "summing in" occurs, the total peak area, compared to what it would have been otherwise, is  $1 + [K(a,b,c)\epsilon_p(a)\epsilon_p(b)/\epsilon_p(c)]$ , where indices a and b represent the cascade gamma rays and c represents the crossover, and  $K(a,b,c)$  is the probability for the a and b gamma rays to be emitted in cascade relative to the probability for the emission of c. If more than one pair of gamma rays can sum to the crossover energy, other terms like that in the square bracket must be added. Therefore, an observed peak must be divided by  $1 + \sum [K(a_j, b_j, c)\epsilon_p(a_j)\epsilon_p(b_j)/\epsilon_p(c)]$  in order to get the counts due to c alone. Table 2 contains values of  $K(a,b,c)$  which have been calculated for the three radionuclides.



Two factors usually make "summing out" of a peak due to the simultaneous detection of a correlated radiation much more significant. It is not required that the summing pulse is one that otherwise would have been stored in a peak; therefore, the total efficiency ( $\epsilon_t$  = the fraction of radiation emitted at a given energy that generates pulses of any size in the system) must be considered. This efficiency is often much greater than the corresponding  $\epsilon_p$ , so that it is easy to underestimate the effect if the areas of sum peaks are used as a measure. Secondly, the narrow peaks characteristic of germanium spectrometers suffer losses with any summed pulse, even quite small ones. Summing pulses smaller than those which would correspond to a full-energy peak for correlated radiations can result from Compton or photoelectric interactions in the shielding or can result from partial energy loss or incomplete charge collection in the detector.

It would then appear that the total efficiency would also have to be measured at many energies, but in general it varies slowly with energy above 100 keV, and attenuation in detector housings or added absorbers often reduce it in a calculable way at lower energies. Suggested radionuclides for total-efficiency measurements are  $^{125}\text{I}$ ,  $^{241}\text{Am}$ ,  $^{109}\text{Cd}$ ,  $^{139}\text{Ce}$ ,  $^{137}\text{Cs}$ ,  $^{54}\text{Mn}$ ,  $^{60}\text{Co}$ , and  $^{88}\text{Y}$ . All of these are issued as NBS standards, which are also useful for determining peak efficiencies. Alternatively, radionuclides can be calibrated with sufficient accuracy for total-efficiency measurements by the user from an efficiency-energy relation established with this long-lived standard at a sufficient distance from the detector that summing is small. Note that the effect of correlated summing may be significant, even for total-efficiency measurements, with  $^{125}\text{I}$ ,  $^{60}\text{Co}$ , and  $^{88}\text{Y}$ , if the geometry is tight. In any case, the contribution of x rays and other gamma rays must be removed by subtraction of known lower-energy contributions or extrapolation of the spectrum through low-energy-peak regions. A curve of the total efficiency vs energy for a point source at 26 centimeters from a 60-cm<sup>3</sup> wrap-around coaxial germanium detector is shown in Figure 3.

Beta-ray or conversion electron efficiencies may be appreciable if sufficient absorbers are not present, and can also cause "summing out". In most calculations, including the ones we are going to suggest, it is assumed that electrons, and L and higher-shell x rays, are not detected. K x rays often are important, especially in nuclides decaying by K-electron capture.

The peak area for the rth radiation with summing out by radiation s is related to that which would be measured without the effect by  $1 - K(s,r)\epsilon_t(s)$ , where  $K(s,r)$  is the probability for the simultaneous emission of the two. If there are other summing possibilities, the total effect is not simply  $1 - \sum K(s_j,r)\epsilon_t(s_j)$ . If the efficiency is large, additional additive terms such as  $\sum K(s_j,s_k,r)\epsilon_t(s_j)\epsilon_t(s_k)$  can be significant (and possibly analogous terms containing the product of three efficiencies must be subtracted, and so forth). We have calculated all pertinent Ks for these three radionuclides (and many other), and will supply the full set on request. However, the first-order terms given in Table 2 will probably be sufficient unless the source is close to the detector and the required accuracy is high.

There are two further complications. In general, angular correlations between pairs of correlated gamma-rays (not x rays) must be taken into account by introducing factors multiplying each  $K$ . For the present radionuclides these are sufficiently close to 1 that we do not list them here. This may not be true of other radionuclides that users wish to measure. The second complication is that the discussion so far has been for point sources; if the sources are extended, high accuracy results will require a measurement of  $\epsilon_t$  and a calculation of the summing effect at different locations, and then an integration over the volume of the source.

This discourse on summing effects does not appear because these standards are especially troublesome in this respect; quite the opposite is true. (Compare them with  $^{166}\text{Ho}$ !) If users must count at high efficiencies and yet require accuracies of better than 10 percent (or even 50 percent, in extreme cases), there is another alternative to the admittedly laborious summing corrections. They should ignore the concept of an efficiency-energy relation, and calibrate the detector directly in terms of apparent peak efficiency for selected gamma rays of the radionuclides which will be measured. If standards are not available, the radionuclides can be calibrated in the laboratory by establishing an efficiency-energy relation with this standard at a source-detector distance where summing is a fraction of a percent for all radionuclides (probably 25 centimeters or more). Concentrated solutions of the radionuclides (or mixtures thereof) can be calibrated at this distance, using tabulated  $P_{\gamma}$ s and taking into account container and source absorption and other corrections. These solutions can then be quantitatively diluted (to probably better than 1 percent by simple volume measurements, if the initial volume is greater than a few ml) and counted in the usual geometry.

#### 5. Other Gamma Rays

We have intentionally not given emission rates for weaker gamma rays, although many users might find them convenient. In many cases the values have not been measured well, as evidenced by the considerable discrepancy with literature values. If accurate values become available, purchasers of standards will be informed, although our feeling is that more accurate efficiencies will result from using separate standards with less background.

#### 6. Sample Preparation Considerations

The solution SRMs 4276 and 4276-B are provided in 4 M hydrochloric acid, which has a density of  $1.06 \text{ g cm}^{-3}$  at  $23^\circ\text{C}$ . They also contains 30  $\mu\text{g}$  each of  $\text{Sb}^{+3}$  and  $\text{Eu}^{+3}$  per gram of solution. A similar carrier solution should be used for dilutions.

If sources of this mixture are to be evaporated to dryness, care must be taken to avoid loss of  $^{125}\text{Sb}$  through volatilization. The present point-source standards (SRM 4275 and 4275-B) were prepared by taking to dryness deposited sources in a hydrogen sulfide gas atmosphere such that the antimony is precipitated as the orange  $\text{Sb}_2\text{S}_3$ .

TABLE 1

## Considerations for Peak Analysis for SRM's 4275-B and 4276-B

<u>Gamma Ray Energy (keV)</u>	<u>Source</u>	<u>Conflict</u>
27.4	$^{125}\text{Sb}$ - $^{125\text{m}}\text{Te}$ K $\alpha$ x ray	24.36 keV germanium escape peak from a 35.46 keV $\gamma$ in $^{125}\text{Sb}$ 26.51 keV $\gamma$ in $^{155}\text{Eu}$ 0.35% of the 27.4 keV K $\alpha$ -ray emission
42.8	$^{154}\text{Eu}$ - $^{155}\text{Eu}$ K $\alpha$ x ray	a) see footnotes
86.6	$^{155}\text{Eu}$	86.062 keV $\gamma$ in $^{155}\text{Eu}$ 0.49% of the 86.6 keV $\gamma$ emission
105.3	$^{155}\text{Eu}$	104.3 keV backscatter peak of the 176.4 keV $\gamma$ in $^{125}\text{Sb}$ 109.27 keV $\gamma$ in $^{125\text{m}}\text{Te}$ 0.49% of the 105.3 keV $\gamma$ emission
123.1	$^{154}\text{Eu}$	122.2 keV Compton edge of the 248.04 keV $\gamma$ in $^{154}\text{Eu}$
176.4	$^{125}\text{Sb}$	172.6 keV $\gamma$ in $^{125}\text{Sb}$ , 3.9% 178.8 keV backscatter peak of the 591.7 keV $\gamma$ in $^{154}\text{Eu}$ 179.35 keV average backscatter peaks of the 600.6 and 606.7 keV $\gamma$ 's in $^{125}\text{Sb}$
248.0	$^{154}\text{Eu}$	252.5 keV double-escape peak of the 1274.4 keV $\gamma$ in $^{154}\text{Eu}$
380.5	$^{125}\text{Sb}$	a) see footnotes
427.9	$^{125}\text{Sb}$	421.3-426.9 keV Compton edges of the 600.6 and 606.7 keV $\gamma$ 's in $^{125}\text{Sb}$
463.4	$^{125}\text{Sb}$	a) see footnotes
591.7	$^{154}\text{Eu}$	a) see footnotes
600.6	$^{125}\text{Sb}$	606.7 keV $\gamma$ in $^{125}\text{Sb}$ , 27.5% of the 600.6 keV $\gamma$ emission
635.9	$^{125}\text{Sb}$	a) see footnotes
723.3	$^{154}\text{Eu}$	715.8 keV $\gamma$ in $^{154}\text{Eu}$ 0.89% of the 723.3 keV $\gamma$ emission, b)
873.2	$^{154}\text{Eu}$	a) see footnotes
996.4	$^{154}\text{Eu}$	1004.8 keV $\gamma$ in $^{154}\text{Eu}$ 168.9% of the 996.4 keV $\gamma$ emission, b)
1004.8	$^{154}\text{Eu}$	996.4 keV $\gamma$ in $^{154}\text{Eu}$ 59.2% of the 1004.8 keV $\gamma$ emission, b)
1274.4	$^{154}\text{Eu}$	a) see footnotes
1596.5	$^{154}\text{Eu}$	a) see footnotes

a) No significant conflicts are expected for semiconductor detectors of good resolution.

b) Conflicts may depend on specific detector resolution and counting rates.

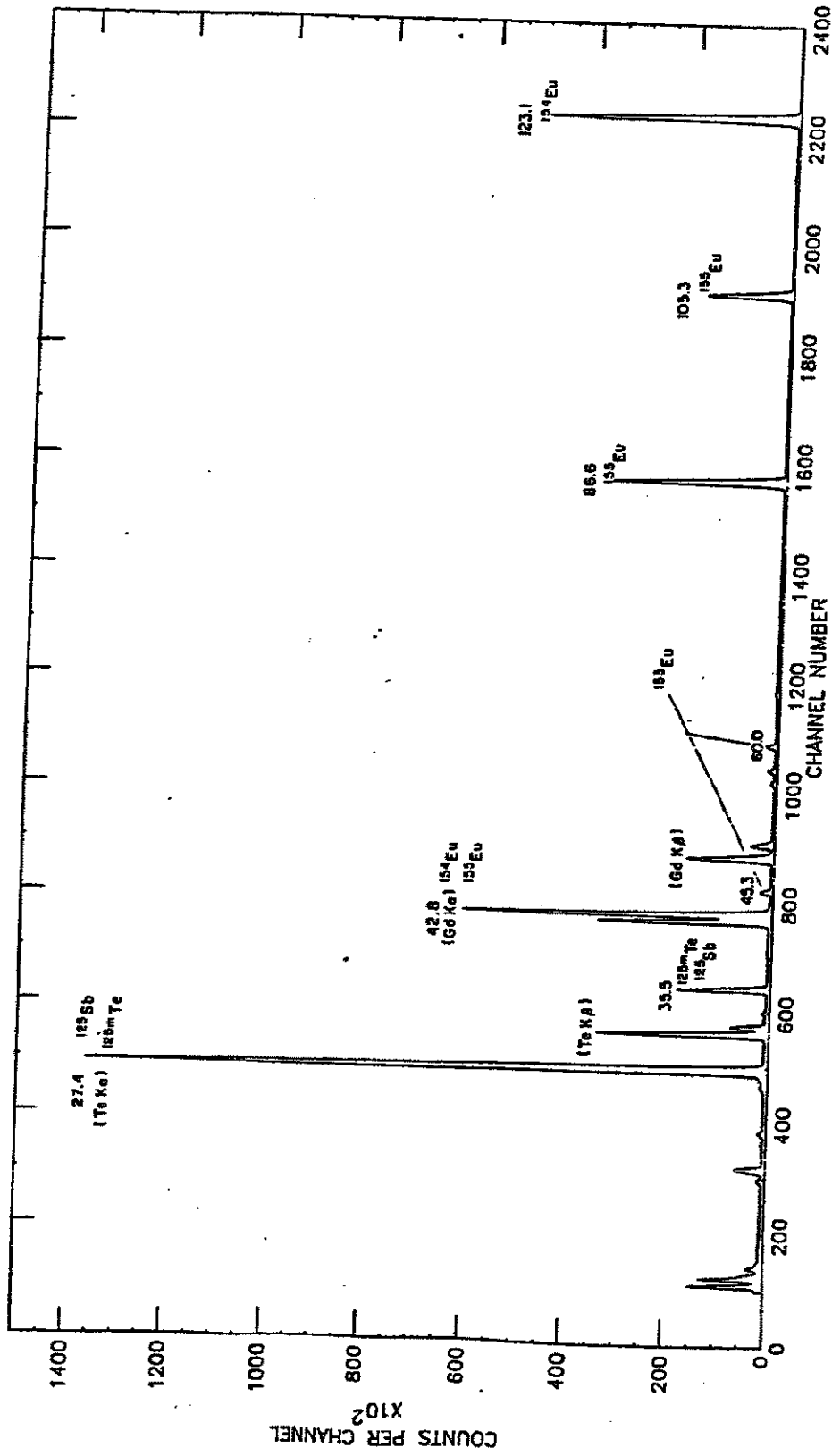


Figure 1. Spectrum of low-energy photons from SRM 4275 taken with a 200-mm<sup>2</sup> area, 5-mm-thick planar germanium detector at a source-to-detector distance of 15 cm.

---

# Origin and Effects of Impurities in High Purity Gold<sup>1</sup>

*David J Kinneberg and Stephen R Williams*

*Metalor USA Refining Corporation, PO Box 255, North Attleborough, Mass., USA*

*and D P Agarwal*

*Leach and Garner Company, PO Box 200, North Attleborough, Mass., USA*

Chemical specifications for high purity gold have grown increasingly stringent as manufacturers strive to improve quality control. Once 999.9-fine grain and bullion bars were accepted without question; today sophisticated users insist on knowing impurity levels or, at least, the source of the gold. This paper demonstrates why. Using glow discharge mass spectrometry, concentrations of seventeen elements were measured in hallmarked bullion bars and grain from different sources. In 89 percent of the samples, gold bullion met or exceeded hallmarked purities. As expected, the principal impurity was silver followed by iron, copper and lead. At surprisingly low levels, some impurities can impact manufacturing processes, resulting in hard spots, embrittlement, blistering, and discoloration. After reviewing why various impurities are not entirely removed by the prevalent refining processes, this paper examines the effect of the significant impurities on manufacturing processes. Since the only means of dealing with excessive impurity levels is to refine contaminated metal, we conclude that manufacturers are exercising reasonable prudence by carefully evaluating incoming gold bullion in order to hold down overall production costs.

Markets for gold bullion are robust and diverse; a wide array of choices is available to purchasers of gold bullion for jewelry manufacture. Commodity products range in purity from 995-fine 'good delivery' bars to kilobars and grain hallmarked at 999.9 fineness. (Fineness refers to gold content measured in parts per thousand; a fineness of 999.9 equals 99.99 per cent gold.) The option also exists for higher purities or bullion purchased against a company specification. Each of these products carries its own availability and price, on top of the usual variations in the market value of the gold.

How should a purchaser respond? On the one hand, lower grades (less than 999.5 fine) command little or no premium and are generally more readily available. On the other hand, while the gold content of bullion is precisely known, what else is present that could lead to manufacturing difficulties? Just how serious is the risk of impurities disrupting the manufacturing process or compromising product quality?

The purpose of this paper is to provide information on the quality of gold bullion. Since 999.9-fine gold has become the standard in the

marketplace, we focus on this commodity. What are the impurities in 999.9-fine gold and where do they originate? Which refining processes result in the lowest concentrations of impurities? And most important of all, which impurities carry the highest risk of disrupting a manufacturing operation? These are the questions we address as we explore whether buyers should purchase against a clearly defined specification of impurity levels or be content with a simple measurement of gold content. After all, 999.9 is almost 1000 - are further specifications warranted?

## CLASSIFICATION OF IMPURITIES

A natural starting point for discussing impurities in gold bullion is ASTM Specification B-562, the only widely accepted criteria for high-purity gold bullion. (This is not to say that ASTM B-562 is widely used in

---

<sup>1</sup> This article is based on a presentation given at the Santa Fe Symposium on Jewelry Manufacturing Technology, 1997

the industry as a purchasing specification; to enhance liquidity, bullion sellers and traders generally resist efforts to characterize impurities.) Table 1 summarizes impurity levels by bullion grade. At the low end of the spectrum, 99.5 grade (995 parts per thousand) simply requires a minimum gold content. This is the only grade that actually requires that the gold content be measured; gold contents for the other grades are calculated by difference. Five elements are considered in the specification of 999.5-fine gold. These include three elements commonly used as alloying agents (silver, copper and palladium) that will probably be added during manufacturing anyway. The other two elements, iron and lead, are recognized as having serious consequences during processing. The number of specified elements increases substantially in the 99.99 grade; thirteen elements are listed, from arsenic, bismuth and chromium to nickel, manganese and magnesium and ending with silicon and tin. Of course, the five elements of the 99.95 grade are included as well. Surprisingly, the list decreases in going to the 99.995 grade — arsenic and nickel are dropped. (For reference, Figure 1 graphically compares the magnitude of impurity levels by bullion grade.)

Now that the elements specified in ASTM B-562 have been presented, something must be said about the omissions. Platinum, a common impurity in gold, is not listed, presumably because it has a higher monetary value than gold and confers few deleterious effects during manufacturing. Other platinum group metals, rhodium, ruthenium, osmium and iridium, are also not specified, nor are any of the classic non-metallic

**Table 1** *Chemical requirements for gold bullion as given by ASTM B-562*

Gold Grade (%)	Concentration, mg/kg			
	99.5	99.95	99.99	99.995
Silver	-	350	90	10
Copper	-	200	50	10
Palladium	-	200	50	10
Iron	-	50	20	10
Lead	-	50	20	10
Silicon	-	-	50	10
Magnesium	-	-	30	10
Arsenic	-	-	30	-
Bismuth	-	-	20	10
Tin	-	-	10	10
Chromium	-	-	3	3
Nickel	-	-	3	-
Manganese	-	-	3	3

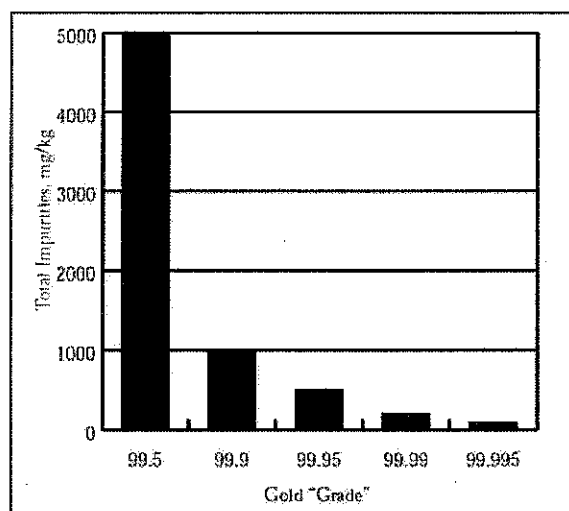


**Figure 1** *Total impurities as a function of gold grade*

elements. By this we mean, oxygen, sulfur and carbon. Chlorine, used in most gold refining processes in one form or another, is not mentioned. Again one assumes that these elements have been found historically to be irrelevant in characterizing gold or do not have a major impact on gold alloys (a potentially risky assumption in the case of chlorine which can react with all major constituents of jewelry alloys). Other elements that impact alloy properties and would be suspected to be present in gold from primary sources, yet are not included in ASTM B-562, are antimony, selenium, tellurium and mercury. Thus ASTM B-562 presents a variety of metallic elements for consideration but omits many others. To protect themselves, industrial buyers often target other elements. (In fact ASTM B-562 clearly states that, "by agreement between purchaser and manufacturer, analyses may be required and limits established for elements not specified" by ASTM B-562.)

Of the approximately one hundred elements, relatively few require measurement by industrial or commercial agreements. Of course, analyzing for all elements would be difficult and costly and serve no practical purpose. In this regard, the argument for 'indicator' elements has merit. By this, we mean selecting one element from a chemical family whose concentration serves as an indicator for other elements in the family. Thus palladium can be viewed as an 'indicator' for platinum-group metals; high palladium concentrations point to the need to check for other family members while low values indicate that other platinum-group metals are probably not present. Combining the use of 'indicators' with a knowledge of which elements may be

---

present in refined gold and which may be deleterious to manufacturing operations allows the list of candidate elements to be dramatically reduced.

Nadkarni and Agarwal (1) classified gold impurities into three categories: metallic or elemental, non-metallic and radioactive. Radioactive impurities in gold, such as uranium and thorium, are important to industrial users because of the effects of small amounts of radiation on electronic components but are not generally a concern to jewelry manufacturers. We will not consider radioactive impurities further. Similarly, non-metallic impurities, for example oxide particles containing chromium or magnesium that cause problems when gold is formed into very thin wires or strips for industrial products, will not be discussed. Elemental impurities, fortunately the easiest to detect, form the most important class of impurities with regard to jewelry fabrication. Here we will consider silver (more because it serves as a convenient model for discussing mechanisms of impurity transport during refining than because of manufacturing implications), lead, iron, and silicon and other related metals. But before discussing the effect of impurities during manufacturing, it is necessary to consider methods for measuring the concentrations of these elements in gold bullion and review how small concentrations of these elements traverse the refining process.

## ANALYTICAL METHODS

Fire assay, one of the most precise and robust analytical techniques developed by mankind, has little or no place in a discussion of impurities in gold bullion. Since a fire assay consists of collecting the precious metals from a particular sample into a bead and comparing the weight of that bead against the original sample weight, the technique is limited to measuring overall precious metal content. While fire assay can determine whether bullion is 995 or 999 fine, up to a limit of 999.9 fine, it cannot identify which impurities are present nor their respective concentrations. For this reason, ASTM B-562 requires a minimum gold content, performed by fire assay, only for the 99.5 grade. For higher purities, the concentrations of significant trace elements are measured and the balance assumed to be gold. Obviously when using such a method, all significant impurities must be considered, otherwise the calculated gold content will be in error. Fire assay can be used as a check.

Several techniques exist for measuring impurity levels in gold bullion. Most commonly, a sample is dissolved

into solution and the concentrations of the various elements are measured by spectroscopic means. This can be done by atomic absorption spectrometry or D.C. plasma spectroscopy (2). I.C. plasma spectrometry can be used for solutions or, in some cases, can analyse a solid sample directly. The advantages of eliminating the dissolution step are twofold: (1) if an impurity does not dissolve, its concentration cannot be determined in solution; and (2) impurities from glassware and laboratory reagents do not contribute to the measurement. Other techniques that avoid dissolution are mass spectroscopy, X-ray fluorescence and spark or arc emission techniques. Of these, mass spectroscopy has emerged as the technique of choice for high-purity materials because of its ability to measure trace concentrations of virtually all elements. This feature alone minimizes the risk of overlooking a particular element when determining gold content by difference.

While bullion producers rely on several techniques for measuring 'average' or 'bulk' concentrations of impurities in gold, other techniques are more appropriate for jewelry manufacturers. In particular, a scanning electron microscope (SEM) equipped with an EDS (Energy Dispersive Spectrometer) probe allows one to 'focus' into very specific areas on a specimen and determine 'localized' concentrations (3). If a fracture occurs, or a hard spot exists, those elements present at the point of trouble can be determined. This is crucial since deleterious elements tend to segregate along grain boundaries and lattice imperfections leading to 'localized' concentrations that are many times larger than 'bulk' concentrations. While bullion producers must rely on 'bulk' methods to characterize their homogeneous product, jewelry manufacturers must recognize that small 'bulk' concentrations can lead to highly concentrated 'localized' impurity levels.

## REFINING PROCESSES

### *Process Descriptions*

There are basically two approaches for refining gold (4). The first and oldest (dating back to the discovery of nitric acid in the Middle Ages) is dissolution followed by precipitation. Impure gold is dissolved into a chloride solution using a strong oxidant such as nitric acid. The solution is then filtered to separate undissolved or precipitated impurities (principally silver chloride) from dissolved species. After filtering, a selective reductant, generally a sulfur compound such as sodium sulfite or sulfur dioxide gas, is added to precipitate gold as a sponge. The sponge is rinsed several times, dried and melted.

---

Much research has been performed on improving the dissolution/precipitation process in recent years. Besides examining a wide range of oxidants and precipitation agents, solvent extraction has been incorporated into the process. In this step, dissolved gold is selectively transferred from an impure aqueous solution into an organic phase and then returned to a relatively pure aqueous phase for reduction. Direct reduction from the organic phase is also possible. The selective action of the organic reagent rejects unwanted impurities and allows reduction to be carried out from a 'purified' process stream.

The other established refining process, and the one practiced by most diversified refineries, is chlorination followed by electrorefining. This process has been in existence, basically unchanged, for over one hundred years. During chlorination, impure gold is charged to a furnace, and after melting, chlorine gas is sparged into the bath. Chlorine bubbles, rising upwards through the molten metal, initially react with base metal impurities such as iron and zinc to form volatile metal chlorides that leave the furnace. Once the gaseous metal chlorides are removed, molten chlorides of copper and silver form and float to the surface of the melt to be removed as a slag. Given enough chlorine, essentially all the base metals and silver can be removed, resulting in gold purities of up to 99.5% if platinum-group metals are not present. (Platinum-group metals do not react with chlorine.) At this point, however, gold begins to react with chlorine and form gaseous chlorides. To prevent gold losses, most refineries stop chlorinating well below 99.5% and pour off the product to be refined electrolytically. Chlorination is commonly known as the Miller process after one of its first practitioners.

Relatively pure gold from the chlorination furnace containing small amounts of base metals along with platinum-group metals is next cast into anodes. The anodes are immersed in a warm solution of gold chloride opposite cathodes made of titanium or thin gold strips. An electric current is forced to flow between electrodes causing gold in the anodes to dissolve into solution and gold in the solution to deposit on the cathodes. Impurities in the anodes either form insoluble particles (principally silver chloride) or dissolve into solution but do not deposit on the cathodes. Over time, soluble impurities build up in solution requiring that it be replaced. Cathode deposits from the cells are stripped (if titanium blanks are used), thoroughly rinsed and melted. Electrolytic refining of gold is known as the Wohlwill process after its inventor.

Each of the two refining schemes has its advantages and disadvantages (5). Miller/Wohlwill requires a significant capital expenditure (both for equipment and operating capital), but is capable of handling a wide diversity of incoming feedstocks. Dissolution/precipitation can be carried out at any scale at a rapid pace but is only applicable to acid-soluble feedstocks. Since both processes rely on aqueous chloride chemistry, the mechanisms by which impurities contaminate the final product are similar.

### *Mechanisms of Contamination*

Inevitably, the principal contaminant in high purity gold is silver. Comprehensive discussions of silver as an impurity can be found in the literature (6). Other than diminishing the intrinsic value of the final product, the small concentrations of silver found in 999.9-fine gold have little deleterious effect on jewelry manufacturing processes; in most cases, much greater amounts of silver are being added anyway. (Typically, 10K and 14K alloys contain over 10 percent silver.) However, the mechanisms by which silver contaminates refined gold are worthy of discussion since other impurities follow similar paths; and, as a chloride salt, silver can carry with it a much less tolerable impurity, namely chloride.

In oxidizing solutions with high excess chloride concentrations, silver is soluble to a surprising degree. A typical solution at room temperature can hold over 1 g/l Ag as a complexed chloride species  $\text{Ag}(\text{Cl})_x^{1-x}$  where  $x$  can range from 1 to 3. Other factors further enhance silver chloride solubility, principally temperature (elevated in refining solutions to promote rapid kinetics) and aging time (silver chloride particles are freshly formed in refining solutions and as such are very amenable to dissolution). Thus silver is present as finely divided silver chloride particles and as dissolved silver chloride complexes. At least three avenues therefore exist for contamination to occur:

- 1 Migration/convection of particles to a porous gold surface followed by entrapment in the solid;
- 2 Entrainment of solution in the porous gold surface; and
- 3 Reduction from solution and incorporation into the lattice.

Of these, the first predominates. Cathodes from a Wohlwill operation or sponge from precipitation are always rinsed in solutions specially selected to dissolve silver chloride.

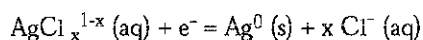
Accepting that process solutions always contain solid silver chloride particles, various strategies have been developed to prevent particle transport into the gold product. Here the leach/precipitation process



offers advantages over electrowinning (assuming, of course, that feedstocks do not contain so much silver that dissolution is impeded by the formation of tightly adhering silver chloride, in which case, dissolution cannot be used). Leach solutions generally are allowed to cool before being passed through highly retentive filters prior to precipitation. Besides removing silver chloride, other insoluble or 'slimes' constituents are removed as well. These include platinum-group metals (rhodium, osmium and iridium). Even after filtration, silver chloride particles can precipitate out of solution because of dilution effects when gold is precipitated. In the Miller/Wohlwill process, most silver is removed during chlorination. But the small amount remaining is not captured during electrolysis by filtering solutions. Instead, quiescent or mildly stirred conditions are maintained to allow particulates to settle to the bottom of electrolytic cells. Some operations utilize porous bags to retain silver chloride slimes in the vicinity of the anode.

Any solution caught in porous cathodes or gold sponges carries with it all of its dissolved constituents. These impurities precipitate as salts during drying or melting. At that point, whether the impurity dissolves into molten bullion depends on salt stability at high temperatures and in the presence of reducing agents (for example, graphite in the crucible). While silver chloride is thermally stable, it can be reduced relatively easily into a gold matrix. Thus, most dissolved silver chloride carried out of the precipitation reactor or electrolytic cell, ends up in the final product as metallic silver. Other soluble impurities such as palladium and platinum will also be reduced to the metallic state during melting while others such as calcium and sodium will not be. Copper, found in high concentrations in dissolution liquors and electrolytes, can be captured by suitable fluxing.

The last mode of silver contamination is reduction to the metallic state in the precipitation stage or by the cathodic potential. The chemical reaction for silver chloride reduction can be written:



where electrons are supplied either by the reducing agent during precipitation or at the cathode during electrorefining. Thermodynamically, this reaction should not proceed if even small concentrations of gold are present in solution, assuming a unit activity for the solid. However, silver is actually being reduced onto a gold lattice containing little silver. This additional driving force must contribute to some

reduction. A detailed investigation of this mechanism would be useful but to date nothing has been reported in the open literature. Other elements may also be reduced. Lead, thallium and bismuth and mercury all act as depolarizers in gold plating baths (7). These elements form adsorbed monolayers on gold surfaces at potentials positive to those at which bulk cathodic deposition begins. Such phenomena may also occur in chloride solutions.

The rationale for solvent extraction should be apparent from this discussion. By extracting gold from leach solutions into another liquid phase, one can avoid the carry-over of impurity elements and subsequent contamination of precipitated gold. Nevertheless, small concentrations of some impurities such as silver still find a route into the final product, either by physical entrainment or coextraction.

## GOLD BULLION SURVEY

To get an idea of the range of impurities found in fine gold bullion in today's market, we purchased gold grain or small bars from nine different refineries and analyzed the gold bullion by glow discharge mass spectroscopy. Refineries were selected based on the availability of their product to US jewelry manufacturers. Large, integrated facilities known to practice chlorination/electrorefining were selected along with smaller refineries which practice dissolution/precipitation. No attempt was made to make the sampling statistically meaningful. Rather, grain or bars were purchased from standard sources on a 'grab' basis - the sample grabbed by the seller was the sample analyzed. If the purchase was grain, a small amount of sample was melted in a laboratory induction furnace and poured into a pin mold. If the sample was a bar, drill samples were taken and the drillings melted in the laboratory furnace to produce a pin. (To confirm that no contamination occurred during drilling, a drill sample from one bar was compared with a sample taken with an evacuated glass tube after the entire bar was melted.) Concentrations of seventeen metallic elements were measured in the samples. Results are presented in Table 2.

Of the samples acquired, nearly 89 percent met or exceeded their hall-marked purity levels. Sample A failed. In this case, the gold grain contained over 2000 mg/kg of various impurities. While conclusions should not be drawn about the marketplace as a whole from a non-statistical survey, this illustrates why consumers must deal with reputable sources capable of providing certified analyses of their products.

**Table 2** Concentration of impurities in bullion products from nine different precious metal refineries as measured by glow discharge mass spectroscopy. All values given in mg/kg (ppm), except for gold which is given in parts per thousand

Element	Concentration, mg/kg								
	A	B	C	D	E	F	G	H	I
Mg	0.1	0.2	0.1	0.1	0.5	0.3	0.1	0.5	0.1
Si	0.6	0.7	1.0	0.5	0.0	0.0	0.0	0.0	2.6
Cr	0.3	0.1	0.1	0.1	0.5	0.2	0.2	0.3	0.6
Mn	0.5	0.2	0.1	0.1	0.3	0.2	0.1	0.3	0.4
Fe	8.8	2.4	4.5	2.4	4.1	6.8	3.5	4.0	1.7
Ni	2.7	0.4	0.1	0.3	0.2	0.2	0.1	0.2	0.2
Cu	103.7	4.9	1.6	1.3	4.3	0.8	0.9	1.4	12.4
As	0.2	0.0	0.0	0.0	0.1	0.1	0.1	0.1	0.0
Zr	0.2	0.0	0.0	0.0	0.1	0.9	0.1	0.2	0.0
Pd	4.3	1.3	1.2	0.7	0.9	0.8	2.4	0.5	7.3
Ag	2300.0	43.2	57.8	55.9	35.5	40.4	18.5	115.8	26.3
In	0.5	0.1	0.0	0.1	0.1	0.0	0.0	0.1	0.0
Sn	13.3	0.4	0.4	1.2	0.3	0.2	0.5	0.6	0.3
Ir	0.0	0.0	0.3	0.2	0.4	0.1	0.2	0.0	0.6
Pt	0.1	0.9	0.3	0.2	0.6	0.2	1.2	0.0	3.6
Pb	6.2	2.3	0.1	0.1	0.2	0.1	0.2	1.9	0.1
Bi	0.3	0.3	0.1	0.3	0.0	0.1	0.3	0.6	0.5
SUM	2441.7	57.2	67.8	63.4	48.2	51.5	28.4	126.6	56.6
Au (measured) ppt	997.56	999.94	999.93	999.94	999.95	999.95	999.97	999.87	999.94
Au (as purchased) ppt	999.5+	999.9+	999.9+	999.5+	999.9+	999.9+	999.9+	999.5+	999.9+
Form	Grain	Bar	Bar	Bar	Grain	Grain	Grain	Grain	Grain

The data in Table 2 show that, as expected, silver was the predominant impurity in all samples, at much higher concentrations than any other element. For 999.9+ fine gold, silver concentrations ranged from less than 20 mg/kg in two cases, to about 70 mg/kg. For 999.5-fine gold, silver was up to 120 mg/kg. (Sample A had 2000 mg/kg). Other elements were found at levels substantially less than 10 mg/kg. Next to silver, iron and copper were the next most prevalent impurities at concentrations of about 5 mg/kg. Lead was measured at approximately 1 mg/kg. Other elements found at about the 1 mg/kg level were palladium, platinum and silicon.

The range of impurity concentrations from batch to batch for two different refineries is presented in Table 3. Here four different batches of 999.9-fine gold grain from each refinery were analysed separately. Variation is plainly evident but not so much as to negate the observations given above.

Lastly, for the sake of completeness, two samples were subjected to a complete elemental scan to determine if any impurities had been overlooked. The

results are presented in Table 4. Because of the need for precise standards when performing such analyses and the fact that these standards are not available for many of the elements included in Table 4, results are given as 'less than 1 mg/kg' for elements measured at the parts per billion level. Results for nitrogen, oxygen and chlorine are not reported for similar reasons. As indicated, there are no other elements in these samples at concentrations above 1 mg/kg except those that were initially selected for analysis.

Overall, the fineness of 89 percent of the gold bullion acquired in this survey met ASTM specifications. In these samples, few elements other than gold were found in gold bullion at measurable levels. Of these impurities, silver predominated. Significant concentrations of copper, platinum, palladium, lead and, in some cases, silicon, were found. (All of these elements, except platinum, are included in ASTM B-562, more or less validating its selection of impurities.) Given that silver and copper are common alloying elements, we will only further address the other

**Table 3** Variation in impurity concentrations for bullion products from two different precious metal refineries as measured by glow discharge mass spectroscopy. All values given in mg/kg (ppm), except for gold which is given in parts per thousand

Element	Concentration, mg/kg							
	E1	E2	E3	E4	I1	I2	I3	I4
Mg	0.2	0.4	0.1	0.5	0.1	0.0	0.0	0.1
Si	0.0	0.0	0.4	0.0	2.6	0.9	0.7	1.6
Cr	0.2	0.4	0.1	0.5	0.6	0.1	0.2	0.2
Mn	0.2	0.3	0.1	0.3	0.4	0.1	0.2	0.2
Fe	6.0	9.7	3.2	4.1	1.7	0.7	0.7	2.8
Ni	0.2	0.2	0.1	0.2	0.2	0.1	0.1	0.1
Cu	5.0	7.2	3.3	4.3	12.4	4.5	6.9	7.4
As	0.1	0.2	0.1	0.1	0.0	0.0	0.0	0.0
Zr	0.1	0.2	0.1	0.1	0.0	0.0	0.1	0.0
Pd	1.2	1.5	0.7	0.9	7.3	3.4	4.5	3.3
Ag	32.4	42.1	18.8	35.5	26.3	72.5	49.8	69.9
In	0.1	0.1	0.0	0.1	0.0	5.8	3.8	0.1
Sn	0.3	0.3	0.2	0.3	0.3	0.2	0.2	0.3
Ir	0.5	0.5	0.4	0.4	0.6	0.3	1.2	1.1
Pt	0.8	1.0	0.7	0.6	3.6	1.7	2.5	2.0
Pb	0.4	0.1	0.1	0.2	0.1	0.0	0.0	0.0
Bi	0.3	0.8	0.3	0.0	0.5	0.3	0.5	0.3
SUM	48.1	65.2	28.7	48.2	56.6	90.9	71.4	89.3
Au (measured) ppt	999.95	999.93	999.97	999.95	999.94	999.91	999.93	999.91
Au (as purchased) ppt	999.9+	999.9+	999.9+	999.9+	999.9+	999.9+	999.9+	999.9+
Form	Grain	Grain	Grain	Grain	Grain	Grain	Grain	Grain

three significant contaminants, lead, iron and silicon, which are known to have deleterious effects during manufacturing.

## EFFECTS OF IMPURITIES

Given that measurable quantities of lead, iron and silicon are found in most bullion products, it is appropriate to review at what concentration levels these elements begin causing problems during the manufacturing process.

### Lead

Lead is one of the most (if not the most) detrimental of bullion impurities in applications requiring mechanical working and high ductility. Rose (8) noted as early as 1894 that "less than 0.1 percent bismuth, tellurium or lead renders the gold brittle, owing to the distribution of Bi, AuTe<sub>3</sub>, or Au<sub>2</sub>Pb between the grains." Rose referred to Nowack (9) who showed that at 600 mg/kg lead, both a 10% copper-gold alloy and pure gold

are unrollable but that additions of 50 mg/kg had no effect. Even so, many manufacturers set 50 mg/kg as their upper limit for acceptable lead concentrations. Without question, the concentration at which lead causes embrittlement is low, probably less than 100 mg/kg.

Figures 2 and 3 present visual proof of the effect of lead on gold alloys. Figure 2 shows an SEM micrograph of a gold-lead compound at the grain boundary of 14K white gold. In this case, the average concentration of lead in the sample was 400 mg/kg. Figure 3 shows another example of lead segregation at grain boundaries. Here, the light-colored particles are gold-lead precipitates covering the surface of a grain exposed after a fracture occurred in a 14K alloy.

### Iron

From a solubility viewpoint, iron should not segregate in gold alloys. Alloys containing up to 25 percent iron have been used for jewelry in Europe. Rose (8) noted that additions of even more than 1 percent iron have only a slight effect on the rolling properties of gold. The phase diagram for gold-iron bears this out.

**Table 4** Concentration ranges for elements detected in gold bullion samples by glow discharge mass spectroscopy

		Concentration, mg/kg			
Sample J		Sample K			
<1	1-10	>10	<1	1-10	>10
Be, B	Si	Li	Li, Be	Ti	Ag
Mg, Al	P	Na	B, Na	Cu	
Cl, K	Ti	Cu	Mg, Al	Ru	
Ca, Sc	Fe	Ag	Si, P	Pd	
V, Cr	Zn		Cl, K	Ir	
Mn, Co	Ga		Ca, Sc	Pt	
Ni, Ge	Pd		V, Cr		
As, Br	Pt		Mn, Fe		
Se, Rb	Pb		Co, Ni		
Sr, Y			Zn, Ga		
Zr, Nb			Ge, As		
Mo, Ru			Br, Se		
Rh, Cd			Rb, Sr		
In, Sn			Y, Zr		
Sb, I			Nb, Mo		
Te, Cs			Rh, Cd		
Ba, La			In, Sn		
Ce, Pr			Sb, I		
Nd, Eu			Te, Cs		
Sm, Gd			Ba, La		
Tb, Dy			Ce, Pr		
Ho, Er			Nd, Eu		
Tm, Yb			Sm, Gd		
Lu, Hf			Tb, Dy		
Ta, W			Ho, Er		
Re, Os			Tm, Yb		
Ir, Hg			Lu, Hf		
Tl, Bi			Ta, W		
Th, U			Re, Os		
			Hg, Tl		
			Pb, Bi		
			Th, U		

However, as anyone who has ever tried to prepare gold standards containing a small amount of iron knows, it is not a trivial matter to add 100mg/kg iron to pure gold and end up with a homogeneous alloy. While iron should dissolve into pure gold from a thermodynamic standpoint, its relatively high melting point makes the addition of small amounts of iron to gold difficult. Conversely, small amounts of iron can solidify in casting alloys, causing 'hard spots', if conditions are right.

Figure 4 demonstrates this point. Shown at 144 X magnification is a hard spot on the surface of a 10K casting ring. An EDS analysis showed that iron was present in the alloy along with boron. Figures 5 and 6 give further evidence of iron inclusions. Figure 5 shows the surface of a casting at low magnification while Figure 6, at higher magnification, indicates iron particles as dark spots in the alloy matrix. Thus iron, when crudely added to gold alloys, can lead to surface imperfections and hard spots. However, the small concentrations of iron found in gold bullion are already dissolved in gold and unless another element is added to the mixture that would cause iron to coprecipitate, such phenomena are unlikely.

### Silicon

A classic example of the insolubility of one element in the solid matrix of another is the gold-silicon system. There is practically no solubility of silicon in gold. It has been shown that silicon tends to segregate as separate particles in gold at levels as low 200 mg/kg (10). Figure 7 presents an SEM micrograph from this work showing black specks of segregated silicon whose 'bulk' concentration was measured to be 200 mg/kg. Levels of silicon above 200 mg/kg typically result in the formation of a gold-silicon eutectic at grain boundaries. The segregation of the eutectic at the boundaries makes gold extremely brittle and can cause problems during soldering operations (11).

Silicon is commonly added to karat gold castings as a brightening agent. Occasionally, however, some castings exhibit 'hard spots', a defect typically associated with silicon segregation. Figure 8 shows a hard spot consisting of segregated particles of silicon. This type of casting defect was found in the cross section of a 10K yellow ring.



**Figure 2** SEM micrograph of lead segregation at the grain boundaries of a continuously cast 14K white gold. Average lead concentration measured at 400mg/kg by atomic absorption spectroscopy (2,420 x magnification)



**Figure 3** SEM micrograph of the surface of a grain exposed after fracture occurred in a 14K alloy. Light areas represent lead precipitate (7,500 x magnification)

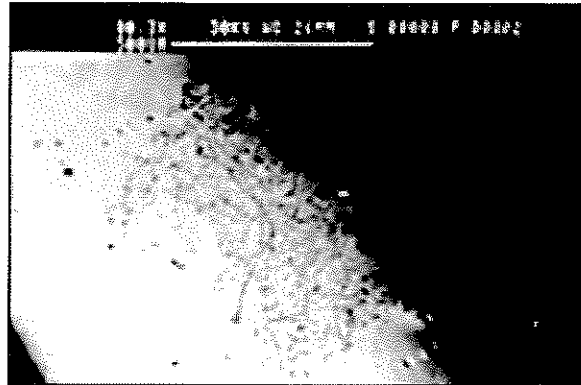


**Figure 5** SEM micrograph of the surface of a gold alloy showing iron inclusions (80.3 x magnification)

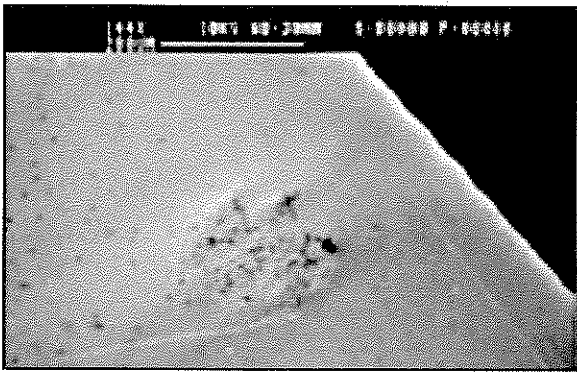


**Figure 4** SEM micrograph of the surface of a 10K casting ring showing a hard spot caused by iron and boron (144 x magnification)

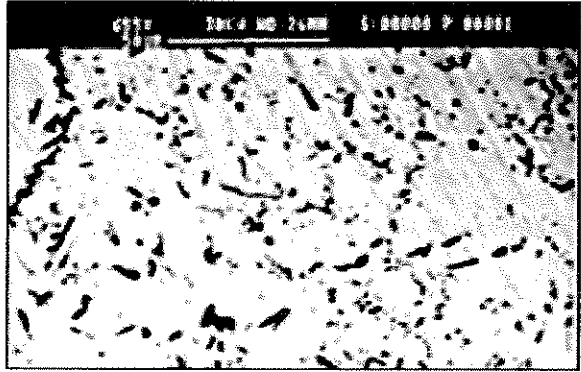


**Figure 6** SEM micrograph of the iron inclusions shown in Figure 5 at higher magnification. Dark areas represent iron particles (655 x magnification)

Silicon can also combine with other elements in the gold alloy and precipitate as a compound at grain boundaries. The segregation of silicon and iridium is shown in Figure 9. In this micrograph of a 14K yellow ring, the dark areas show silicon and the bright areas iridium. This type of segregation appeared as a white discoloration on the cast surface. Silicon can also combine with nickel, forming nickel silicide in 10K white castings (10). Once again, nickel silicide forms at the boundaries between the alloy grains leading to embrittlement of the casting.

## CONCLUSIONS

In this paper, we have reviewed the various issues associated with impurities in gold bullion. After discussing the two basic refining processes in use

today, we described how it is possible that small amounts of some elements can traverse the purification sequence and contaminate fine gold. Several mechanisms exist for contamination to occur and one refining process, per se, does not have a particular advantage over the other with regard to purity. If properly operated, both the classical chlorination/electrorefining and dissolution/precipitation refining processes result in high-quality gold. If operated improperly, neither does. We then surveyed the output from nine different refineries that produce gold grain and bars commonly used by jewelry manufacturers. Using glow discharge mass spectroscopy, we found that in nearly 89 percent of the samples acquired in our survey, the gold bullion met or exceeded hallmarked purities. The distribution of impurities was remarkably similar regardless of refining technique. As expected the major impurity in

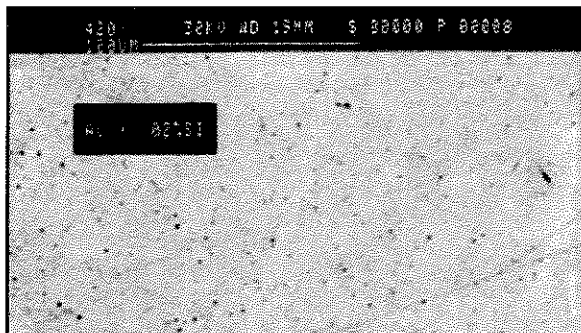


**Figure 7** SEM micrograph of silicon particles dispersed in gold matrix. Average concentration of silicon measured at 200 mg/kg (424 x magnification)

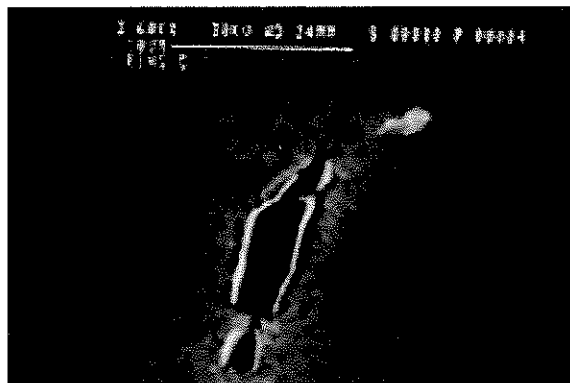


**Figure 8** SEM micrograph of silicon segregation at the grain boundaries of a 10K alloy (3,360 x magnification)

fine gold was silver. Other elements found in significant concentrations were iron, copper, lead and silicon.

Of the elements found in refined gold, lead and iron typically have the most potential to disrupt the jewelry manufacturing process. We reviewed how lead, iron and silicon, as well as combinations of silicon with other elements, can lead to embrittlement and hard spots. Because these impurities segregate at grain boundaries, low levels measured in 'bulk' techniques can be misleading. It is only by carefully controlling the purity of all constituents in a jewelry alloy, including additives, that the quality of the final product can be assured. In this respect, having certified analyses of all materials, including fine gold, minimizes the risks and simplifies investigations of problems should they arise.

## ABOUT THE AUTHORS

David Kinneberg is Director of Research and Development and Stephen Williams is Vice President of Sales and Marketing in Metalor Refining Corporation, USA; D.P. Agarwal is Vice President of Leach and Garner Company. They each have a special interest in the production of pure gold.

## REFERENCES

- 1 R.M. Nadkarni and D.P. Agarwal, 'Impurities in Gold: Pedigree versus Specification', *Precious Metals 1988*, Int. Precious Metals Inst., Allentown, PA, p.283
- 2 A. Savolainen, 'Modern Gold Assaying', *Precious Metals 1988*, Int. Precious Metals Inst., Allentown, PA, p.55

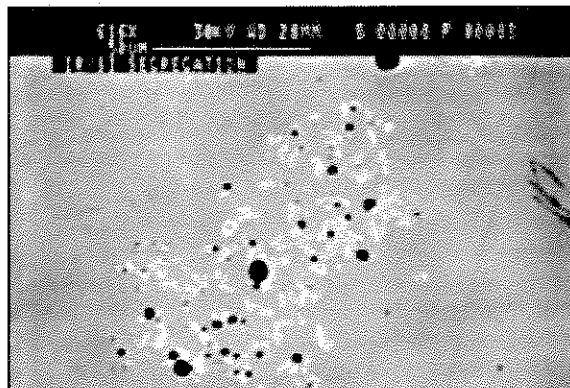


**Figure 9** SEM micrograph of iridium/silicon segregation in a gold alloy (616 x magnification)

- 3 D.P. Agarwal and G. Raykhtsaum, 'Materials Characterization and Failure Analysis in Jewelry Scientific Instrumentation', presented at the Santa Fe Symposium on Jewelry Manufacturing Technology, 1992
- 4 R.M. Nadkarni, D.J. Kinneberg, M.B. Moolman and P. Cettou, 'Precious Metals Processing', Elliott Symposium, Iron and Steel Society, Warrendale PA, 1990, p.96
- 5 D.J. Kinneberg, M.B. Moolman and W.D. Müller, 'Gold Refining - Past, Present and Future', *Precious Metals 1986*, Int. Precious Metals Inst., Allentown, PA, 1986, p.433
- 6 D. Schneller, 'Silver Contamination in Fine Gold', presented at 'Refining and Recovery of Precious Metals', Int. Precious Metals Inst., Los Angeles, CA, March 1986
- 7 J.D. McIntyre and W.F. Peck, Jr., 'Electrodeposition of Gold', *J. Electrochem. Soc.*, 1976, 123 (12), 1800
- 8 T.K. Rose and W.A.C. Newman, 'The Metallurgy of Gold', Reprint of 7th Ed., Met-Chem Research, Inc., Boulder, CO, 1986, p.36
- 9 Z. Nowack, *Z. anorg. Chem.*, 1926, 154, 395
- 10 G. Raykhtsaum and D.P. Agarwal, 'Gold in Jewelry', *Precious Metals 1993*, Int. Precious Metals Inst., Allentown, PA, p.169
- 11 G. Raykhtsaum and D.P. Agarwal, 'Defects in Castings and Wrought Products Associated with the Phenomenon of Segregation in Karat Golds', presented at the Santa Fe Symposium on Jewelry Manufacturing Technology, 1993

### Equipment Required

- |  |   |
|--|---|
| <ul style="list-style-type: none"><li>• <b>GEM10-70/CFG-SV-70/DWR-30</b> Coaxial Germanium Detector System (Includes detector, preamplifier, cryostat, liquid-nitrogen dewar, and 12-ft. cable pack); typical specifications: 10% relative efficiency, 1.75 keV resolution at 1.33 MeV, 41:1 peak-to-Compton ratio.</li><li>• <b>659</b> 5 kV Detector Bias Supply</li><li>• <b>672</b> Spectroscopy Amplifier</li><li>• <b>480</b> Pulser</li><li>• Four each <b>C-24-4</b> RG-62A/U 93-Ω Coaxial Cables with BNC Plugs, 4-ft. (1.2-cm) length</li><li>• <b>C-29</b> BNC Tee Connector</li><li>• <b>4001A/4002D</b> NIM Bin and Power Supply</li><li>• <b>EASY-MCA-8K</b> System including a USB cable, and MAESTRO software (other ORTEC MCAs may be substituted)</li><li>• <b>TDS3032C</b> Oscilloscope with bandwidth <math>\geq 150</math> MHz</li><li>• <b>GF-057-M-20*</b> 20 <math>\mu\text{Ci}</math> <math>^{57}\text{Co}</math> (272-d half life). A license is required for this source.</li></ul> | <ul style="list-style-type: none"><li>• <b>GF-137-M-20*</b> 20 <math>\mu\text{Ci}</math> <math>^{137}\text{Cs}</math> (30-y half life). A license is required for this source.</li><li>• <b>GF-060-M-10*</b> 10 <math>\mu\text{Ci}</math> <math>^{60}\text{Co}</math> (5.3-y half life). A license is required for this source.</li><li>• <b>GF-228-D-10*</b> 10 <math>\mu\text{Ci}</math> <math>^{228}\text{Th}</math> (698-d half life). A license is required for this source.</li><li>• Personal Computer with a USB port and Windows operating system</li><li>• Small, flat-blade screwdriver for tuning screwdriver-adjustable controls</li><li>• OPTIONAL FOR EXPERIMENT 7.4<ul style="list-style-type: none"><li>• <b>POSK22-10*</b> 10 <math>\mu\text{Ci}</math> <math>^{22}\text{Na}</math> thin source for observing positron annihilation peak broadening. A license is required for this source.</li><li>• <b>Foil-AL-30</b> 10 ea ½-inch (1.27-cm) dia. Aluminum foils, 0.030-inch (0.076 cm) thick</li><li>• <b>Foil-NI-10</b> 10 ea ½-inch (1.27-cm) dia. Nickel foils, 0.010-inch (0.025 cm) thick</li></ul></li></ul> |
|--|---|

\*Sources are available direct from supplier. See the ORTEC website at [www.ortec-online.com/Service-Support/Library/Experiments-Radioactive-Source-Suppliers.aspx](http://www.ortec-online.com/Service-Support/Library/Experiments-Radioactive-Source-Suppliers.aspx)

### Purpose

Gamma-ray energies will be measured with a High-Purity Germanium (HPGe) detector and research-grade electronics. The principles behind the response characteristics of the detector are explained. The high-resolution measurement results are contrasted with those obtainable from the NaI(Tl) (sodium iodide) scintillation detector previously explored in Experiment 3.

### Introduction

Most of the experiments in this series are written for use with lower-cost detectors and electronic modules. However, in this experiment, which illustrates the superior resolution capabilities of the high-performance HPGe detector systems, research-grade signal processing modules have been incorporated to fully utilize the detector's capabilities.

Many colleges, universities, and national research laboratories have Nuclear Spectroscopy Centers that employ high-resolution gamma-ray spectrometry to investigate decay schemes of radioisotopes. Given the plethora of isotopes, opportunities continue to arise in exploring the details of the decay schemes. Improved energy resolution allows additional lines to be found in spectra. Occasionally, a doublet is discovered, whereas earlier measurements with NaI(Tl) detectors indicated only a single energy line.

High-Purity Germanium (HPGe) detectors are also extensively used to detect and monitor radioactivity in the environment, and to detect contraband radioisotopes and fissionable material. It is the excellent energy resolution of the HPGe detector that enables ultra-low detection limits in these applications.

## Experiment 7 High-Resolution Gamma-Ray Spectroscopy

Decay schemes for isotopes are included in refs. 10 and 12. More recent information on certain nuclei can be found in ORTEC's Nuclide Navigator Master Library software package (Model C53-B32). An up-to-date on-line resource for such information is sponsored by:

National Nuclear Data Center  
Building 197D  
Brookhaven National Laboratory  
Upton, NY 11973-5000  
Phone: (631) 344-2902  
Fax: (631) 344-2806  
Email: nndc@bnl.gov  
Internet: <http://www.nndc.bnl.gov>

In Experiment 3, gamma-ray spectroscopy with NaI(Tl) detectors was studied. The typical energy resolution that can be obtained with NaI(Tl) is circa 7% for the 0.662 MeV  $^{137}\text{Cs}$  gamma-ray line. For NaI(Tl) detectors, the resolution is a strong function of energy. The resolution is primarily controlled by the statistical fluctuation of the number of photoelectrons produced at the photocathode surface in the photomultiplier tube. Table 7.1 illustrates some typical resolutions for a NaI(Tl) detector as a function of the gamma-ray energy. Note that it is conventional to express the resolution in percent for NaI(Tl) detectors.

$$\% \text{ Resolution (FWHM)} = \frac{\delta E}{E} \times 100\% \approx \frac{k \times 100\%}{\sqrt{E}} \quad (1)$$

Where

$E$  is the energy of the peak,

$\delta E$  is the FWHM of the peak in energy units, and

$k$  is a proportionality constant characteristic of the particular detector.

The development of germanium detectors in the late 1960s completely revolutionized gamma spectroscopy. Fig. 7.1 illustrates the striking contrast in results obtained with the two common types of gamma-ray detectors. Compared to NaI(Tl), there is a factor of 30 improvement in the full-width at half-maximum (FWHM) resolution. As a result of this improved resolution, many nuclear energy levels that could not be resolved with NaI(Tl) detectors are easily identified by using HPGe detectors.

Concurrently, the development of lithium-drifted silicon detectors [Si(Li)] with drastically-improved energy resolution revolutionized x-ray spectrometry. These Si(Li) devices are studied in Experiment 8.

The purpose of this experiment is to explore some of the properties of HPGe detector systems. This experiment deals only with the

**Table 7.1. Typical Resolutions of a NaI(Tl) Detector for Various Gamma-Ray Energies.**

Isotope	Gamma Energy (keV)	Resolution (%)
$^{166}\text{Ho}$	81	16.19
$^{177}\text{Lu}$	113	13.5
$^{133}\text{Te}$	159	11.5
$^{177}\text{Lu}$	208	10.9
$^{203}\text{Hg}$	279	10.14
$^{51}\text{Cr}$	320	9.89
$^{198}\text{Au}$	411	9.21
$^7\text{Be}$	478	8.62
$^{137}\text{Cs}$	662	7.7
$^{54}\text{Mn}$	835	7.26
$^{207}\text{Bi}$	1067	6.56
$^{65}\text{Zn}$	1114	6.29
$^{22}\text{Na}$	1277	6.07
$^{88}\text{Y}$	1850	5.45

The information for this table was taken from *IRE Trans. Nucl. Sci.* NS-3(4), 57 (Nov. 1956). "Intrinsic Scintillator Resolution," by G. G. Kelley *et al.*, quoting results from F. K. McGowan, *et al.*

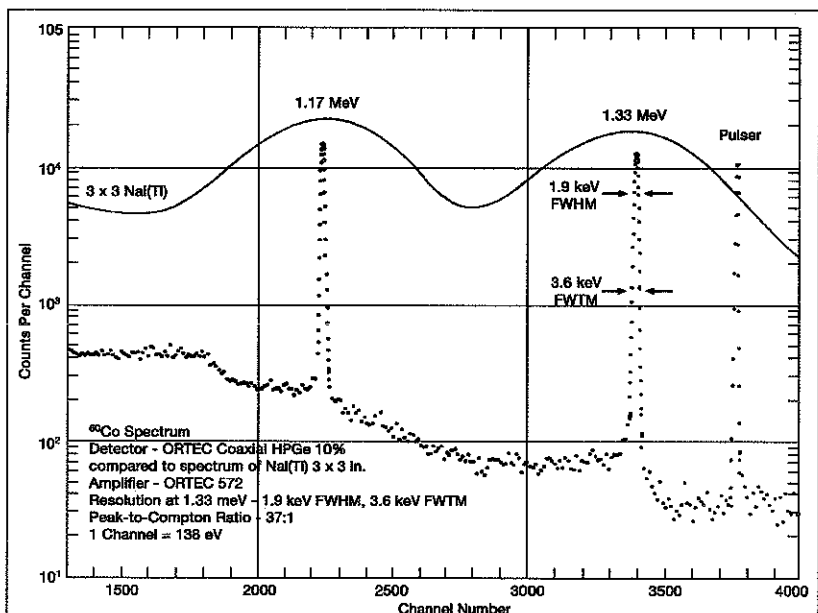


**Fig. 7.1. A Portion of a  $^{60}\text{Co}$  Spectrum, Illustrating the Energy Resolutions and Peak-to-Compton Ratios for a Coaxial HPGe Detector Compared to a NaI(Tl) Detector.**



practical aspects of making measurements with these detectors. To understand the properties of these detector systems, the following brief review of gamma-ray interactions and pair-production processes is included.

### Gamma-Ray Interactions in HPGe Detectors

Fig. 7.2 shows graphs for the three important gamma-ray interactions in both germanium and silicon. The absorption cross sections for germanium are of interest in this experiment. The corresponding values for silicon will be used in Experiment 8.

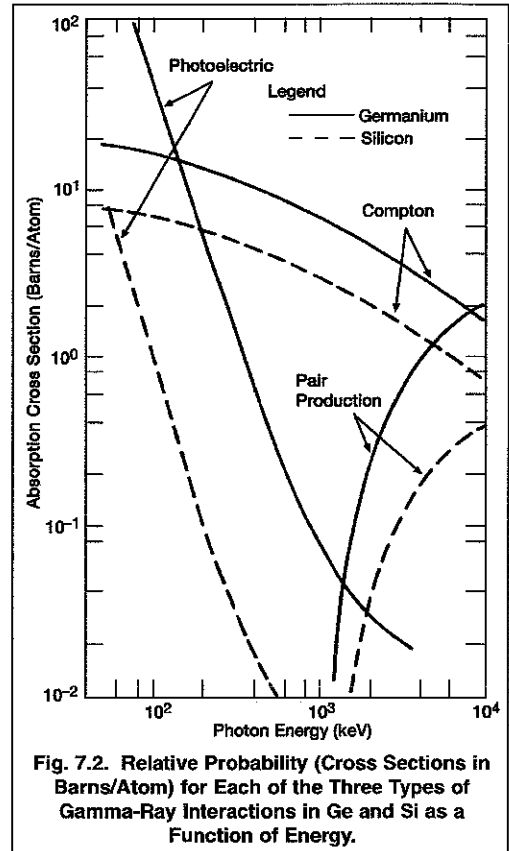
When a gamma-ray photon enters a detector, it must produce a recoil electron by one of three processes before it is recorded as an event: (1) the photoelectric effect, (2) the Compton effect, or (3) pair production.

In the **photoelectric process**, the gamma-ray or x-ray photon transfers all of its energy to an electron in the detector. Consequently, the photon vanishes. The recoiling electron loses energy by causing ionization of the detector material, resulting in a trail of electron-hole pairs. The bias voltage applied across the detector sweeps the electrons and holes to opposite electrodes, where the charge is collected to form the preamplifier pulse. For the photoelectric process, the total charge in the output pulse from the detector is proportional to the energy of the gamma-ray or x-ray that produced the interaction. These events will show up as full-energy photopeaks in the spectrum.

In the **Compton process**, the photon is scattered from an electron that is essentially not bound to an atom. Because the scattering angle can vary from 0 to 180 degrees, there is a range of energies that can be transferred from the photon to the recoiling electron. The scattered photon survives and carries off the remainder of the energy. It is the recoiling electron that loses energy by ionizing the detector material. Consequently, the charge collected from the detector will yield a distribution of pulse amplitudes at the preamplifier output up to some maximum pulse height. This maximum pulse height corresponds to the Compton edge in the energy spectrum, as explained in Experiment 3. There is a statistical probability that each Compton scattering event has an approximately equal chance to produce a pulse with any height up to this maximum. Thus, Compton events will provide a well-distributed low-energy continuum in the spectrum.

In large detectors with high peak-to-Compton ratios, some Compton events also contribute to the full-energy peak, when the scattered photons undergo one or more additional interactions, and finally terminate in complete absorption by the photoelectric interaction.

The **pair-production process** can also provide a total absorption of the gamma-ray energy. The gamma-ray photon enters the detector and creates an electron-positron pair. All the energy of the initial photon is transferred to the electron-positron pair. Consequently, the initial photon disappears in the process. From the law of conservation of mass and energy, it follows that the initial gamma-ray must have an energy of at least 1.022 MeV, because it takes that much energy to create both the negative and positive electrons. The net mass that is produced is two electron masses, and this satisfies the law of conversion of energy,  $E$ , into mass,  $m$ , i.e.,  $E = mc^2$ . If the initial photon has an energy in excess of 1.022 MeV, that excess energy is transferred into the recoil energies of the positron and electron. Both the positron and the electron lose energy by causing ionization of the atoms in the detector. Once the positron is moving slowly enough, it can be captured by a free electron, and the two can combine. In this annihilation of the positron with an electron, both particles disappear, and their rest mass energies are converted into two photons travelling in opposite directions, with each photon having an energy of 511 keV. Note that the sum of the energies of these two annihilation gamma rays is 1.022 MeV.



## Experiment 7 High-Resolution Gamma-Ray Spectroscopy

The optional experiment 7.4 explores this process of positron annihilation when the positron is obtained from  $\beta^+$  decay of a  $^{22}\text{Na}$  radioactive source.

Fig. 7.3 illustrates what happens in the detector in the pair-production process. In Fig. 7.3 the  $e^-$  (ordinary electron) will produce a pulse whose magnitude is proportional to the energy of  $e^-$ , i.e.,  $E_{e^-}$ . The positron,  $e^+$ , will produce a pulse proportional to its energy,  $E_{e^+}$ . Since these two pulses are produced simultaneously, the output pulse from the detector would be the sum of the two pulses. When the positron annihilates in the detector, the annihilation radiation  $\gamma_1$  and  $\gamma_2$ , will be produced. In Fig. 7.3, both  $\gamma_1$  and  $\gamma_2$  are shown escaping from the boundaries of the detector without making any further interactions. (Note:  $E_{\gamma_1} = E_{\gamma_2} = 0.511 \text{ MeV}$ ).

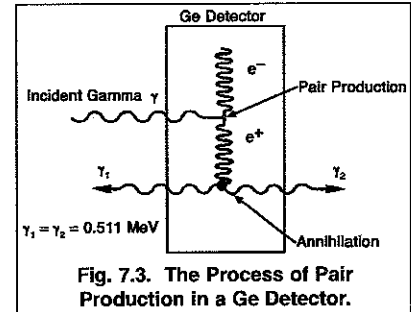


Fig. 7.3. The Process of Pair Production in a Ge Detector.

Thus, in this example, an energy of exactly 1.022 MeV escapes from the detector, and is subtracted from the total energy that entered the detector. It is possible for only one, either  $\gamma_1$  or  $\gamma_2$ , to make a photoelectric interaction in the detector while the other escapes. In such cases, the total energy absorbed is 0.511 MeV less than the original incident gamma-ray energy. It is also possible for both gammas to make photoelectric interactions without escaping, with all the original energy being left in the detector. Therefore, in the spectrum being measured, there will be three peaks for each incident gamma-ray having an energy well in excess of 1.022 MeV. These peaks, labeled Full-Energy Peak, Single-Escape Peak, and Double-Escape Peak, will be separated by 0.511 MeV increments. Fig. 7.4 shows a typical spectrum that would be obtained for an incident gamma-ray energy of 2.511 MeV. The lower end of the spectrum that shows the Compton distribution has not been included. The Single-Escape Peak occurs at 2.00 MeV ( $E_\gamma - 0.511 \text{ MeV}$ ), and the Double-Escape Peak occurs at 1.49 MeV ( $E_\gamma - 1.022 \text{ MeV}$ ). Of course, the full-energy peak represents those events for which there was a combination of pair production and photoelectric effect in which all the energy was absorbed in the detector.

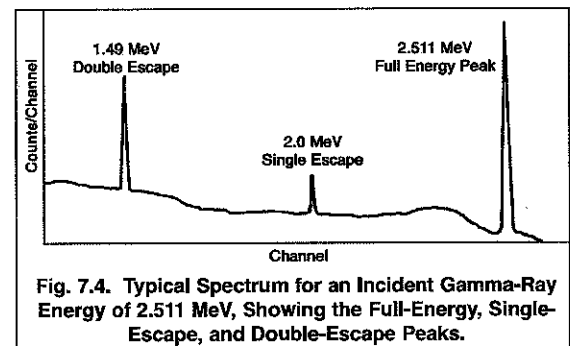


Fig. 7.4. Typical Spectrum for an Incident Gamma-Ray Energy of 2.511 MeV, Showing the Full-Energy, Single-Escape, and Double-Escape Peaks.

Now refer again to Fig. 7.2, and specifically to the curves for the interaction in germanium. The absorption cross section, plotted in the y direction, is a measure of the relative probability that an interaction will occur in a thin slab of the germanium detector. These probabilities of relative interactions, for the most part, determine the shape of the observed spectrum. For example, a photon with an energy of 100 keV has an absorption cross section of approximately 55 barns/atom for the photoelectric process. The corresponding Compton cross section is about 18 barns/atom. There is no pair production. These two cross sections are in the approximate ratio of 3:1, at 100 keV, implying that there are 3 times as many photoelectric interactions as Compton interactions. Fig. 7.5 shows the shape of a spectrum that could be expected for measurement of the 100 keV energy events.

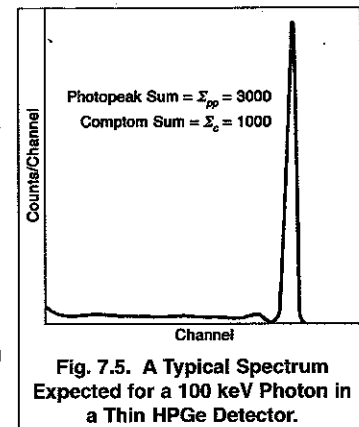


Fig. 7.5. A Typical Spectrum Expected for a 100 keV Photon in a Thin HPGe Detector.

The shape of the spectrum changes drastically from 100 keV to 1 MeV. Fig. 7.6 shows the gamma spectrum that could be expected for the 1 MeV gammas incident on a thin HPGe detector. From Fig. 7.2, the ratio of Compton cross section to photoelectric cross section is approximately 90; so, in Fig. 7.6, the sum of the counts in the Compton distribution is  $\Sigma_c = 90,000$  and the sum of the counts in the photopeak is  $\Sigma_{pp} = 1000$ .

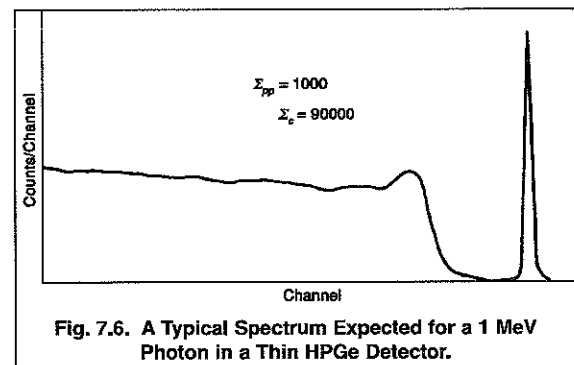


Fig. 7.6. A Typical Spectrum Expected for a 1 MeV Photon in a Thin HPGe Detector.

## Experiment 7 High-Resolution Gamma-Ray Spectroscopy

The relative efficiencies for HPGe and Si(Li) detectors can also be approximated from Fig. 7.2. For example, at  $E_\gamma = 400$  keV the photoelectric cross section for germanium is 6 barns/atom, and that for silicon is approximately 0.1 barn/atom. This is a ratio of 60:1, and indicates that there will be 60 times as many counts under the photopeak for a germanium detector as for a silicon detector at 400 keV, assuming that the detectors are the same size. This ratio of detector efficiencies reflects the fact that the photoelectric cross section varies as  $Z^5$ , where  $Z$  is the atomic number of the absorbing material. The atomic number of Ge is 32 and for Si it is 14. The ratio of these two numbers raised to the 5th power is 62.2, which agrees remarkably well with the above cross-section ratios. Higher atomic numbers offer greater photopeak efficiencies.

Fig. 7.2 shows that the cross-section for photoelectric absorption drops rapidly with increasing energy. From 300 keV to 3 MeV, the Compton-scattering cross-section dominates. The higher the energy, the more deeply the gamma-ray can penetrate the detector before it interacts with an electron. Consequently, the efficiency can be improved by increasing the dimensions of the Ge detector along the original direction of the photon, and in directions perpendicular to the path of the photon. According to the Beer-Lambert law for absorption (Experiments 2 and 3), a larger detector increases the probability that the photon will interact in the detector. If the initial interaction is a Compton scattering, the larger detector dimensions improve the chances that the scattered photon will be stopped by a photoelectric absorption before it leaves the detector volume, placing the event in the full-energy peak. Consequently, a larger detector improves the ratio of counts in the full-energy peak to the counts in the Compton continuum. This improves detection limits for weak peaks that would be obscured by statistical fluctuations in the Compton continuum from higher-energy gamma rays.

### Detector Structure

Basically, a HPGe detector is a very large semiconductor diode, with a reverse bias voltage applied to its two electrodes to deplete virtually all free charge carriers from the bulk of the detector. Small detectors can be obtained in the planar geometry that is similar to the structure of the silicon charged-particle detectors studied in experiments 4, 5 and 6. Figure 7.7 illustrates the planar geometry. The detector is a cylinder of HPGe with electrodes applied to its two circular ends.

Significantly larger detectors benefit from using the coaxial geometry depicted in Fig. 7.8. The P-type HPGe (GEM) is the type of detector used in this experiment. The detector is composed of a large cylinder of high-purity germanium. A hole is drilled from one end, along the centerline of the cylinder. One electrode is applied to the outer surface of the cylinder and to the closed end. The other electrode is applied to the inside surface of the central hole. The surface of the end from which the hole is drilled (open end) is passivated to reduce surface leakage currents between the two electrodes. The coaxial detector shape is mounted in the end cap of the cryostat, with the cylindrical axis of the detector diode aligned coaxially with the centerline of the end cap. The closed end of the detector is located a few millimeters behind the circular surface of the end cap.

The detector and the first amplifying stage of the preamplifier are operated near the boiling temperature of liquid nitrogen (77°K) to reduce noise. Consequently, the detector and the first stage of the preamplifier are mounted in a vacuum cryostat. The cryostat establishes operation at the desired low temperature via a copper cooling rod dipped in the liquid nitrogen contained in the associated dewar. Operation at the cryogenic temperature dramatically reduces the leakage current in the HPGe detector and also diminishes thermally generated noise in the FET input stage of the preamplifier. The preamplifier feedback capacitor and feedback resistor are also cooled to reduce their noise contribution. As will be seen next, decreasing these sources of noise improves the energy resolution.

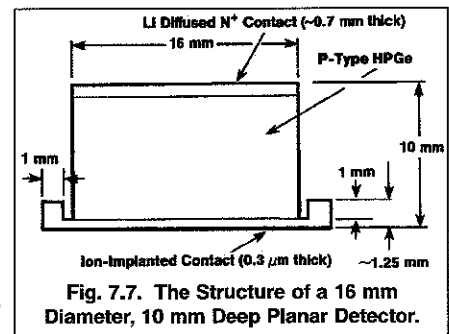


Fig. 7.7. The Structure of a 16 mm Diameter, 10 mm Deep Planar Detector.

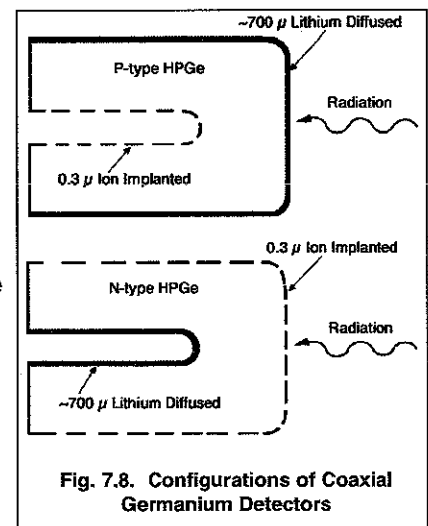


Fig. 7.8. Configurations of Coaxial Germanium Detectors

## Experiment 7

### High-Resolution Gamma-Ray Spectroscopy

---

#### Energy Resolution

The energy resolution of a HPGe detector is described by equation (2).

$$\Delta E_{total} = \sqrt{(\Delta E_{noise})^2 + (\Delta E_{ion})^2 + (\Delta E_{incomplete})^2} \quad (2a)$$

where

$$\Delta E_{ion} = 2.35\sqrt{\epsilon FE} \quad (2b)$$

$\Delta E_{total}$  is the full width at half maximum amplitude (FWHM) of the gamma-ray peak at energy E in the spectrum.  $\Delta E_{noise}$  is the contribution from the noise caused by the detector leakage current and the preamplifier. It is most readily measured as the FWHM of a pulser peak artificially introduced into the spectrum by injecting a pulser signal into the input of the preamplifier. The noise contribution is independent of the gamma-ray energy. But, it does depend on the shaping time constant of the spectroscopy amplifier. If the shaping time constant is too small or too large, the noise contribution will be higher than the optimum. Check the detector data sheet for the optimum shaping time constant to minimize the noise. The optimum will likely lie in the range of 3 to 6 microseconds.

$\Delta E_{ion}$  describes the variation in the number of electron-hole pairs generated as a result of ionization statistics. It depends on the average energy required to create an electron-hole pair (i.e.,  $\epsilon = 2.95$  eV), the energy of the gamma-ray, E, and the Fano factor, F. Note that the same units of energy must be used throughout equation (2). The Fano factor accounts for the fact that the ionization process lies somewhere between completely independent random ionization events at one extreme ( $F = 1$ ), and an absolutely deterministic conversion of energy into electron-hole pairs at the other extreme ( $F = 0$ ). For HPGe a Fano factor,  $F \approx 0.1$ , indicates the process is closer to the latter than the former condition.

$\Delta E_{incomplete}$  accounts for the variation in the ability to collect all of the electron-hole pairs that are created by the ionization process. Primarily, this applies to electron-hole pairs that recombine before they can be collected, or charge carriers that fall into traps while drifting to their respective electrode. Additionally, there is potential for a ballistic deficit effect when the shaping time constant is too small. For large coaxial HPGe detectors the charge collection time can vary from 50 to 700 ns, depending on the position at which the charge was created. If the amplifier shaping time constant is not large compared to these collection times, the pulse height will show additional fluctuations caused by random variations in the charge collection times. If the incomplete charge collection term is ignored in equation (2), spectral resolution measurements may lead to an inflated value for the implied Fano factor.

#### Maximum Counting Rate Deduced from the Percent Dead Time

Because gamma rays arrive at the detector with random spacing in time, the width of the pulse from the amplifier limits the counting rate that can be processed without distortion. Probably the most efficient way to ensure that the maximum counting rate is not exceeded is to adjust the source-to-detector distance so that the percent dead time observed on the Multichannel Analyzer is less than 63%. The dominant dead time in the gamma-ray spectrometer specified for this experiment is a paralyzable (a.k.a., extending) dead time (ref. 11, 14 and 15). For a paralyzable dead time, the maximum analyzed throughput is accomplished when the dead time is 63%. Operation at counting rates that yield slightly less than 63% dead time will provide optimum performance.

#### Further Information on HPGe Detectors

Consult references 11, 13, 14 and 15 for further details on HPGe detectors.

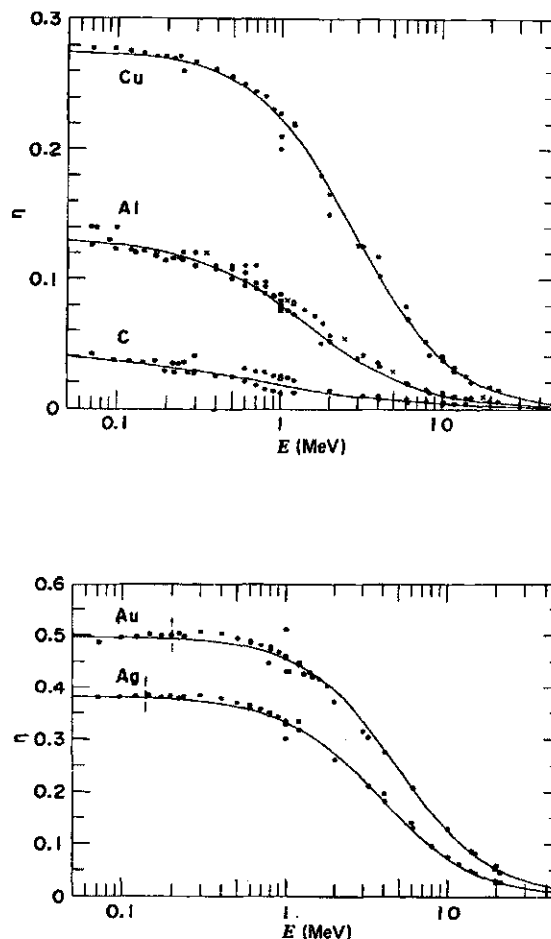


**Figure 2.17** Fraction  $\eta$  of normally incident electrons that are backscattered from thick slabs of various materials, as a function of incident energy  $E$ . (From Tabata et al.<sup>27</sup>)

### III. INTERACTION OF GAMMA RAYS

Although a large number of possible interaction mechanisms are known for gamma rays in matter, only three major types play an important role in radiation measurements: *photoelectric absorption*, *Compton scattering*, and *pair production*. All these processes lead to the partial or complete transfer of the gamma-ray photon energy to electron energy. They result in sudden and abrupt changes in the gamma-ray photon history, in that the photon either disappears entirely or is scattered through a significant angle. This behavior is in marked contrast to the charged particles discussed earlier in this chapter, which slow down gradually through continuous, simultaneous interactions with many absorber atoms. The fundamentals of the gamma-ray interaction mechanisms are introduced here but are again reviewed at the beginning of Chapter 10 in the context of their influence on the response of gamma-ray detectors.

## A. Interaction Mechanisms

### 1. PHOTOELECTRIC ABSORPTION

In the photoelectric absorption process, a photon undergoes an interaction with an absorber atom in which the photon completely disappears. In its place, an energetic *photoelectron* is ejected by the atom from one of its bound shells. The interaction is with the atom as a whole and cannot take place with free electrons. For gamma rays of sufficient energy, the most probable origin of the photoelectron is the most tightly bound or *K* shell of the atom. The photoelectron appears with an energy given by

$$E_{e^-} = h\nu - E_b \quad (2.15)$$

where  $E_b$  represents the binding energy of the photoelectron in its original shell. For gamma-ray energies of more than a few hundred keV, the photoelectron carries off the majority of the original photon energy.

In addition to the photoelectron, the interaction also creates an ionized absorber atom with a vacancy in one of its bound shells. This vacancy is quickly filled through capture of a free electron from the medium and/or rearrangement of electrons from other shells of the atom. Therefore, one or more characteristic X-ray photons may also be generated. Although in most cases these X-rays are reabsorbed close to the original site through photoelectric absorption involving less tightly bound shells, their migration and possible escape from radiation detectors can influence their response (see Chapter 10). In some fraction of the cases, the emission of an Auger electron may substitute for the characteristic X-ray in carrying away the atomic excitation energy.

As an example of the complexity of these interactions, consider incident photons with energy above 30 keV that undergo photoelectric absorption in xenon. About 86% interact through *K*-shell absorptions in the xenon atom.<sup>28</sup> Of these, 87.5% result in *K*-shell characteristic (or “fluorescent”) X-rays (a mixture of *K*- $\alpha$  and *K*- $\beta$ ) and 12.5% de-excite through the emission of Auger electrons. The remaining 14% of the incident photons that do not undergo *K*-shell interactions are absorbed through photoelectric interaction with the *L* or *M* shells. These result in much lower energy characteristic X-rays or Auger electrons that are very short range and, to first approximation, are reabsorbed very near the site of the original interaction. Another example of such a “cascade sequence” is shown in Chapter 10 as Fig. 10.20.

The photoelectric process is the predominant mode of interaction for gamma rays (or X-rays) of relatively low energy. The process is also enhanced for absorber materials of high atomic number  $Z$ . No single analytic expression is valid for the probability of photoelectric absorption per atom over all ranges of  $E_\gamma$  and  $Z$ , but a rough approximation is

$$\tau \cong \text{constant} \times \frac{Z^n}{E_\gamma^{3.5}} \quad (2.16)$$

where the exponent  $n$  varies between 4 and 5 over the gamma-ray energy region of interest.<sup>1</sup> This severe dependence of the photoelectric absorption probability on the atomic number of the absorber is a primary reason for the preponderance of high- $Z$  materials (such as lead) in gamma-ray shields. As further detailed in Chapter 10, many detectors used for gamma-ray spectroscopy are chosen from high- $Z$  constituents for the same reason.

A plot of the photoelectric absorption cross section for a popular gamma-ray detection material, sodium iodide, is shown in Fig. 2.18. In the low-energy region, discontinuities in the curve or “absorption edges” appear at gamma-ray energies that correspond to the binding energies of electrons in the various shells of the absorber atom. The edge lying highest in energy therefore corresponds to the binding energy of the *K*-shell electron. For gamma-ray energies slightly above the edge, the photon energy is just sufficient to undergo a photoelectric interaction in which a *K*-electron is ejected from the atom. For gamma-ray

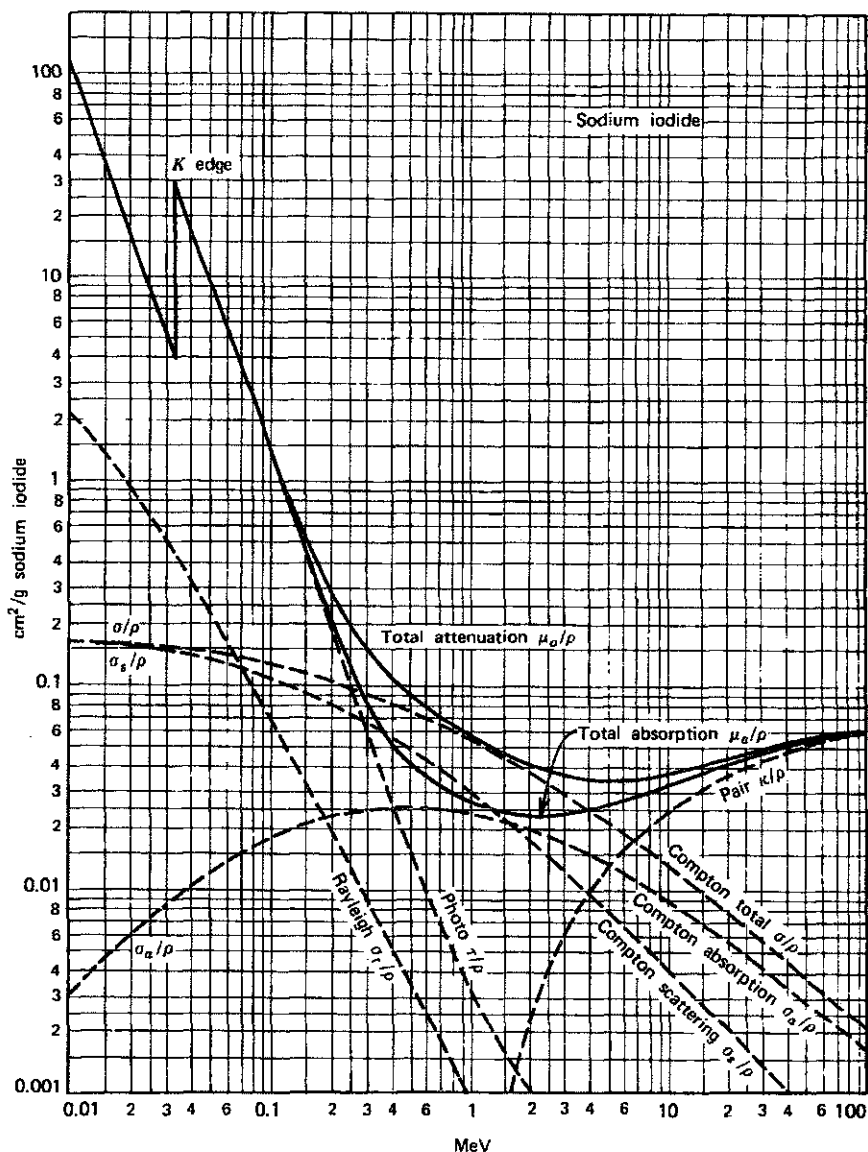


**Figure 2.18** Energy dependence of the various gamma-ray interaction processes in sodium iodide. (From *The Atomic Nucleus* by R. D. Evans. Copyright 1955 by the McGraw-Hill Book Company. Used with permission.)

energies slightly below the edge, this process is no longer energetically possible and therefore the interaction probability drops abruptly. Similar absorption edges occur at lower energies for the *L*, *M*, . . . electron shells of the atom.

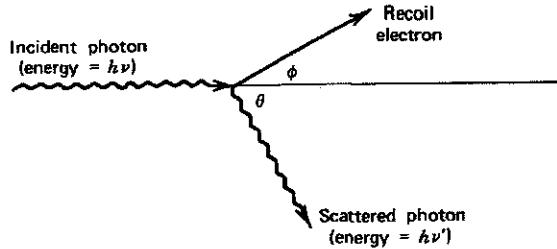
**2. COMPTON SCATTERING**

The interaction process of Compton scattering takes place between the incident gamma-ray photon and an electron in the absorbing material. It is most often the predominant interaction mechanism for gamma-ray energies typical of radioisotope sources.

In Compton scattering, the incoming gamma-ray photon is deflected through an angle  $\theta$  with respect to its original direction. The photon transfers a portion of its energy to the electron (assumed to be initially at rest), which is then known as a *recoil electron*. Because

all angles of scattering are possible, the energy transferred to the electron can vary from zero to a large fraction of the gamma-ray energy.

The expression that relates the energy transfer and the scattering angle for any given interaction can simply be derived by writing simultaneous equations for the conservation of energy and momentum. Using the symbols defined in the sketch below



we can show<sup>1</sup> that

$$h\nu' = \frac{h\nu}{1 + \frac{h\nu}{m_0c^2}(1 - \cos \theta)} \quad (2.17)$$

where  $m_0c^2$  is the rest-mass energy of the electron (0.511 MeV). For small scattering angles  $\theta$ , very little energy is transferred. Some of the original energy is always retained by the incident photon, even in the extreme of  $\theta = \pi$ . Equations (10.3) through (10.6) describe some properties of the energy transfer for limiting cases. A plot of the scattered photon energy predicted from Eq. (2.17) is also shown in Fig. 10.7.<sup>†</sup>

The probability of Compton scattering per atom of the absorber depends on the number of electrons available as scattering targets and therefore increases linearly with  $Z$ . The dependence on gamma-ray energy is illustrated in Fig. 2.18 for the case of sodium iodide and generally falls off gradually with increasing energy.

The angular distribution of scattered gamma rays is predicted by the *Klein-Nishina formula* for the differential scattering cross section  $d\sigma/d\Omega$ :

$$\frac{d\sigma}{d\Omega} = Zr_0^2 \left( \frac{1}{1 + \alpha(1 - \cos \theta)} \right)^2 \left( \frac{1 + \cos^2 \theta}{2} \right) \left( 1 + \frac{\alpha^2(1 - \cos \theta)^2}{(1 + \cos^2 \theta)[1 + \alpha(1 - \cos \theta)]} \right) \quad (2.18)$$

where  $\alpha \equiv h\nu/m_0c^2$  and  $r_0$  is the classical electron radius. The distribution is shown graphically in Fig. 2.19 and illustrates the strong tendency for forward scattering at high values of the gamma-ray energy.

### 3. PAIR PRODUCTION

If the gamma-ray energy exceeds twice the rest-mass energy of an electron (1.02 MeV), the process of pair production is energetically possible. As a practical matter, the probability of this interaction remains very low until the gamma-ray energy approaches several MeV and therefore pair production is predominantly confined to high-energy gamma rays. In the interaction (which must take place in the coulomb field of a nucleus), the gamma-ray photon disappears and is replaced by an electron-positron pair. All the excess energy carried in by the photon above the 1.02 MeV required to create the pair goes into kinetic energy shared by the positron and the electron. Because the positron will subsequently annihilate

<sup>†</sup>The simple analysis here neglects the atomic binding of the electron and assumes that the gamma-ray photon interacts with a free electron. If the small binding energy is taken into account, the unique energy of the scattered photon at a fixed angle predicted by Eq. 2.17 is spread into a narrow distribution centered about that energy (see Fig. 13.9).



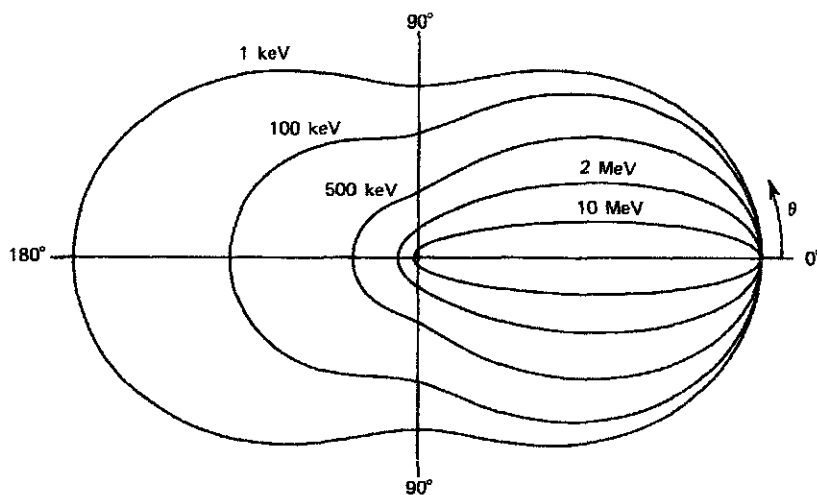


**Figure 2.19** A polar plot of the number of photons (incident from the left) Compton scattered into a unit solid angle at the scattering angle  $\theta$ . The curves are shown for the indicated initial energies.

after slowing down in the absorbing medium, two annihilation photons are normally produced as secondary products of the interaction. The subsequent fate of this annihilation radiation has an important effect on the response of gamma-ray detectors, as described in Chapter 10.

No simple expression exists for the probability of pair production per nucleus, but its magnitude varies approximately as the square of the absorber atomic number.<sup>1</sup> The importance of pair production rises sharply with energy, as indicated in Fig. 2.18.

The relative importance of the three processes described above for different absorber materials and gamma-ray energies is conveniently illustrated in Fig. 2.20. The line at the left represents the energy at which photoelectric absorption and Compton scattering are equally probable as a function of the absorber atomic number. The line at the right represents the energy at which Compton scattering and pair production are equally probable. Three areas are thus defined on the plot within which photoelectric absorption, Compton scattering, and pair production each predominate.

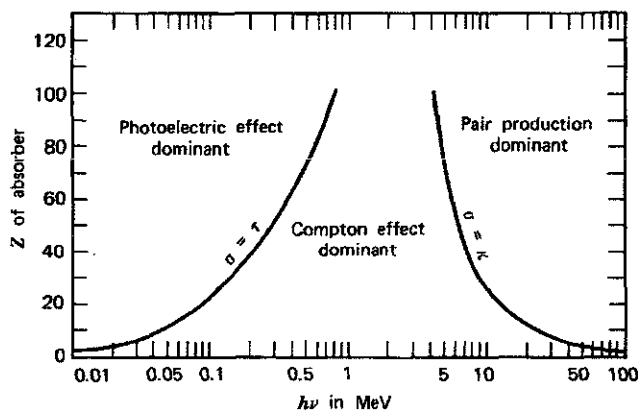


**Figure 2.20** The relative importance of the three major types of gamma-ray interaction. The lines show the values of  $Z$  and  $h\nu$  for which the two neighboring effects are just equal. (From *The Atomic Nucleus* by R. D. Evans. Copyright 1955 by the McGraw-Hill Book Company. Used with permission.)

#### 4. COHERENT SCATTERING

In addition to Compton scattering, another type of scattering can occur in which the gamma-ray photon interacts coherently with all the electrons of an absorber atom. This *coherent scattering* or *Rayleigh scattering* process<sup>1</sup> neither excites nor ionizes the atom, and the gamma-ray photon retains its original energy after the scattering event. Because virtually no energy is transferred, this process is often neglected in basic discussions of gamma-ray interactions, and we will also ignore it in the discussions that follow. However, the direction of the photon is changed in coherent scattering, and complete models of gamma-ray transport must take it into account. The probability of coherent scattering is significant only for low photon energies (typically below a few hundred keV for common materials) and is most prominent in high- $Z$  absorbers. The average deflection angle decreases with increasing energy, further restricting the practical importance of coherent scattering to low energies.

### B. Gamma-Ray Attenuation

#### 1. ATTENUATION COEFFICIENTS

If we again picture a transmission experiment as in Fig. 2.21, where monoenergetic gamma rays are collimated into a narrow beam and allowed to strike a detector after passing through an absorber of variable thickness, the result should be simple exponential attenuation of the gamma rays as also shown in Fig. 2.21. Each of the interaction processes removes the gamma-ray photon from the beam either by absorption or by scattering away from the detector direction and can be characterized by a fixed probability of occurrence per unit path length in the absorber. The sum of these probabilities is simply the probability per unit path length that the gamma-ray photon is removed from the beam:

$$\mu = \tau(\text{photoelectric}) + \sigma(\text{Compton}) + \kappa(\text{pair}) \quad (2.19)$$

and is called the *linear attenuation coefficient*. The number of transmitted photons  $I$  is then given in terms of the number without an absorber  $I_0$  as

$$\frac{I}{I_0} = e^{-\mu t} \quad (2.20)$$

The gamma-ray photons can also be characterized by their *mean free path*  $\lambda$ , defined as the average distance traveled in the absorber before an interaction takes place. Its value can be obtained from

$$\lambda = \frac{\int_0^{\infty} x e^{-\mu x} dx}{\int_0^{\infty} e^{-\mu x} dx} = \frac{1}{\mu} \quad (2.21)$$

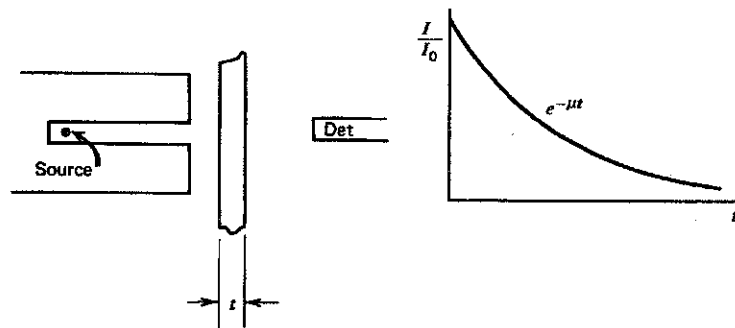


**Figure 2.21** The exponential transmission curve for gamma rays measured under "good geometry" conditions.

and is simply the reciprocal of the linear attenuation coefficient. Typical values of  $\lambda$  range from a few mm to tens of cm in solids for common gamma-ray energies.

Use of the linear attenuation coefficient is limited by the fact that it varies with the density of the absorber, even though the absorber material is the same. Therefore, the *mass attenuation coefficient* is much more widely used and is defined as

$$\text{mass attenuation coefficient} = \frac{\mu}{\rho} \quad (2.22)$$

where  $\rho$  represents the density of the medium. For a given gamma-ray energy, the mass attenuation coefficient does not change with the physical state of a given absorber. For example, it is the same for water whether present in liquid or vapor form. The mass attenuation coefficient of a compound or mixture of elements can be calculated from

$$\left(\frac{\mu}{\rho}\right)_c = \sum_i w_i \left(\frac{\mu}{\rho}\right)_i \quad (2.23)$$

where the  $w_i$  factors represent the weight fraction of element  $i$  in the compound or mixture.

## 2. ABSORBER MASS THICKNESS

In terms of the mass attenuation coefficient, the attenuation law for gamma rays now takes the form

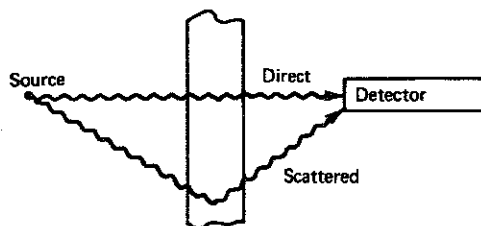
$$\frac{I}{I_0} = e^{-(\mu/\rho)\rho t} \quad (2.24)$$

The product  $\rho t$ , known as the *mass thickness* of the absorber, is now the significant parameter that determines its degree of attenuation. Units of mass thickness have historically been  $\text{mg}/\text{cm}^2$ , and this convention is retained in this text. The thickness of absorbers used in radiation measurements is therefore often measured in mass thickness rather than physical thickness, because it is a more fundamental physical quantity.

The mass thickness is also a useful concept when discussing the energy loss of charged particles and fast electrons. For absorber materials with similar neutron/proton ratios, a particle will encounter about the same number of electrons passing through absorbers of equal mass thickness. Therefore, the stopping power and range, when expressed in units of  $\rho t$ , are roughly the same for materials that do not differ greatly in  $Z$ .

## 3. BUILDUP

The gamma-ray attenuation experiment of Fig. 2.21, in which the gamma rays are collimated to a narrow beam before striking the absorber, is sometimes characterized as a “narrow beam” or “good geometry” measurement. The essential characteristic is that only gamma rays from the source that escape interaction in the absorber can be counted by the detector. Real measurements are often carried out under different circumstances (as sketched below) in which the severe collimation of the gamma rays is absent.



Now the detector can respond either to gamma rays directly from the source, to gamma rays that reach the detector after having scattered in the absorber, or to other types of secondary photon radiation. Many types of detectors will be unable to distinguish between these possibilities, so that the measured detector signal will be larger than that recorded under equivalent “good geometry” conditions. The conditions that lead to the simple exponential attenuation of Eq. (2.20) are therefore violated in this “broad beam” or “bad geometry” measurement because of the additional contribution of the secondary gamma rays. This situation is usually handled by replacing Eq. (2.20) by the following:

$$\frac{I}{I_0} = B(t, E_\gamma)e^{-\mu t} \quad (2.25)$$

where the factor  $B(t, E_\gamma)$  is called the *buildup factor*. The exponential term is retained to describe the major variation of the gamma-ray counting rate with absorber thickness, and the buildup factor is introduced as a simple multiplicative correction. The magnitude of the buildup factor depends on the type of gamma-ray detector used, because this will affect the relative weight given to the direct and secondary gamma rays. (With a detector that responds only to the direct gamma rays, the buildup factor is unity.) The buildup also depends on the specific geometry of the experiment. As a rough rule of thumb, the buildup factor for thick slab absorbers tends to be about equal to the thickness of the absorber measured in units of mean free path of the incident gamma rays, provided the detector responds to a broad range of gamma-ray energies.

## IV. INTERACTION OF NEUTRONS

### A. General Properties

In common with gamma rays, neutrons carry no charge and therefore cannot interact in matter by means of the coulomb force, which dominates the energy loss mechanisms for charged particles and electrons. Neutrons can also travel through many centimeters of matter without any type of interaction and thus can be totally invisible to a detector of common size. When a neutron does undergo interaction, it is with a nucleus of the absorbing material. As a result of the interaction, the neutron may either totally disappear and be replaced by one or more secondary radiations, or else the energy or direction of the neutron is changed significantly.

In contrast to gamma rays, the secondary radiations resulting from neutron interactions are almost always heavy charged particles. These particles may be produced either as a result of neutron-induced nuclear reactions or they may be the nuclei of the absorbing material itself, which have gained energy as a result of neutron collisions. Most neutron detectors utilize some type of conversion of the incident neutron into secondary charged particles, which can then be detected directly. Specific examples of the most useful conversion processes are detailed in Chapters 14 and 15.

The relative probabilities of the various types of neutron interactions change dramatically with neutron energy. In somewhat of an oversimplification, we will divide neutrons into two categories on the basis of their energy, either “fast neutrons” or “slow neutrons,” and discuss their interaction properties separately. The dividing line will be at about 0.5 eV, or about the energy of the abrupt drop in absorption cross section in cadmium (the *cadmium cutoff energy*).